PRECLINICAL EVALUATION OF SOMATOSTATIN ANALOGUES FOR BREAST

CANCER IMAGING USING POSITRON EMISSION TOMOGRAPHY

by

Iulia Gabriela Dude

B.Sc., The University of Waterloo, 2014

A THESIS SUBMITTED IN PARTIAL FULFILLMENT OF

THE REQUIREMENTS FOR THE DEGREE OF

MASTER OF SCIENCE

in

THE FACULTY OF GRADUATE AND POSTDOCTORAL STUDIES

(Interdisciplinary Oncology)

THE UNIVERSITY OF BRITISH COLUMBIA

(Vancouver)

March 2017

Abstract

Somatostatin receptors (sstrs) are G-protein coupled receptors that modulate hormone secretions. Their overexpression on neuroendocrine tumours (NETs) has enabled successful imaging of these cancers with radioactive peptides using positron emission tomography. Luminal A breast cancers also overexpress sstr, but with a lower and more heterogeneous density than NETs. Recently, several authors demonstrated higher tumour binding with sstr antagonists compared to agonists. Antagonists are hypothesized to bind to target receptors in multiple configurations, thus labeling more binding sites than high-affinity agonists. This property could result in better visualization of tumours with lower sstr density, such as breast cancers.

We hypothesized that the somatostatin agonist peptides TOC and TATE and antagonist peptide JR11 could be radiolabeled with ^{68}Ga and ^{18}F, and that antagonist radiotracers will show higher tumour uptake when evaluated *in vivo* using the human breast cancer xenograft ZR-75-1. We synthesized the literature compounds ^{68}Ga-DOTATOC, ^{68}Ga-DOTATATE and antagonist ^{68}Ga-NODAGA-JR11 and evaluated binding affinity and tumour uptake. The agonist ^{68}Ga-DOTATOC had the highest tumour uptake (18.4 ± 2.87 %ID/g), and the antagonist ^{68}Ga-NODAGA-JR11, the lowest (12.1 ± 0.78 %ID/g). We radiolabeled the same peptide analogues with ^{18}F using the easy and robust AmBF$_3$ method. ^{18}F is an excellent isotope for peptide radiolabeling, having low positron energy (634 keV), a half-life well-matched to peptide kinetics (110 min), and an established cyclotron production method. We synthesized the compounds ^{18}F-AmBF$_3$-TOC, ^{18}F-AmBF$_3$-TATE and ^{18}F-AmBF$_3$-JR11 and found that all were kinetically stable (determined by *in vivo* plasma stability studies) and successfully visualized the tumour with high intensity and contrast at both 1 hour and 2 hours post-injection (p.i.). At 1 h p.i. uptake means

were between 10.0 – 13.4 %ID/g for all three radiotracers, and differences were not statistically significant.

Imaging with ^{18}F- and ^{68}Ga-labeled JR11 antagonists did not confer any additional advantages compared to agonists in this tumour model. However, the high tumour uptake of both ^{68}Ga- and ^{18}F-labeled antagonists is striking, despite their significantly poorer binding affinity (inhibition contrast (K_i) > 18 nM) compared to agonist (K_i < 1.5 nM). With modifications to improve affinity, antagonist somatostatin analogues may be very promising for breast cancer visualization.

Preface

A version of Chapter 3 has been accepted for publication [**I Dude**, Z Zhang, J Rousseau, N Hundal-Jabal, N Colpo, H Merkens, KS Lin, F Bénard. Evaluation of Agonist and Antagonist Radioligands for Somatostatin Receptor Imaging of Breast Cancer using Positron Emission Tomography. *European Journal of Nuclear Medicine and Molecular Imaging (EJNMMI) Radiopharmacy and Chemistry]*. Z Zhang and I were the lead members on this project. Z Zhang performed the chemical and radiochemical synthesis of cold standards and radiotracers. I conducted the biological evaluation experiments (binding assays, qPCR, biodistribution). H Merkens assisted with animal procedures and monitoring. N Colpo, N Hundal-Jabal and J Rousseau performed PET/CT image acquisition. KS Lin and F Bénard were the supervisory authors and were both heavily involved in experimental design and manuscript input. The manuscript was drafted and finalized by me with critical input from Z Zhang, KS Lin and F Bénard.

A version of Chapter 4 is currently being prepared for submission [**I Dude**, Z Zhang, C Zhang, N Hundal-Jabal, N Colpo, H Merkens, D Perrin, KS Lin, F Bénard. Synthesis and Preclinical Evaluation of ^{18}F-labeled Ammoniomethyl- Trifluoroborate Somatostatin Analogues for Breast Cancer Imaging]. In this work, Z Zhang was responsible for chemistry and radiochemistry. I was responsible for all aspects of the biological evaluation. C Zhang provided assistance with internalization assays and *in vivo* stability measurements (Figure 4.3 and Figure 4.4). H Merkens assisted with animal procedures and monitoring. N Hundal-Jabal and N Colpo performed PET/CT image acquisition. D Perrin, KS Lin, and F Bénard were the supervisory authors. KS Lin, and F Bénard were heavily involved in both experimental design and

manuscript input. The manuscript was drafted and finalized by me with critical input from Z Zhang, KS Lin and F Bénard.

The research in this thesis was conducted under animal protocol A11-0238, "Radiolabeled peptides to improve cancer diagnosis by positron emission tomography and single-photon emission tomography" which was approved by the Institutional Animal Care Committee of the University of British Columbia in compliance with the Canadian Council on Animal Care Guidelines.

Table of Contents

List of Tables

List of Figures

List of Abbreviations

%ID/g: Percent injected dose per gram of tissue

[111]In-pentetreotide: ^{111}In-DTPA-D-Phe[1]-octreotide

^{125}I-SRIF14: ^{125}I-Tyr[11]-somatostatin-14

^{18}F-DOPA: ^{18}F-dihydroxyphenylalanine

^{18}F-FDG: 2-deoxy-2-[^{18}F]fluoro- D-glucose

^{18}F-FES: 16-α-[^{18}F] fluoro-17-β-estradiol

^{18}F-FLT: ^{18}F-fluoro-L-thymidine

^{18}F-FMISO: ^{18}F-fluoromisonidazole

1-Na1: 1-naphthyl-alanine

2D: 2-dimensional

3D: 3-dimensional

^{68}Ga-DOTANOC: ^{68}Ga-DOTA-Na1[3]-octreotide

^{68}Ga-DOTATATE: ^{68}Ga-DOTA-Tyr[3]-octreotate

^{68}Ga-DOTATOC: ^{68}Ga-DOTA-Phe[1]-Tyr[3]-octreotide

[99m]T-sestamibi: ^{99m}Tc-methoxyisobutylisonitrile

AmBF$_3$: Ammonimethyl-trifluroborate

ANOVA: Analysis of variance

Aph(Hor): Amino-Phe-hydroorotic acid

bp: Base pair(s)

Bq: Becquerel

BSA: Bovine serum albumin

CCK: Cholecytokinin

cDNA: Coding DNA

Cpa: 4-Cl-pheny-alanine

CT: Computed tomography

C$_t$: Threshold cycle

CXCR4: Chemokine receptor 4

d: Day(s)

D-Aph (Cbm): D-4-amino-carbamoyl-phenylalanine

DI: Deionized

DMEM: Dulbecco's modified Eagle's medium

DMF: Dimethylformamide

DNA: Deoxyribonucleic acid

DOTA: 1,4,7,10-tetraazacyclododecane-1,4,7,10-tetraacetic acid

DTPA: Diethylenetriamine pentaacetic acid

E2: 17β-estradiol

EC: Electron capture

EDDA: Ethylenediamine-N,N'-diacetic acid

ER: Estrogen receptor

eV: Electron volt(s)

FBS: Fetal bovine serum

FDA: Food and Drug Administration

g: Gram(s)

GEP-NET: Gasteroenteropancreatic neuroendocrine tumour

GLP: Good laboratory practice

GLP-1R: Glucagon-like peptide-1 receptor

GPCR: G-protein coupled receptor

GRPR: Gastrin-releasing peptide receptor

GTP: Guanosine tri-phosphate

h: Hour(s)

HEK: Human embryonic kidney

HEPES: 4-(2-hydroxyethyl)-1-piperazineethanesulfonic acid

HER2: Human epidermal growth factor 2

HPLC: High performance liquid chromatography

HPRT1: Hypoxanthine phosphoribosyltransferase 1

HYNIC: N-hydroxysuccinimidyl hydrazinonicotinamide

IC$_{50}$: Half-maximal inhibitory concentration

IEX: Isotope exchange reaction

IGF-1: Insulin-like growth factor-1

IHC: Immunohistochemistry

IT: Isomeric transition

k: Kilo

K_i: Inhibition constant

L: Litre(s)

LET: Linear energy transfer

LOR: Line of response

M: Mega

m: Meter(s)

m: Milli

M: Molar

MC1R: Melanocortin 1 receptor

MeCN: Acetonitrile

MIBG: Metaiodobenzylguanidine

min: Minute(s)

mol: Mole(s)

MRI: Magnetic resonance imaging

mRNA: Messenger RNA

n: Nano

NaCl: Sodium Chloride

NaI: Sodium Iodide

NET: Neuroendocrine tumours

NMP: *N*-methyl-2-pyrrolidone

NOD *scid* gamma: NOD.Cg-*Prkdc^{sci}Il2rg^{tm1Wjl}*/SzJ

NODAGA: 1,4,7-triazacyclononane,1-glutaric acid-4,7-acetic acid

NOPO:1,4,7-triazacyclononane-1,4-bis(methylene(hydroxymethyl)phosphinic acid)

NOTA: 1,4,7-triazacyclononane-1,4,7-trisacetic acid

NPY: Neuropeptide Y

NTR1: Neurotensin-1 receptor

Octreotide LAR: Octreotide long-acting release

p.i.: Post-injection

p: pico

PBS: Phosphate buffered saline

PCR: Polymerase chain reaction

PEM: Positron emission mammography

PET: Positron emission tomography

PR: Progesterone receptor

PRRT: Peptide receptor radionuclide therapy

PTP: Phosphotyrosine phosphatase

PTPη: Density-enhanced phosphatase 1

QC: Quality control

qPCR: Quantitative polymerase chain reaction

RCY: Radiochemical yield

RGD: Arg-Gly-Asp

RNA: Ribonucleic acid

RPMI: Roswell Park Memorial Institute medium

s: Second(s)

SHP-1 and -2: Src-homology phosphatase type 1 and type 2

SiFA: Silicon-fluoride acceptor

SPECT: Single photon emission computed tomography

SRIF-14 and SRIF-28: Somatotropin-release inhibiting factor-14 and -28 (or somatostatin-14 and -28)

sstr1-5: Somatostatin receptor subtype 1-5

$T_{1/2}$: Half-life

TFA: Trifluoroacetic acid

Thr(ol): Threoninol

TRAP: (3,30,3''-(((1,4,7-triazonane-1,4,7-triyl)tris(methylene))tris(hydroxy-phosphoryl))tripropanoic acid

Tricine: N-[tris(hydroxyl-methyl)-methyl]glycine

VPAC: Vasoactive intestinal peptide receptor

α: Alpha particle (2 protons, 2 neutrons)

β⁻: Beta minus particle (electron)

β⁺: Beta plus particle (positron)

γ: Gamma ray

μ: Micro

Acknowledgements

I would like to thank Dr. François Bénard for his guidance and advice. Your breadth of knowledge, creativity, and work proficiency is inspiring to a young graduate. Secondly, I would like to thank Dr. Kuo-Shyan Lin for his invaluable teaching efforts and insights into all research related matters. Your tenacious drive and extraordinary work efficiency is both admirable and inspiring. Thank you to the members of my supervisory committee, Dr. Urs Hafeli and Dr. Paul Schaffer for meaningful discussions. Thank you Dr. David Perrin, for a productive collaboration.

My sincerest gratitude goes to the members of the Bénard and Lin lab, past and present. I would like to acknowledge Dr. Zhengxing Zhang (Johnson) for his indispensable contribution to this project. I am grateful to have worked with such a reliable and diligent researcher. I would also like to thank Gemma for her immense kindness, Julie for her cheerful nature, Joseph for valuable advice, and Chengcheng for perspective in both research and life. Thank you Guillaume, Ting, Hwan, Maral, Carlos, Milena, Marin, Martha, Jinhe, Etienne, and Frederic for both your guidance and your friendship. Thank you Silvia, Helen and Jutta for fostering my hands-on lab skills. Thank you Nav and Nadine for your help and expertise in animal imaging. Thank you Gayle, Tina and the ARC staff for animal assistance. Thank you Amy, Ester and Adrian from the Huntsman and Aparicio labs for your help with DNA/RNA work.

Lastly, I want to acknowledge my parents for their unyielding efforts to provide the best for their children. I am in awe of the courage and perseverance they displayed through the early years of our immigration to Canada. I also want to acknowledge my partner and best friend, D'arcy, without whom, this work would not have been possible. Thank you for your support and for sharing every one of my hardships and successes with me throughout this journey.

Pentru cei mai buni parinți

Mihaela și Mihai Dude

Chapter 1: Introduction

1.1 Nuclear Medicine

Nuclear medicine is a medical practice that uses radionuclides for both imaging and therapy of various diseases. Specific molecular mechanisms or physiological processes can be targeted by probing key proteins (*i.e.,* receptors, enzymes, and transporters) with radioactive compounds, known as radiopharmaceuticals. A radiopharmaceutical is comprised of a biological component (*i.e.,* small-molecule, peptide, or antibody) specific for a certain protein or disease state, and a radioactive isotope which can have either photon emissions for diagnostic purposes, particle emissions for therapeutic purposes, or a combination of both. For imaging, patients undergoing a nuclear medicine scan will be administered (usually intravenously) a radiopharmaceutical and scanned by either positron emission tomography (PET) or single photon emission tomography (SPECT) based on the decay properties of the radionuclide in use[1]. Based on its biological characteristics, the radiopharmaceutical homes to various organs or lesions, and its spatial localization is determined by detection of the radioactive emissions. Nuclear medicine scans provide functional information on physiological processes (*i.e.,* metabolism, proliferation, hypoxia, angiogenesis, apoptosis), protein expression profiles or presence of disease biomarkers[2]. PET and SPECT instruments are commonly paired with anatomical imaging modalities such as computed tomography (CT)[3] or magnetic resonance imaging (MRI)[4], allowing for co-registration of functional and anatomical information. Table 1.1 outlines various isotopes used in nuclear medicine.

Table 1.1 Commonly used radionuclides for imaging and therapy. Table adapted with permission from Fani and Maecke[5] with some modifications[6-10].

Isotopes for single photon emission computed tomography (SPECT)

Radionuclide	$T_{1/2}$	Decay Mode (%)	E_γ (keV) (%)	Principal Production Mode
^{99m}Tc	6.02 h	IT (100), γ	141 (91)	^{99}Mo/^{99m}Tc generator
^{111}In	2.83 d	EC (100) Auger, γ	171 (90) 245 (94)	Cyclotron, ^{111}Cd(p,n)^{111}In
^{67}Ga	3.26 d	EC (100) Auger, γ	93 (39) 185 (21) 300 (17)	Cyclotron, ^{68}Zn(p,2n)^{67}Ga
^{123}I	13.2 h	EC (100), γ	15 (84) 27 (71) 31 (16)	Cyclotron, ^{124}Te(p,2n)^{123}I

Isotopes for positron emission tomography (PET)

Radionuclide	$T_{1/2}$	Decay Mode (%)	$E_{\beta+}$ (keV) (%)	Principal Production Mode
^{11}C	20.4 min	β^+ (99.8)	385 (99.8)	Cyclotron, ^{14}N(p,α)^{11}C
^{18}F	110 min	β^+ (97) EC (3)	634 (97)	Cyclotron, ^{18}O(p,n)^{18}F
^{68}Ga	68 min	β^+ (89) EC (11)	1899 (88)	^{68}Ge/^{68}Ga generator
^{89}Zr	3.27 d	β^+ (23) EC (77)	897 (23)	Cyclotron, ^{89}Y(p,n)^{89}Zr
^{124}I	4.15 d	EC (77) β^+ (23)	3160 (24) 2556 (25) 2137 (11) 1535 (12) 866 (11)	Cyclotron, ^{124}Te(p,n)^{124}I

Isotopes for radionuclide therapy

Radionuclide	$T_{1/2}$	Decay Mode (%)	$E_{\beta-}$ (keV) (%)	Principal Production Mode
^{90}Y	2.67 d	β^- (100)	2280 (99.9)	^{90}Sr/^{90}Y Generator
^{177}Lu	6.71 d	β^-, γ	498 (79) 385 (9) 177 (12)	Reactor, ^{176}Lu(n,γ)^{177}Lu
^{188}Re	17 h	β^-, γ	2120 (71.1) 1965 (25.6) 1487 (1.6)	^{188}W/^{188}Re generator
^{211}At	7.2 h	α (42) EC (58)	E_α = 5870 (42)	Cyclotron, ^{209}Bi(α,2n)^{211}At

β^+ decay is always accompanied with 511 keV annihilation gamma emission. IT = isomeric transition. EC = electron capture.

1.1.1   SPECT and Planar Scintigraphy

SPECT and planar scintigraphy modalities rely on the detection of gamma photons emitted from the radioactive nucleus[1]. Planar scintigraphy scans are 2D projections acquired by detecting the incoming radioactive signal on a large-scale detector, called an Anger or gamma camera, placed near the patient. SPECT uses the same principle, but acquires several 2D projections at different angles around the patient, which are reconstructed to create a tomographic representation[1]. Both modalities require collimation of the incoming gamma rays, done by mounting a collimator (thick sheet of lead containing thousands of small pin holes) parallel to the Anger camera, which allows only photons travelling perpendicular to the detector to be registered[1]. Collimation ensures a representative spatial distribution of the radiotracer, but significantly reduces detection sensitivity leading to low counts and high noise levels[1]. Among its many applications, SPECT is clinically used in the detection of bone metastases (^{99m}Tc-phosphate compounds), coronary artery disease (^{99m}Tc-sestamibi), brain abnormalities (^{99m}Tc-ethyl cysteinate dimer/^{99m}Tc-exametazime) and cancer[11]. Oncological applications include diagnosis of neuroendocrine/neurological tumours using ^{123}I-metaiodobenzylguanidine (^{123}I-MIBG), an analogue of norepinephrine. ^{111}In-radiolabeled antibodies detecting tumour specific antigens such as ^{111}In-capromab-pentetide in prostate cancer and ^{111}In-ibritumomab tiuxetan in non-Hodgkin lymphoma are also used[11].

1.1.2   Positron Emission Tomography

PET scanning can detect signals from positron emitting isotopes. A positron, or β^{+} particle, is the anti-matter counterpart of the electron and is emitted from certain unstable nuclei. When emitted, it travels a short distance in the tissue before annihilating with a nearby electron. The annihilation event produces two 511 keV photons, which are ejected 180° apart and will be

3

simultaneously detected by a pair of sensors mounted around the patient[1] (See Figure 1.1). When two photons are detected in coincidence (within a 5-15 ns window), the annihilation can be localized along the imaginary line connecting the affected sensors, called the "line of response" (LOR). Coincidence events from many LORs are reconstructed to create a 3D image[1]. This system obviates the need for collimation, allowing PET to have improved sensitivity compared to SPECT. However, PET image resolution is limited by the distance between the emission and annihilation sites, which depends on the kinetic energy of the positron[1]. Overall clinical PET scanners have a higher sensitivity and resolution compared to SPECT[1].

Examples of PET radiotracers include ^{11}C-choline for recurrent prostate cancer, ^{18}F-dihydroxyphenylalanine (^{18}F-DOPA) for brain imaging, ^{68}Ga-DOTA-Phe^1-Tyr^3-octreotide for neuroendocrine tumours, ^{18}F-NaF for bone lesions, and ^{18}F-fluoromisonidazole (^{18}F-FMISO) for visualization of hypoxia[12]. However, the most frequently used PET radiotracer is 2-deoxy-2-[^{18}F]fluoro-D-glucose (^{18}F-FDG), an analogue of glucose with the C-2 hydroxyl replaced by ^{18}F[13]. Clinical applications for ^{18}F-FDG are primarily in oncology, with moderate use in cardiology and neurology[14,15].
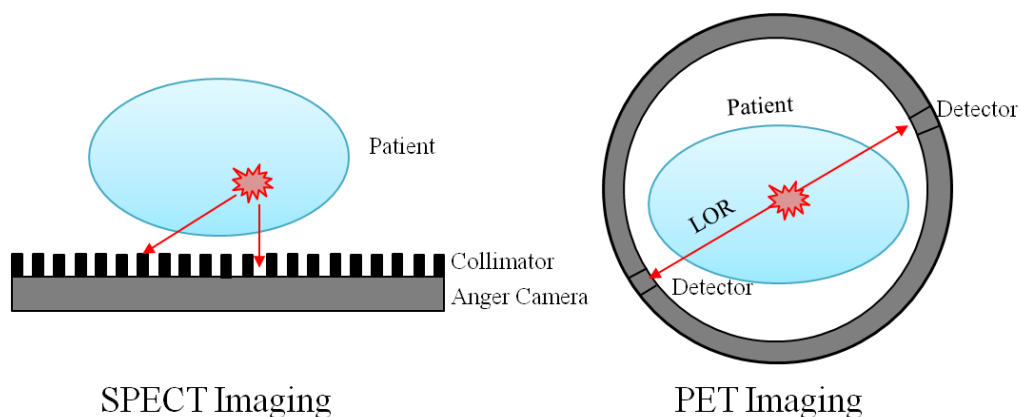
Figure 1.1 Principles of SPECT and PET imaging. SPECT detects only photons emitted parallel to the Anger camera. PET detects 511 keV photons emitted in coincidence.[1]

1.1.2.1   ^{18}F-FDG in Oncology

Tumour uptake of ^{18}F-FDG is driven by the Warburg effect, a phenomenon resulting in overexpression of glucose transporters and propensity of aerobic glycolysis in malignant versus non-malignant tissues[13,16]. Like glucose, ^{18}F-FDG is actively transported into the cytoplasm and engages in the first step of glycolysis: conversion to ^{18}F-FDG-6-phosphate by hexokinase. The next step cannot be performed, as it requires the C-2 oxygen (replaced by ^{18}F), and thus ^{18}F-FDG-6-phosphate continues to accumulate in the cell providing an enhanced PET signal[13]. ^{18}F-FDG is used extensively in clinical care, for initial staging and evaluation of recurrent disease in lung cancers, melanoma, colorectal carcinoma, lymphomas, head and neck cancers, esophageal cancer, breast cancer and gynecological cancers (cervical and ovarian)[17]. ^{18}F-FDG plays a major role in predicting early response to therapy and informing clinical management. However, ^{18}F-FDG suffers from poor detection of small lesions (< 7 mm) or negative results in tumours with low metabolic rates (differentiated neuroendocrine tumours, prostate cancer, and hepatocellular carcinoma)[17]. ^{18}F-FDG is not a tumour-specific tracer and will also accumulate in other metabolically active regions, such as benign inflammatory processes[17]. The development of tumour-specific radiotracers is currently an active and prolific area of research.

1.1.2.2   Impact of PET on Cancer Care

Currently, the clinical use of PET in cancer care is dominated by ^{18}F-FGD imaging. The National Oncologic PET Registry collected data from 22,975 studies (1,178 centers) across the United States, and found that ^{18}F-FDG PET imaging changed the clinical course of 36.5% of cancer cases[18]. In patients with planned biopsy before imaging, ^{18}F-FDG PET obviated the need for any further invasive procedures in 70% of cases[18].

As of 2015, Canada has 45 publicly funded PET scanners (and 7 privately funded), all mainly used for oncology applications[19]. The British Columbia Cancer Agency in Vancouver, British Columbia is equipped with two scanners and has the capacity to perform 7,775 scans/year. ^{18}F-FDG PET imaging will continue to be an important cancer management tool, especially in Canada's aging population. In most developed countries, PET imaging is a standard of care, with approximately 2,000 PET scanners installed in the United States (as of 2009)[20] and 724 in Europe (as of 2014)[21].

Aside from ^{18}F-FDG, several radiopharmaceuticals specific for unique cancer proteins have been developed and evaluated[2]. Similar to current drug development approaches, radiotracer development is inspired by the "magic bullet" approach – synthesizing tracers that target and visualize key proteins and biomarkers, providing information on the patient's unique molecular phenotype or potential response to treatment[22]. As an example, radiotracers targeting the somatostatin receptors in neuroendocrine tumours can visualize the extent of disease, but can also predict response to therapy with somatostatin-receptor specific agents[23].

1.2 Peptide Radiopharmaceuticals

Regulatory peptides (2-50 amino acids in size) act with high affinity and specificity on their respective cell surface receptors to modulate physiological processes. The majority of peptide receptors are G-protein coupled receptors (GPCRs), and their aberrant overexpression has been well documented in several cancer types[24,25].

Peptides are excellent imaging probes. Their small size enables efficient tumour penetration, fast clearance from non-target organs, and rapid excretion[25,26]. They have minimal side effects, no immunogenicity, and can be tuned to bind with high affinity to target receptors[25,26]. Peptides can be easily modified to accommodate a radiolabeling prosthetic, or

6

chemically engineered to modulate pharmacokinetics[25,26]. Challenges include a short biological half-life due to degradation by proteolytic enzymes, high specific activity requirements to avoid receptor saturation, high radiation dose to excretory organs (commonly kidneys and bladder), and a sensitive structure-activity relationship easily perturbed by the addition of a radiolabeling moiety[25,26].

1.2.1 Peptide Radiopharmaceuticals for Cancer Imaging

Table 1.2 outlines specific examples of receptors targeted with radio-peptides; somatostatin receptors (sstrs) being the most common. The SPECT analogue ^{111}In-pentetreotide (OctreoScan, Mallinckrodt) was approved by the U.S. Food and Drug Administration (FDA) for imaging somatostatin-positive neuroendocrine tumours (NETs) in 1994[27]. This strategy will likely be replaced by the higher-resolution PET procedure using ^{68}Ga-DOTATATE (NetSpot, Advanced Accelerator Applications USA, Inc), which recently gained FDA approval in 2016[28]. Several other experimental somatostatin analogues are in preclinical phases[26].

Gastrin-releasing peptide receptors (GRPR) are overexpressed on prostate and breast tumours. The GRPR-specific compounds ^{68}Ga-RM2[29], ^{68}Ga-SBS[30], ^{18}F-BAY-864367[31] and ^{64}Cu-CB-TE2A-AR06[32] have been explored in clinical studies with promising results, albeit in small sample sizes. A notable challenge of imaging prostate lesions and pelvic lymph nodes with these radio-peptides is the high background uptake due to bladder and urine excretion[33].

Neoangiogenesis, a hallmark of tumour growth and metastasis[34], can be visualized by targeting the $\alpha_v\beta_3$ integrin receptor overexpressed on active endothelial cells. The tri-peptide core sequence Arg-Gly-Asp (RGD), specific for $\alpha_v\beta_3$, has been used in the development of angiogenesis-specific PET tracers: ^{18}F-Galacto-RGD, ^{18}F-Fluciclatide, ^{18}F-RGD-K5, ^{18}F-FPPRGD2, ^{18}F-Alfatide, ^{68}Ga-NOTA-RGD and ^{68}Ga-NOTA-PRGD2 which have been evaluated

in clinical studies[35]. Heteromultivalent RGD peptide tracers, in which RGD is conjugated to either a somatostatin or bombesin analogue, have also been explored. These compounds increase tumour avidity by simultaneously targeting co-expressed receptors[36].

Other receptors visualized clinically with ^{111}In-, ^{99m}Tc-, ^{123}I-, and ^{68}Ga- labeled analogues include cholecystokinin (CCK) receptor expressed on medullary thyroid carcinomas[37,38], glucagon-like peptide-1 receptor (GLP-1R) overexpressed on insulinomas[39-41], vasoactive intestinal peptide receptor overexpressed in many epithelial neoplasms[42], and neurotensin receptor (NTR1) in ductal pancreatic adenocarcinoma[43]. Peptide and small-molecule radiotracers (labeled with ^{18}F, ^{68}Ga and ^{64}Cu) specific to chemokine receptor 4 (CXCR) have also been developed[44], and a select few were evaluated in multiple myeloma[45] or glioma[46] patients. Development of PET and SPECT analogues targeting neuropeptide Y receptor (NPY), and melanocortin 1 receptor (MC1R) are currently in preclinical stages[47,48].

Table 1.2 Receptors targeted with radio-peptides in human tumours. Table adapted with permission from Fani *et al.*[5]

Target Receptor	Peptide	Overexpression on Tumour Type	Status
Somatostatin receptors (sstr1-5)	Somatostatin	Neuroendocrine and gastroenteropancreatic tumours, non-Hodgkin's lymphoma, paragangliomas, breast, small cell lung cancer	Clinical Use
Gastrin-releasing peptide receptor (GRPR)	Bombesin/GRP	Prostate, breast, pancreas, gastric, small cell lung cancer, colorectal cancer	Clinical Trials
Cholecystokinin B/gastrin receptor (CCK$_2$/CCK-B)	CCK/gastrin	Medullary thyroid cancer, small cell lung cancer, gastrointestinal stromal cancer, stromal ovarian cancer, astrocytomas	Clinical Trials
Glucagon-like peptide-1 receptor (GLP-1)	Exendin	Insulinomas, gastrinomas, phaeochromocytomas, paragangliomas and medullary thyroid carcinomas	Clinical Trials
$\alpha_v\beta3$-integrin	RGD	Neoangiogenic vessels in brain, lung, ovary, breast, skin	Clinical Trials
Vasoactive intestinal peptide receptors (VPAC$_1$ VPAC$_2$)	Vasoactive Intestinal Peptide	Neuroendocrine tumours, brain tumours, adenocarcinoams of the pancreas, prostate, breast, colon, stomach and liver	Studies in Patients
Melanocortin 1 receptor (MC1R)	α-MSH	Melanomas	Preclinical
Neurotensin receptor (NTR1)	Neurotensin	Small cell lung cancer, colon, exocrine pancreatic cancer, Ewing's sarcoma, breast, prostate	Studies in Patients
Chemokine receptor 4 (CXCR4)	CXCR4	Lymphatic system, lung, breast and prostate cancer	Clinical Trials

1.2.2 Antagonist Peptide Radiopharmaceuticals

Upon binding to target receptors, agonist peptides stimulate downstream effects, and in some cases, trigger internalization of the peptide-receptor complex. Antagonist peptides, which also bind with high affinity and specificity, do not initiate signal transduction or receptor internalization. Until recently, agonist radiopeptides were preferred to antagonists, as internalization of the peptide-receptor complex was believed essential for successful imaging. However, recent studies using antagonist radiotracers to target sstr and GRPR (which both require receptor internalization for signal transduction) demonstrate otherwise[49,50]. In a preclinical study, Ginj *et al.* showed that ^{111}In-labeled somatostatin antagonists outperformed agonists in targeting sstr-expressing tumours, having higher tumour uptake and contrast despite similar binding affinities[49]. *In vitro* binding assays revealed that antagonists bound to more sites on the tumour tissue resulting in an overall higher tumour uptake[49]. This phenomenon was also observed in *in vitro* studies with $5-HT_{2A}$[51] and corticotropin releasing factor receptors[52]. Similarly, the GRPR antagonist ^{99m}Tc-Demobesin 1 was a superior imaging agent compared to the agonist ^{99m}Tc-Demobesin 4, having higher tumour uptake and contrast in mice bearing tumours from the human prostate cell line PC3[50]. It is believed that agonist binding is modulated by the degree of receptor/G-protein coupling, as opposed to antagonists which are independent of this effect and hence can bind receptors in multiple conformations[52]. These studies suggest that antagonist radio-peptides may hold more value than originally believed.

1.2.3 Peptide Receptor Radionuclide Therapy

Peptide receptor radionuclide therapy (PRRT) is a treatment approach that uses cancer-targeting peptides labeled with therapeutic isotopes to deliver a lethal dose of radiation to the tumour specifically[26]. Only isotopes with high linear energy transfer (LET) emissions can be

10

used for PRRT, to effectively damage DNA and induce tumour cell death. LET is defined as the amount of energy deposited per unit length on the radiation path[24,53]. High LET emissions include beta (β^-), alpha (α) and Auger electron emissions (see Table 1.1)[24]. Currently, the most frequently used therapeutic isotopes are ^{177}Lu and ^{90}Y, which are both β^- emitters. ^{177}Lu β^- particles (E_{β^-} (max) = 177, 385 and 498 keV) have a short-range of ~ 2 mm in tissue, which is appropriate for small tumours or metastases[26]. ^{90}Y has a long-range emission (E_{β^-} (max) = 2280 keV) of ~12 mm in tissue, which is desirable for larger tumours with heterogeneous receptor distribution or hypoxic regions[26].

The primary toxicological concerns of PRRT are of the bone marrow (mild and reversible), and the kidneys (the main dose-limiting organ)[54]. Partial re-absorption of the tracer in the tubular cells of the kidneys causes high renal exposure and radiotoxicity. Kidney protection strategies, such as amino acid infusions (L-lysine and L-arginine), are employed and very effective, however these agents cause severe nausea, vomiting and discomfort[54].

1.2.4 Peptide Radiolabeling

Peptides have relatively fast pharmacokinetics and require radiolabeling with short half-life isotopes to minimize patient exposure (when used for diagnostic purposes). In this respect, ^{68}Ga ($t_{1/2}$ = 68 min) and ^{18}F ($t_{1/2}$ = 110 min) are ideal isotopes, however, several other radiometals have been previously used[47,55]. Other considerations include type of emission (γ or β^+), positron range, γ energy, isotope cost, isotope availability and radiolabeling methods[5]. The radiolabeling moiety must not interfere with receptor binding, and must be able to conjugate the radioisotope with high thermodynamic and kinetic stability[5]. The radio-peptides investigated in this thesis are labeled with the isotopes ^{18}F and ^{68}Ga, therefore only ^{18}F- and ^{68}Ga-radiochemistry will be further discussed.

1.2.4.1 ^{68}Ga Radiolabeling

^{68}Ga is a positron-emitting radionuclide, generally produced using a ^{68}Ge/^{68}Ga generator. The high positron emission abundance (90%) and minimal gamma emissions of ^{68}Ga enables easier data collection, lower activities needed and lower patient exposure[55]. ^{68}Ga has a high positron energy (1,880 keV) translating to ~8.9 mm max range in water[56], which compromises resolution and detection of small lesions. The ^{68}Ge/^{68}Ga generator has a shelf life of approximately 1 year (^{68}Ge $T_{1/2}$ = 271 d), and can be easily mobilized to hospitals or research settings[55]. ^{68}Ga is easily eluted with HCl solution, while the ^{68}Ge remains bound on the stationary-phase of the generator column[55].
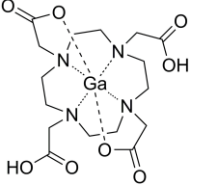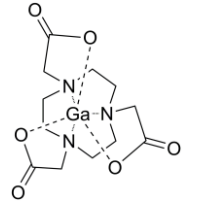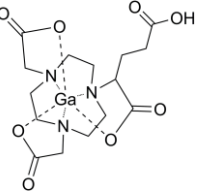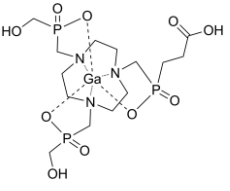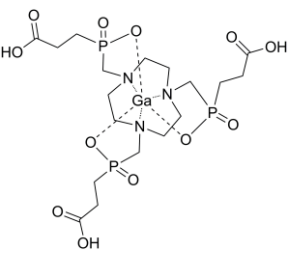
^{68}Ga benefits from robust and thermodynamically stable coordination chemistry with macrocyclic ligands, most commonly 1,4,7,10-tetraazacyclododecane-1,4,7,10-tetraacetic acid (DOTA) and 1,4,7-triazacyclononane-1,4,7-trisacetic acid (NOTA)[47,55] (Table 1.3). DOTA is the most frequently used, and binds ^{68}Ga with fairly stable hexadentate co-ordination (although the ideal denticity of DOTA is octadentate)[47,55]. Protected forms of DOTA compatible with standard peptide synthesis methods can be purchased commercially, and enables simple peptide conjugation[47]. Additionally, DOTA has the advantage of stably binding other trivalent and divelent lanthanide isotopes (^{111}In^{3+}, ^{90}Y^{3+}, ^{177}Lu^{3+}, and ^{64}Cu^{2+}), allowing the same chelated biomolecule to be used for longer time-point imaging or therapy[55].

NOTA has a smaller cavity size compared to DOTA, and can bind ^{68}Ga with perfect hexadentate co-ordination, forming an extremely thermodynamically and kinetically stable complex[47]. Conjugation of NOTA to a peptide is possible by introducing a coupling moiety at the alpha position of one carboxylate arm. 1,4,7-triazacyclononane,1-glutaric acid-4,7-acetic acid

(NODAGA) is a glutamic acid functionalized version of NOTA that maintains hexadentate co-ordination and excellent stability[47].

Other ^{68}Ga chelators currently gaining popularity are TRAP (3,30,3"-(((1,4,7-triazonane-1,4,7-triyl)tris(methylene))tris(hydroxy-phosphoryl))tripropanoic acid) and NOPO (1,4,7-triazacyclononane-1,4-bis(methylene(hydroxymethyl)phosphinic acid)-

7-(methylene(2-carboxyethyl)phosphinic acid))[57,58]. Both exhibit very high ^{68}Ga-radiolabelling efficiency over a broad pH range (0.5-5) and without the need for heating[57]. [68]Ga binding to TRAP and NOPO is very specific and relatively unaffected by metal ion contaminants potentially present in the [68]Ge/^{68}Ga generator eluate[57].

Table 1.3 Commonly used ^{68}Ga chelators for peptide radiolabeling.

Chelator	[68]Ga Radio-Chemistry	Advantages	Disadvantages	Ref
DOTA	37-90 ℃, 10-30 min, pH 4.0 - 5.5, RCY > 90%	-Binds multiple lanthanide radiometals -Bifunctional without loss of ^{68}Ga affinity	-Large cavity size not ideal for ^{68}Ga binding -Sensitive to trace metal contaminants	[57-59]
NOTA	95 ℃, 10 min, pH 4.0 - 5.5, RCY > 95	-Optimal cavity size for ^{68}Ga enables excellent stability	-One carboxyl arm required for peptide conjugation, which lowers overall hydrophilicity of tracer -Sensitive to trace metal contaminants	[57-59]
NODAGA	95 ℃, 25 min, pH 4.0 - 5.5 RCY = 95	-Bifunctional without loss of ^{68}Ga affinity -Excellent ^{68}Ga stability	-Sensitive to trace metal contaminants	[57-59]
TRAP	25 ℃, 5 min, pH 3, RCY = 99%	-Bifunctional -Excellent ^{68}Ga affinity -Room temperature radiolabeling -Robust against generator impurities -Functional over a wide pH range (0.5 – 5) -Increases hydrophilicity of radiotracer -Trimeric (TRAP) and monomeric (NOPO) applications	-Difficult to synthesize -Not extensively used in clinical applications yet	[57,58, 60,61]
NOPO				

RCY: Radiochemical yield

1.2.4.2 ^{18}F Radiolabeling
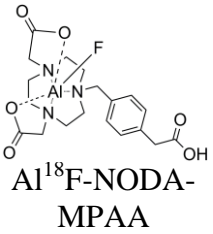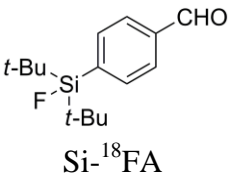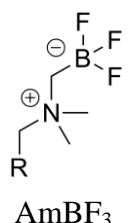
^{18}F is an excellent PET isotope with 97% positron emission, an ideal half-life of 110 min, and a low positron range (634 keV, ~2.3 mm max range in water[56]) enabling good image resolution[62]. ^{18}F is cyclotron-produced by bombardment of an enriched ^{18}O-water target with high-energy protons, resulting in high levels of radioactivity[62]. The slightly longer half-life of ^{18}F compared to ^{68}Ga allows more time for radiolabeling, quality control and distribution to imaging centers lacking a cyclotron facility[63].

Direct nucleophilic substitution with ^{18}F at a carbon center is often done at high temperatures and non-aqueous conditions, which are unsuitable for peptides. Typically, ^{18}F-fluoride requires drying to promote reactivity, as water molecules form a tight hydration sphere around the ^{18}F anion inhibiting its nucleophilic action[62-64]. Drying is accomplished by repetitive and time-consuming azeotropic distillation[62-64]. To avoid exposing the peptide to highly basic and non-aqueous solvents, a prosthetic group is first radiolabeled, followed by conjugation to the peptide under milder conditions. This requires multiple reaction steps with adequate purification for each[62-64].

There have been a number of advances in ^{18}F radiochemistry that reduced or eliminated the need for aziotropic drying. These approaches rely on ^{18}F binding to boron, silicon or aluminum elements conjugated to the peptide cold-standards[62-65]. Al-^{18}F chelation scaffolding developed by McBride *et al.* is a convenient labeling method reminiscent of radiometal approaches[66]. The Al-^{18}F complex is stably bound by macrocyclic chelator NOTA, with minimal *in vivo* defluorination. Another approach is Silicon-Fluoride Acceptor chemistry (SiFA), which involves functionalization of the peptide with a Si-F moiety, followed by isotope exchange reaction (IEX) for radiolabeling[67]. Using IEX obviates the need for extensive purification, as the

precursor is chemically identical to the radiotracer; however, IEX requires large amounts of starting ^{18}F to achieve acceptable specific activity[64]. A disadvantage of SiFA chemistry is the poor hydrolytic stability of the Si-F bond, requiring stabilization by bulky and hydrophobic *tert*-butyl groups. Hydrophobic-reducing auxiliaries (like polyethylene glycol and carbohydrate linkers) are subsequently needed to modulate the pharmacokinetics and excretion mechanism[65,67]. Lastly, the Perrin group has developed a radiolabeling approach using an ammoniomethyl-trifluroborate (AmBF$_3$) moiety that can be click-reacted to the N- or C-terminus of a peptide resulting in a chemically identical non-radioactive standard. Radiolabeling is done by IEX within 25-30 minutes, without the need for azeotropic drying or high performance liquid chromatography (HPLC) purification[68-70]. We have employed the latter method to radiolabel several biomolecules and show that this construct is stable, efficient, and does not severely interfere with specific receptor binding[70]. Work using this radiolabeling method is described in Chapter 4 of this thesis.

Table 1.4 Al-F, Si-F and B-F ^{18}F labeling methods

Radiosynthon	Chemisty	Advantages	Disadvantages	Ref
Al[18]F-NODA-MPAA	Ligand exchange and solid-phase extraction 100 ℃, 20 min, RCY = 5-20%	-Can be prepared as a lyophilized kit -One step aqueous radiolabeling -Metabolically stable	-Variable yields and specific activity -Heating is not ideal for sensitive biomolecules	[63,65,71]
Si-[18]FA	IEX and solid-phase extraction 25 ℃, 15 min, RCY = 80-95%	-Little precursor amount needed -High RCY - Simple purification	-Si-F is prone to hydrolysis and requires shielding by hydrophobic *tert*-butyl groups -Requires large amounts of starting [18]F	[63,65,68]
AmBF$_3$	IEX and solid-phase extraction 80 ℃, 25 min, RCY = 20-25%	-One step aqueous radiolabeling -Metabolically stable -Fast radiolabeling and purification	-Requires large amounts of starting ^{18}F and HPLC purification to achieve high specific activity -Moderate RCY	[63,65,70]

RCY: Radiochemical yield

1.3 Somatostatin Receptors and Somatostatin Radiotracers

Somatostatin receptors (sstr) are GPCRs expressed on cells of the brain, gut, pituitary, endocrine and exocrine pancreas, adrenals, thyroid, kidneys, and immune system[72]. There are five subtypes (sstr1-5) encoded by non-allelic genes on different chromosomes[72].

Sstrs have two known endogenous ligands, namely somatotropin-release inhibiting factor-14 and -28 (SRIF-14 and SRIF-28). SRIF-14 and SRIF-28 are comprised of 14 or 28 amino acids respectively[73]. Both bind with nanomolar affinity to all five receptor subtypes, and act as inhibitors of both endocrine (growth hormone, insulin, glucagon, gastrin, cholecystokinin,

vasoactive intestinal peptide, and secretin) and exocrine secretions (gastric acid, intestinal fluid, and pancreatic enzymes)[73]. SRIF analogues, notably octreotide, have been used to regulate hormone hypersecretion associated with various diseases, such as acromegaly and functional neuroendocrine tumours[73].

1.3.1   Somatostatin Receptor Signal Transduction

As is characteristic of GPCRs, ligand binding to sstr induces a conformational change in the receptor that stimulates guanosine tri-phosphate (GTP) to bind to the α-subunit of the G-protein. The G-protein is a trimeric complex (α, β and γ), which dissociates into two parts upon GTP binding: the GTP-bound α subunit, and the β/γ dimer. Both parts can interact with various second messenger enzymes to initiate signaling cascades[74]. For somatostatin receptors, the intracellular pathways that are triggered are subtype-, cell- and organ-dependent, and predominantly regulate hormone secretions, cell proliferation and neurotransmission. The inhibition of adenylyl cyclase and reduction of intracellular Ca^{2+} through co-ordination of Ca^{2+} and K^+ channels are responsible for the anti-secretory effects. The activation of phosphotyrosine phosphatases (PTPs), notably Src-homology phosphatase type 1 (SHP-1), type 2 (SHP-2), and density-enhanced phosphatase 1 (PTPη) account for the apoptotic and anti-mitogenic effects. In neuronal cells, SRIFs stimulate neuronal K^+ channels and inhibit Ca^{2+} channels leading to reduced action potential. See Figure 1.2 for a simplified schematic of intracellular SRIF signaling pathways[73,75].

Dimerization of somatostatin receptors is both constitutive and ligand-dependent, and can occur between receptors of the same or different species[75]. Once activated, sstr is phosphorylated and binds β-arrestin, which desensitizes the receptor by blocking its interaction with G-proteins.

Desensitized receptors are internalized into vesicles where they are dephosphorylated and recycled back to the cell membrane[75].
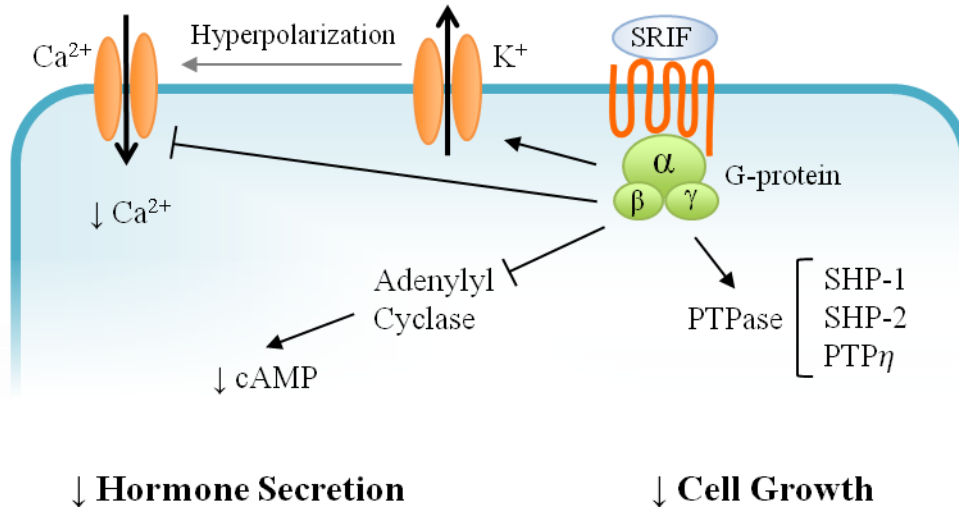
Figure 1.2 Simplified representation of somatostatin receptor intracellular signaling. Somatostatin decreases hormone sections by simultaneous inhibition of adenylyl cyclase and decreased intracellular Ca^{2+}. Growth inhibitory effects are mediated by phosphotyrosine phosphatases[73,75].

1.3.2   Somatostatin Receptor Expression in Cancer

Somatostatin receptors are overexpressed on several different tumour types, most notably neuroendocrine tumours (NETs). Sstrs are also present (although at lower density) on breast tumours, brain cancers (meningiomas, astrocytomas, and medulloblastomas), renal cell carcinomas, hepatomas, gastric carcinomas, non-Hodgkin's lymphoma, and some immune malignancies (sarcoidosis and tuberculosis)[76-78].

1.3.2.1   Neuroendocrine Tumours

NETs are a heterogeneous group of malignancies that arise from gland-forming neuroendocrine cells (such as those of the pituitary, parathyroid, paraganglia and adrenal

medulla), or from diffusely distributed neuroendocrine cells (found in gastrointestinal tract, pancreas, lung, thymus, thyroid and skin)[79]. NETs are rare and often benign, but can become metastatic at later stages. Some NETs, known as "functioning NETs", produce excessive hormone secretions causing symptoms such as sweating, flushing, diarrhea and bronchospasm[80]. From 1994 to 2009, the incidence of NETs increased from 2.48 to 5.86 per 100,000 people in Ontario, Canada[81] with similar findings observed worldwide[82]. The 5- and 10- year survival rates of NETs are 78% and 63%, respectively[23,83].

Sstr overexpression was reported by Reubi *et al.* on several NETs, such as pituitary adenomas, gasteroenteropancreatic NETs (GEP-NETs), medullary thyroid carcinomas, pheochromocytomas, paragangliomas, neuroblastomas and small cell lung cancers with neuroendocrine features[84,85]. Sstr2 was the most commonly overexpressed subtype, although heterogeneous expression of all five subtypes was observed[86]. Treatment with somatostatin analogues can alleviate symptoms of functioning NET and elicit anti-proliferative effects. However SRIF-14 and -28 have limited therapeutic potential due to their short plasma half-life of 2-3 min[73,75]. Shortening the endogenous peptides and incorporating unnatural amino acids resulted in the development of more kinetically stable analogues[73,75]. The most notable is octreotide, which is 8-amino acid long and has a plasma half-life of 1.5-2 hours[73,75]. The depot formulation, octreotide long-acting release (LAR), is often administered as an intramuscular injection once a month, and is well tolerated and very efficient at managing hormone secretions in patients with GEP-NETs and pituitary adenoma[75]. Octreotide LAR also prolongs progression-free survival in well-differentiated GEP-NETs due to its inhibitory growth effects[80].

1.3.2.2   Breast Tumours

Sstr overexpression has been documented in 15-100% of human breast cancers[87]. The high variability among reports is due to different receptor detection assays (scintigraphy, autoradiography, cross-linking experiments), the innate intra-tumour heterogeneity of sstr2 expression on breast cancer tissue[88], and tumour sampling from a diverse patient population. Sstr2 is the most commonly observed subtype at both the transcriptional and translation level[89], however expression of sstr1, 3 and 5 has also been reported[75,90-93]. Orlando *et al.* demonstrated that sstr2 is differently expressed on malignant breast cancer[94]. A 6-fold upregulation in receptor mRNA was observed on neoplastic tissue compared to corresponding normal tissue[94].

In 1989, Reubi *et al.* analyzed samples from a small cohort of 36 primary breast cancers and found that all samples with expression of estrogen and progesterone receptors (ER and PR respectively) were also sstr-positive[95]. This finding was later confirmed in larger studies[86,88,89]. Overexpression of sstr2 mRNA was found to correlate with a positive ER and PR status, a luminal A molecular profile, negative lymph node involvement, a favorable genomic grade index, and an overall good prognosis[86,88,89]. There is also evidence of a functional interaction between sstr2 and 17β-estradiol stimulation. In the ER-positive breast cancer cell line, T47D, sstr2 mRNA and protein expression levels were regulated by 17β-estradiol in a dose and time dependent manner[96,97]. This was attributed to a 1.5 kilo base-pairs response element in the 5' flanking region of the human sstr2 gene in T47D DNA[98].

Treatment of recurrent breast cancer with octreotide LAR has also been explored[99]. In addition to the anti-proliferative effect of octreotide, sstr activation suppresses the release of insulin-like growth factor-1 (IGF-1). It was speculated that combined treatment with anti-estrogen therapy and octreotide LAR would better control tumour growth by simultaneously

inhibiting the mitogenic effects of both 17β-estradiol and IGF-1. However, when evaluated in a phase III clinical trial with 203 advanced breast carcinoma patients, there was no significant difference between patients treated with tamoxifen and octreotide LAR, or tamoxifen alone[99].

1.3.3 Somatostatin Radiotracers

Somatostatin radiotracers can image NETs by binding to the overexpressed somatostatin receptors on the tumour cell surface. Sstr imaging enables detection of tumour masses, extent of metastases, disease staging and stratification of patients into likely responders to octreotide treatment or PRRT[23]. The next sections will review the progression of somatostatin receptor probes in nuclear medicine.

1.3.3.1 Overview of Somatostatin Radiotracers

Somatostatin receptor imaging has been in practice for the last 20 years, with a steady improvement in radiotracer synthesis and image quality[100]. The first evaluated sstr probe was the iodinated compound [^{123}I]-Tyr^3-octreotide. Although initially promising, [^{123}I]-Tyr^3-octreotide had poor tumour visualization capacity due to high intestinal accumulation and hepatobiliary excretion, and was expensive, difficult and time consuming to radiolabel[101]. Replacement of ^{123}I with diethylenetriamine pentaacetic acid (DTPA)-chelated ^{111}In lead to the development of ^{111}In-DTPA-D-Phe^1-octreotide (^{111}In-pentetreotide), which gained FDA approval in 1994 and was ubiquitously used for NET imaging thereafter[27,100]. However, the high-energy γ emission of ^{111}In compromised resolution and caused high patient dose[100]. This lead to development of ^{99m}Tc-labeled somatostatin tracers by conjugation of ^{99m}Tc to somatostatin analogues via chelator N-hydroxysuccinimidyl hydrazinonicotinamide (HYNIC) and co-ligands N-[Tris(hydroxyl-methyl)-methyl]glycine (tricine) or ethylenediamine-N,N'-diacetic acid (EDDA)[100]. ^{99m}Tc is an excellent isotope for SPECT imaging, with ideal photon energy of 140 keV and convenient

generator production[1]. Both ^{99m}Tc-EDDA/HYNIC-TOC and ^{99m}Tc-EDDA/HYNIC-TATE could detect more lesions with higher uptake compared to ^{111}In-pentetreotide[100].

The next generation of somatostatin analogues was radiolabeled with ^{68}Ga and benefits from imaging with the higher resolution modality PET[55]. Currently, the three most clinically relevant somatostatin PET tracers are ^{68}Ga-DOTA-Phe^1-Tyr^3-octreotide (^{68}Ga-DOTATOC), ^{68}Ga-DOTA-Tyr^3-octreotate (^{68}Ga-DOTATATE) and ^{68}Ga-DOTA-NaI^3-octreotide (^{68}Ga-DOTANOC), which mainly differ in their *in vitro* sstr subtype binding affinity. ^{68}Ga-DOTATOC has high affinity to sstr2 and moderate affinity to sstr5, ^{68}Ga-DOTATATE has exceptional affinity to sstr2 and ^{68}Ga-DOTANOC has high affinity to sstr2, sstr3 and sstr5[100]. However, no significant differences were observed between the three radiotracers in patient studies[102,103].

1.3.3.2   Somatostatin Agonists versus Antagonists

Original reports of somatostatin antagonists come from Bass and colleagues in 1996 who demonstrated that switching the stereochemistry of amino acids at position 1 and 2 of the octreotide peptide converted the agonist binder into an antagonist binder[104]. Bass *et al.* introduced the high-affinity antagonist BASS (or sstr-ANT), which was later radiolabeled with ^{111}In and evaluated preclinically[49]. ^{111}In-DOTA-sstr2-ANT showed high sstr2 binding affinity (IC_{50} = 9.4 nM) but was unable to trigger receptor internalization. When compared with the agonist ^{111}In-DTPA-TATE (IC_{50} = 1.3 nM), ^{111}In-DOTA-sstr2-ANT had twice the *in vivo* tumour uptake at both 4 h and 24 h post-injection (p.i.)[49]. *In vivo* uptake was even more striking for the sstr3 antagonist ^{111}In-DOTA-sstr3-ODN-8 in sstr3-expressing xenografts (60% ID/g, 1 h p.i.)[49]. The improved uptake was attributed to a higher number of receptor binding sites available for the antagonist compared to the agonist, as determined by binding assays[49]. Further *in vitro* autoradiography using human samples from different sstr-expressing cancer types, confirmed

23

these initial results[105]. The antagonist ^{177}Lu-DOTA-BASS, bound more sites on the tumour cell surface compared to agonist ^{177}Lu-DOTATATE, even for tumours with low or heterogeneous sstr density[105]. The first clinical study of antagonist radiotracers compared ^{111}In-DOTA-BASS with ^{111}In-DOTA-octreotide in 5 patients with NETs. The antagonist identified 25 out of 28 lesions, and the agonist identified 17 out of 28 lesions[106].

Several other somatostatin antagonists were developed and tested for binding affinity[107]. As expected, the choice of radiometal and chelating moiety affected the binding affinity and pharmacokinetics of antagonist peptides[108,109]. However, the combination of radiometal ^{68}Ga, chelator NODAGA and peptide JR11 (^{68}Ga-NODAGA-JR11) had a particularly good binding affinity (IC_{50} = 1.2 nM) and striking tumour uptake (30.7% ID/g at 1 h p.i.) in sstr2-positive xenografts[108]. A phase I/II clinical trial (NCT02162446) in metastatic GEP-NETs patients showed that absolute tumour uptake is comparable between antagonist ^{68}Ga-NODAGA-JR11 (^{68}Ga-OPS202) and agonist ^{68}Ga-DOTATOC. However, contrast is improved for the antagonist due to lower uptake in the liver, pancreas and gastro-intestinal tract[110]

Table 1.5 Somatostatin analogues and corresponding peptide sequences. Table adapted with permissions from Fani and Maecke[5,111].

Endogenous Peptide	
SIRF-14	Ala-Gly-cyclo(Cys-Lys-Asn-Phe-Phe-Trp-Lys-Thr-Phe-Thr-Ser-Cys)
Agonists	
Octreotide	D-Phe-cyclo(Cys-Phe-D-Trp-Lys-Thr-Cys)-Thr(ol)
TOC	D-Phe-cyclo(Cys-**Tyr**-D-Trp-Lys-Thr-Cys)-Thr(ol)
TATE	D-Phe-cyclo(Cys-**Tyr**-D-Trp-Lys-Thr-Cys)-**Thr**
NOC	D-Phe-cyclo(Cys-**1-Na1**-D-Trp-Lys-Thr- Cys)-Thr(ol)
Antagonists	
BASS (sstr2-ANT)	**p-NO₂-Phe**-cyclo(**D-Cys-Tyr**-D-Trp-Lys-Thr-Cys)-**D-Tyr-NH₂**
LM3	**p-Cl-Phe**-cyclo(**D-Cys-Tyr-D-Aph(Cbm)**-Lys-Thr-Cys)-**D-Tyr-NH₂**
JR10	**p-NO₂-Phe**-cyclo(**D-Cys-Tyr-D-Aph(Cbm)**-Lys-Thr- Cys)-**D-Tyr-NH₂**
JR11	**Cpa**-cyclo(**D-Cys-Aph(Hor)-D-Aph(Cbm)**-Lys-Thr-Cys)-**D-Tyr-NH₂**

Amino acids in bold indicated substitutions made on the original octreotide sequence.

Thr(ol): Threoninol, 1-Na1: 1-naphthyl-alanine, D-Aph (Cbm): D-4-amino-carbamoyl-phenylalanine, Cpa: 4-Cl-pheny-alanine, Aph(Hor): amino-Phe-hydroorotic acid

1.3.3.3   Somatostatin Peptide Receptor Radionuclide Therapy

Initial attempts at PRRT were done with high doses of ^{111}In-pentetreotide, speculating that the Auger electron emissions of ^{111}In would elicit an anti-tumour response. Although patients experienced symptomatic improvements, there was no tumour regression and it was concluded that the tissue penetration range of Auger electrons was insufficiently short (max 10 µm) to be used for PRRT[26,112].

^{90}Y can deliver higher energy β^- radiation into tumour tissues (E_{β^-} (max) = 2280 keV, ~ 12 mm tissue range). Several clinical studies have evaluated the radio-therapeutic ^{90}Y-DOTATOC using different protocols and patient populations. It was estimated that approximately 10-30% of patients with NETs experienced a positive anti-tumour response upon ^{90}Y-DOTATOC treatments, with GEP-NETs having the most favorable response[112].

^{177}Lu has a lower β^- energy (E_{β^-} (max) = 498 keV), and a shorter β^- emission range (~ 2 mm in tissue) compared to ^{90}Y, making it useful for smaller tumours. Treatments with ^{177}Lu-DOTA-Tyr^3-octreotate (^{177}Lu-DOTATATE) were effective for patients with high ^{111}In-pentetreotide uptake and low tumour burden. ^{177}Lu-DOTATATE also improved symptomatic conditions and quality of life[112]. In a study of 131 GEP-NET patients, treatment with ^{177}Lu-DOTATATE resulted in complete or partial remission in 28% of patients, minor response in 19%, stable disease in 35% and tumour progression in 18%[113]. Recently, the NETTER1-trial, a phase III multi-centric clinical trial of 230 metastatic midgut GEP-NET patients evaluated the tolerability of ^{177}Lu-DOTATATE and compared its efficacy to octreotide LAR[114]. ^{177}Lu-DOTATATE was well tolerated and showed a significant improvement in progression-free survival and overall survival compared to octreotide LAR[114].

Somatostatin antagonists have also recently been explored for PRRT. The antagonist ^{177}Lu-DOTA-JR11 has excellent sstr2 binding affinity (IC_{50} = 0.73)[108]. When evaluated in a preclinical model, ^{177}Lu-DOTA-JR11 delivered a 4.4-fold higher radiation dose to the tumour compared to ^{177}Lu-DOTATATE[115]. Pilot clinical studies in 4 patients with advanced NETs showed that ^{177}Lu-DOTA-JR11 delivered a 1.7-10.6 fold higher dose to the tumour compared to ^{177}Lu-DOTATATE, with only minor and reversible adverse effects[116]. The tolerability and

efficacy of ^{177}Lu-DOTA-JR11 (^{177}Lu-OPS201) in unresectable GEP-NETs is currently being investigated in a phase I/II clinical trial (NCT02592707).
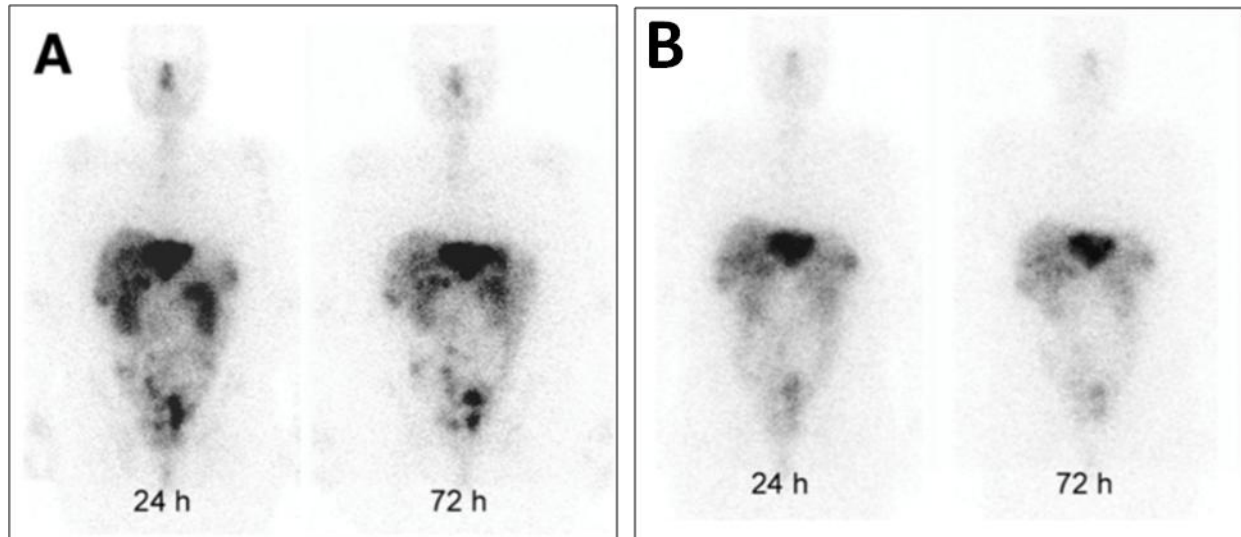
Figure 1.3 Comparison of agonist and antagonist somatostatin radiotracers. Planar scans of the same NET patient injected with 850 MBq ^{177}Lu-DOTA-JR11 (A) and 990 MBq ^{177}Lu-DOTATATE (B) at 24 and 72 h post-injection, showing higher tumour uptake with the antagonist. *This research was originally published in JNM. Wild D, Fani M, Fischer R, Del Pozzo L, Kaul F, Krebs S, Fischer R, Rivier J, Reubi J, Maecke R. Comparison of Somatostatin Receptor Agonist and Antagonist for Peptide Receptor Radionuclide Therapy: A Pilot Study. J Nucl Med. 2014;55:1248-1252.* © *by the Society of Nuclear Medicine and Molecular Imaging, Inc. Figure used with permission*[116].

1.4   Breast Cancer

Breast cancer is the 3rd most common cancer among Canadians[117] and 2nd worldwide[118]. In Canada, breast cancers accounts for 25.8% of cancers among women, with 25,700 new cases in 2016 (1:9 women)[117]. From 1986 to 2016 Canada experienced a 44% decline in breast cancer mortality. In 2016, there were 4,900 breast cancer-related deaths among women, and an estimated 3.3% (1:30) lifetime probability of dying from breast cancers[117].

Breast cancer develops from the cells of the ducts and lobules[119]. If the cancer mass has not broken through the basement membrane, the cancer is considered localized or *in situ*, and can be treated by surgical resection with excellent prognosis[119]. Once the cells have broken through the basement membrane, they are considered invasive and may have a more aggressive phenotype. Based on the type of disease, its molecular markers, stage and level of differentiation breast cancers can be treated with hormone therapies, chemotherapy, surgery, radiation and immunotherapy[120].

1.4.1 Molecular Subtypes of Breast Cancer

Breast cancer is a complex and heterogeneous disease not adequately represented by histological grading and current clinical parameters[121,122]. Gene expression profiling (GEP) studies have provided considerable information on the molecular characteristics of breast cancers, and demonstrated that they can be grouped into four distinct subtypes predictive of risk factors, prognosis and treatment sensitivity[121,122]. The four subtypes are Luminal A, Luminal B, Human Epidermal Growth Factor 2 (HER2)-enriched and Basal-like[121,122]. GEP is not readily available for all patients, and therefore surrogate histological biomarkers (mainly estrogen receptor (ER), progesterone receptor (PR) and HER2) are often used to stratify patients [121,122].

Luminal A breast cancers are the most common (40 – 70%[122-125]). They have low histological grade, low mitotic activity, low recurrence rate, and are responsive to hormone therapies. Pathological biomarkers are ER-positive, PR-positive, HER2-negative and low Ki-67 index (proliferating cell nuclear antigen, a marker for proliferation)[122]. They are often sstr-positive, although sstr status is not typically evaluated in clinical practice. Luminal B cancers are less common (15 – 20%[122-125]) and have a more aggressive phenotype. By immunohistochemistry (IHC) analysis, they are ER-positive, can be HER2 positive or negative

and have high Ki-67 index[122]. HER2-enriched breast cancers (5 – 15%[122-125]) have a high histological grade, high proliferative index, and high propensity for metastasis. They respond well to chemotherapy and treatment with monoclonal antibody, Trastuzumab. By IHC, they show HER2 overexpression, and are ER-negative and PR-negative[122]. Basal-like cancers (10 – 20%[122-125]) have a high histological grade, high mitotic index and rapidly metastasize to brain and lungs. They are ER-negative, PR-negative and HER2-negative[122].

Table 1.6 Clinicopathological surrogate markers for breast cancer.[122]

Intrinsic Subtype	Clinicopathological Surrogate
Luminal A	ER and PR positive HER2 negative Low Ki-67
Luminal B	ER positive HER2 positive or negative High Ki-67
HER2-enriched	HER2-positive or overexpressed ER and PR negative
Basal-like	ER and PR negative HER2 negative

1.4.2   Breast Cancer Imaging

The most commonly used imaging modalities in breast cancer detection and monitoring are mammography, ultrasound and magnetic resonance imaging (MRI). Nuclear medicine procedures are used less frequently, and only in cases of recurrent or metastatic disease. Mammography detects abnormal micro-calcification by irradiating the breast with low dose X-rays. The overall sensitivity of mammography depends on the density of the breast, as highly fibroglandular tissue can obscure potential cancerous lesions. Mammography is the most

common screening and detection tool for breast cancer[126-128]. In British Columbia, asymptomatic women with average risk of breast cancer, 50-69 years old, are encouraged to undergo mammography screening biennially[129,130]. When a lesion is suspected, a higher dose diagnostic mammography is prescribed[127].

Ultrasonography is an excellent and complementary adjunct detection tool to mammography. High frequency sound is transmitted into the breast tissue, and the image is generated based on the quality of the reflected sound waves[128]. Ultrasound is used in patients with dense breast parenchyma. It is commonly used to differentiate between solid masses and cysts and, in combination with mammography, can also characterize lesions as either malignant or benign[127]. Because ultrasound can acquire images in real time, it is often used for guiding invasive procedures such as biopsy[127].

MRI is used as a supplemental tool in cases of inconclusive mammography or ultrasonography[127]. MRI images the magnetic properties of hydrogen atoms found in water molecules of soft tissues and fat[131]. MRI is highly sensitive, however, lacks specificity for tumours smaller than 3 mm[127]. It is a valuable tool for patients with silicone breast implants, or when mammography and ultrasonography are inconclusive. The latter includes cases of breast-conserving surgery, known carcinoma, metastasis, extensive postoperative scaring and very dense breast parenchyma[127]. As a screening tool, it is only used in high-risk patients, such as those with a first-degree relative with proven BRCA1 or BRCA2 mutations[131].

Nuclear medicine procedures are used less for diagnosis, but play a bigger role in monitoring recurrent and metastatic disease[132], and will be further discussed in the next section.

1.4.2.1   Nuclear Imaging

Imaging procedures for breast cancer using SPECT radiotracers are [99mTc]-methoxyisobutylisonitrile ([99mT]-sestamibi) and [99mTc]-diphosphonates (for bone metastases). [99mT]-sestamibi concentrates in breast cancers due to an increase in blood flow, increased density of mitochondria and cancer cell membrane hyperpolarization[133]. [99mT]-sestamibi is used to evaluate patients with a palpable breast abnormality when mammography is negative or inconclusive[131,133].

Several PET tracers have been investigated for breast cancer imaging[132]. The most common is [18F]-FDG, which images the upregulated aerobic glucose metabolism characteristic of advanced tumours. [18F]-FDG-PET was recommended as a routine procedure in patients suspected of recurrent or metastatic disease[132,134]. [18F]-fluoro-L-thymidine ([18F]-FLT) is a radiotracer used to image DNA synthesis. The degree of [18F]-FLT uptake reflects the proliferation rate of tumours. There is currently no established role for [18F]-FLT in routine cancer care, however, it may be valuable in predicting early response to chemotherapy. In a small clinical study (n = 14) a decrease in [18F]-FLT uptake correlated with a positive chemotherapy response, while no correlation was found for [18F]-FDG[132,135]. Lastly, the radiotracer 16-α-[[18F]] fluoro-17-β-estradiol ([18F]-FES) is a ligand for ER and can be used to image ER-positive cancers[132]. [18F]-FES uptake correlates well with estrogen receptor density (as confirmed by IHC) and may play an important role in assessing ER status of lesions that are difficult to biopsy, or in evaluating response to anti-estrogen therapy[132].

Imaging of localized breast lesions using PET radiotracers may benefit from the improved resolution of positron emission mammography (PEM). PEM uses a pair of detectors above and below the breast that scan along the tissue and detect 511 keV photons emitted in

coincidence. Compared to whole-body PET, which has a resolution of 5-7 mm at full width half-maximum, PEM has a resolution of 2.4 mm[136]. In a recent study, Kalinyak *et al.* demonstrated that PEM detected 92% of the tumours studied compared to PET/CT which detected 87% and whole-body PET which detected 56%[137].

1.4.2.2   Somatostatin Receptor Imaging

The expression of somatostatin receptors in breast cancer samples and cell lines has been documented since the early 1990's[87], motivating the use of somatostatin radiotracers for breast cancer visualization[138]. Radiotracers ^{111}In-pentetreotide, ^{99m}Tc-depreotide and ^{99m}Tc-octreotide have been used for this purpose in several studies[138]. Sensitivity ranged from 69-100%, and specificity from 22-100%. 93-100% of visualized lesions were sstr-positive as confirmed by *ex vivo* scintigraphy, *in vitro* autoradiography, IHC, or mRNA studies[138].

Previous studies faced two major limitations in successful detection of somatostatin-positive breast cancers, namely small lesion size and low sstr2 density[138]. The former can be addressed by improvements in imaging resolution and sensitivity. The PET radiotracers ^{68}Ga-DOTATATE, ^{68}Ga-DOTATOC and ^{68}Ga-DOTANOC are more sensitive compared to SPECT tracers[100], and somatostatin antagonists may be even better[49,106]. Additionally, the use of PEM instrumentation could further better resolution [137]. The latter issue, namely of sstr density, can be improved by patient stratification. Luminal A breast cancers, characterized by expression of ER and PR receptors, show a higher expression of sstr, and thus would be eligible for somatostatin imaging.

Somatostatin receptor imaging can be used to monitor response to anti-hormone therapies, and to determined extent of disease to sentinel lymph nodes. Imaging can guide biopsy, or in some cases clarify the nature of lymph node lesions obviating the need for further

surgical intervention. Sstr positive cancers that develop resistance to anti-estrogen therapies, as is the case with ~40% of patients[139], may be eligible for PRRT with somatostatin analogues, which have been shown to be well tolerated in NET patients[114].

1.5 Thesis Objectives

1.5.1 Rationale

Somatostatin antagonists may be superior imaging agents compared to agonists, as demonstrated in recent reports with antagonist ^{68}Ga-NODAGA-JR11[108,110]. However, preclinical studies evaluating ^{68}Ga-NODAGA-JR11 and other somatostatin radiotracers *in vivo* typically use tumour models with high sstr2 density, such as human embryonic kidney cells (HEK) transfected with sstr2[49,108,109]. Although this model may adequately represent tumours with high sstr density, such as NETs, it may not represent the lower sstr density observed in breast cancers. The ZR-75-1 cell line is an invasive ductal carcinoma derived from the metastatic site of a 63-year-old woman[140]. Based on IHC biomarkers, ZR-75-1 cells classify as having a luminal A molecular subtype[141], however, GEP analysis more accurately characterizes this model as Luminal B[142]. Previous studies from our lab showed that ZR-75-1 xenografts express sstr and could be imaged with somatostatin ligand ^{68}Ga-DOTATATE[143].

1.5.2 Hypothesis

We hypothesized that agonist peptides TOC, TATE and antagonist peptide JR11 can be radiolabeled with ^{68}Ga and ^{18}F in high yield, purity and specific activity, and that ZR-75-1 xenografts imaged with antagonist tracers have higher tumour uptake and contrast compared with agonist tracers.

1.5.3 Specific Aims

Aim 1: Synthesize and radiolabel the literature compounds ^{68}Ga-DOTATOC, ^{68}Ga-DOTATATE and ^{68}Ga-NODAGA-JR11. Inject compounds in ZR-75-1 tumour-bearing animals and compare tumour uptake, tumour-to-normal tissue ratios, uptake in excretory organs and general biodistribution.

Aim 2: Use the AmBF$_3$ method described by Perrin and colleagues[69,70] to synthesize the compounds AmBF$_3$-TOC, AmBF$_3$-TATE and AmBF$_3$-JR11 and radiolabel with ^{18}F. Determine the binding affinity, plasma stability, internalization capacity and ZR-75-1 tumour uptake of ^{18}F-fluorinated somatostatin ligands.

Chapter 2: Materials and Methods

2.1 Reagents and Instrumentation

All reagents and solvents were purchased from commercial sources and used without further purification except when otherwise specified. C18 Sep-Pak cartridges (1cc, 50 mg) were obtained from Waters Corporation and pre-washed with ethanol followed by deionized (DI) water prior to use. ^{18}F-fluoride Trap & Release Columns (ORTG Inc.) were pre-washed with saturated NaCl solution followed by DI water. Peptide synthesis was performed on an Endeavor 90 peptide synthesizer (AAPPTec) using Fmoc protection strategy. Mass analyses were performed using a Bruker Esquire-liquid chromotography/mass spectrometry system with an electrospray ionization ion source, a Bruker Autoflex MALDI-TOF spectrometer or a TripleTOF 5600 mass spectrometer (AB/Sciex). High performance liquid chromatography (HPLC) purification and quality control were performed with a semi-preparative column (Phenomenex C18, 5 μ, 250 × 10 mm) or an analytical column (Phenomenex C18, 5 μ, 250 × 4.6 mm) respectively, on an Agilent 1260 infinity platform. HPLC systems were equipped with Infinity Diode Array Detector (DAD, UV to VIS) and/or a Bioscan NaI scintillation detector. ^{68}Ga was eluted from a 50 mCi ^{68}Ge/^{68}Ga generator (iThemba LABS) and purified according to reported methods[144]. ^{18}F-Fluoride was produced by ^{18}O(p,n)^{18}F reaction using a TR19 cyclotron purchased from Advanced Cyclotron Systems Inc. The activity was measured using a Capintec CRC®-25R/W dose calibrator.

2.2 Peptide and Precursor Synthesis

All peptides were synthesized on solid support using standard Fmoc chemistry. The peptides described in Chapter 3, namely DOTATATE, DOTATOC, NODAGA-JR11 and the

non-radioactive standards of their ^{nat}Ga complexes were prepared according to literature procedures[108,145].

The peptides evaluated in Chapter 4 were AmBF$_3$-TATE, which was prepared as previously described by Liu and Pourghiasian *et al.*[146], AmBF$_3$-TOC and AmBF$_3$-JR11, which were prepared as described herein. For TOC, H-Threoninol(But)-2-ClTrt-resin was swelled successively in dichloromethane and dried under N$_2$. Amino acids Fmoc-Cys(ACM)-OH, Fmoc-Thr(But)-OH, Fmoc-Lys(Boc)-OH, Fmoc-D-Trp(Boc)-OH, Fmoc-Tyr(tBu)-OH, Fmoc-Cys(ACM)-OH and Fmoc-D-Phe-OH (3 equivalents, eq.) pre-activated with HBTU/HOBt (3 eq.) and N,N-Diisopropylethylamine (6 eq.) in *N*-methyl-2-pyrrolidone (NMP) were sequentially coupled. The Fmoc group was removed by 20% piperidine in dimethylformamide (DMF). For JR11 synthesis, Fmoc-D-Tyr-Rink amide MBHA resin was swelled and deprotected with 20% piperidine in 15 mL x 2 DMF, followed by sequential amino acid coupling of Fmoc-Cys(ACM)-OH, Fmoc-Thr(But)-OH, Fmoc-Lys(Boc)-OH, Fmoc-D-Aph(Cbm)-OH, Fmoc-Aph(Hor)-OH, Fmoc-D-Cys(ACM)-OH and Fmoc-Cpa-OH. Fmoc-D-Aph(Cbm)-OH and Fmoc-Aph(Hor)-OH were synthesized according to literature procedures[147]. All peptides were cyclized by incubation with thallium(III) trifluoroacetate (1 eq. to the cystine on resin) for 90 min in 15 mL DMF. Azidoacetic acid pre-activated with 1 eq. diisopropylcarbodiimide was coupled to the *N*-terminus of both TOC and JR11 in NMP. Azido containing peptides were deprotected and simultaneously cleaved from the resin by treating with 4 mL 90/2.5/2.5/5 trifluoroacetic acid (TFA)/H$_2$O/triisopropylsilane/phenol for 4 h at room temperature. Peptides were filtered into 10 times the volume of cold diethyl ether and collected by centrifugation. The crude peptides were washed thoroughly with 12 mL x 3 cold ether, dried and purified by HPLC. N$_3$-TOC was eluted with 71% H$_2$O (0.1% TFA) and 29% acetonitrile (MeCN) (0.1% TFA) at a flow rate of 4.5

mL/min. The retention time was 21.4 min, and yield was 27%. The calculated m/z by MALDI-MS was 1118.4 and the measured m/z was 1118.0. Similarly, N_3-JR11 was eluted with 30-35% MeCN (0.1% TFA) in H_2O (0.1% TFA) at a flow rate of 4.5 mL/min. The retention time was 10.1 min, and yield was 19%. The ESI-MS calculated m/z was 1385.5, and measured m/z was 1385.8. *N*-propargyl-*N*,*N*-dimethylammoniomethyltrifluoroborate was synthesized as described previously[146] and click-reacted (3 eq. to peptide) with N_3-TOC (3.5 mg, 3.1 μmol) or N_3-JR11 (8.1 mg, 5.9 μmol) in $CuSO_4$ (1.0 M, 5.0 μL), sodium ascorbate (1.0 M, 12.5 μL) and 5% NH_4OH (MeCN/H_2O=1:1, 100 μL). The reaction mixture was incubated at 45°C for 2 h and directly purified by HPLC using the semi-preparative column. $AmBF_3$-TOC was eluted with 74% H_2O (0.1% TFA) and 26% MeCN (0.1% TFA) at a flow rate of 4.5 mL/min. The retention time was 17.3 min and yield was 54%. ESI-MS calculated m/z was 1283.5, and measured m/z was 1283.6. $AmBF_3$-JR11 was eluted with 25-30% MeCN (0.1% TFA) in H_2O (0.1% TFA) at a flow rate of 4.5 mL/min. The retention time was 13.1 min and the yield was 62%. The ESI-MS calculated m/z was 1550.6 and measured mass was 1550.7.

2.3   Competition Binding Assays

The *in vitro* binding affinity of our tested compounds to sstr2 was determined using a membrane-based competition binding assay. The assay measures binding affinity by evaluating the ability of non-radioactive standards to compete with a radioactive reference ligand for sstr2 binding sites on purified cell membranes overexpressing human sstr2. The assay is performed by co-incubation of purified membranes with non-radioactive standards (at varying concentrations) and the radioactive ligand (at a fixed concentration). The half-maximal inhibitory concentration (IC_{50}) is determined by measuring the amount of bound radioactive ligand in each condition[148].

In our assay, purified Chinese hamster ovary-K1 membranes overexpressing human sstr2 (Perkin Elmer) were incubated with radio-ligand ^{125}I-Tyr^{11}-Somatostatin-14 (^{125}I-SRIF14, Perkin Elmer) and competing non-radioactive ligands in a 96-well, 1.2 μm glass fibre filter plate (EMD Millipore). Prior to assay, the plate filters were pre-soaked in 200 μL 0.1% polyethylenimine (Sigma) for 1 h at ambient temperature. Following pre-incubation, membranes (25 μg/well), ^{125}I-SRIF14 (0.05 nM) and various concentrations of competing non-radioactive standards (10 μM to 1 pM) were diluted in assay buffer (25 mM HEPES pH 7.4, 10 mM MgCl$_2$, 1 mM CaCl$_2$, 0.5% bovine serum albumin (BSA)) and incubated for 1 h at 27°C with moderate shaking (200 μL reaction volume). Once complete, the incubation mixture was aspirated through the filters, followed by 6 washes with 200 μL ice-cold wash buffer (50 mM Tris-HCl pH 7.4, 0.2% BSA). Each filter was removed and counted on a PerkinElmer WIZARD 2480 gamma counter. The data was fit to a one-site Fit-Ki curve in GraphPad Prism v6.07, which calculated the inhibition constant, K_i. Unlike IC$_{50}$, the K_i is an absolute value that does not depend on the radioactive ligand concentration or its binding affinity to receptors. K_i is calculated from IC$_{50}$ using the Cheng-Prusoff equation[149]:

$$K_i = \frac{IC_{50}}{1 + \frac{[A]}{EC_{50}}}$$

where [A] is the radioactive ligand concentration, and EC$_{50}$ is the concentration of radioactive-ligand at half receptor saturation[149].

The endogenous ligand SRIF-28 (Bachem) was used in our assay as a control. To ensure that the concentration of our non-radioactive standards, and hence our determination of K_i, was accurate, our samples underwent amino acid analysis at SPARC BioCentre (Toronto Hospital for Sick Children), where peptides were hydrolyzed and comprising amino acids were separated on

HPLC. The peptide content was calculated by comparing the concentration of selected amino acids to known standards.

2.4 Radiolabeling

2.4.1 ^{68}Ga Radiolabeling

^{68}Ga was eluted from the ^{68}Ge/^{68}Ga generator and purified as previously described[144]. ^{68}GaCl$_3$ in 0.5 mL DI water was added into an 8 mL glass vial preloaded with peptide precursor and HEPES buffer solution (0.7 mL, pH 5). The vial was then sealed with a screw cap and heated in a Danby microwave oven (model number: DMW7700WDB; power set to "2") for 1 min. We used isocratic HPLC to separate the ^{68}Ga-bound peptides from ^{68}Ga-unbound peptides to ensure consistent high specific activity. The reaction mixture was cooled and directly injected into HPLC. The ^{68}Ga-labeled peptide was collected and diluted with 50 mL 0.05 M ammonium formate solution and then passed through C18 light Sep-Pak cartridge. The product was eluted with 0.4 mL 90% ethanol in saline and formulated in saline for animal studies. HPLC solvents were 81% triethylamine-phosphate buffer and 19% MeCN for ^{68}Ga-DOTATATE, 79% phosphate buffered saline (PBS) buffer and 21% MeCN for ^{68}Ga-DOTATOC, and 77% PBS buffer and 23% MeCN for ^{68}Ga-NODAGA-JR11. For purification, the flow rate was 4.5 mL/min. The retention times were 20.4, 19.2 and 14.3 min for ^{68}Ga-DOTATATE, ^{68}Ga-DOTATOC and ^{68}Ga-NODAGA-JR11, respectively. For quality control (QC), the flow rate was 2 mL/min and retention times were 7.4, 6.8 and 5.3 min for ^{68}Ga-DOTATATE, ^{68}Ga-DOTATOC and ^{68}Ga-NODAGA-JR11, respectively. The specific activity of ^{68}Ga-DOTATATE, ^{68}Ga-DOTATOC and ^{68}Ga-NODAGA-JR11 was measured using the same analytical HPLC system. It was calculated by dividing the injected radioactivity by the tracer quantity, which was

interpolated from a UV standard curve. The standard curve was constructed with cold-standard compounds ^{nat}Ga-DOTATATE, ^{nat}Ga-DOTATOC and ^{nat}Ga-NODAGA-JR11.

2.4.2 ^{18}F Radiolabeling

Radiolabeling was performed as described by Liu and Pourghiasian *et al.*[146]. Briefly, cyclotron produced ^{18}F-fluoride was trapped on an ^{18}F-fluoride Trap & Release Column and eluted into a reaction vial preloaded with 100 nmol precursor in aqueous solution (15 µL DMF, 15 µL 1 M pyridazine-HCl buffer pH = 2.0, and 50 nmol KHF$_2$). The mixture was incubated at 80°C for 5 minutes, and again for another 15 min under vacuum. The reaction was quenched with 2 mL 5% NH$_4$OH in water and purified using both Sep-Pak and HPLC. All HPLC purifications were done on a semi-preparative column with flow rate 4.5 mL/min, and used isocratic conditions comprised of MeCN (0.1% TFA) and H$_2$O (0.1% TFA). ^{18}F-AmBF$_3$-TOC was purified with 29% MeCN; ^{18}F-AmBF$_3$-TATE with 28% MeCN, and ^{18}F-AmBF$_3$-JR11 with 26% MeCN. The specific activity of ^{18}F-fluorinated compounds was measured using the analytical HPLC system. It was calculated by dividing the radioactivity of the injected tracer by its mass, which was interpolated from a UV absorbance standard curve constructed with cold-standard compounds AmBF$_3$-TATE, AmBF$_3$-TOC and AmBF$_3$-JR11.

2.5 Internalization Assay

Internalization assays, performed for ^{18}F-AmBF$_3$-TATE, ^{18}F-AmBF$_3$-TOC and ^{18}F-AmBF$_3$-JR11, were used to determine the internalization capacity of radiotracers by determining the membrane-bound or cytosol-internalized fractions. Roughly $3 - 5 \times 10^5$ cells/well (ZR-75-1 model) were seeded onto a 24-well plate (Corning) and grown overnight. On the day of the experiment, growth media was replaced with 500 µL reaction buffer (RPMI with 4.8 mg/mL HEPES, 1 mg/mL penicillin/streptomycin, and 2 mg/mL BSA) and incubated for at least 1 h at

37°C. Approximately 500,000 cpm (~15 kBq) of radiolabeled peptide was added to each well and incubated for 15, 30, 45, and 60 min in triplicates at 37°C. Following incubation, the reaction media was removed and cells were washed twice with 500 μL/well ice-cold PBS. Two acid washes (0.2 M acetic acid, 0.5 M NaCl pH 2.6), each 200 μL/well, were performed for 10 min on ice, and collected to isolate the membrane-bound fraction. Finally, cells were washed once more with ice-cold PBS and trypsinized to collect the internalized fraction. Both fractions were counted on a WIZARD Wallac gamma counter and results were expressed as percent internalized of total bound (% internalized/total bound).

2.6   Quantitative Polymerase Chain Reaction

Quantitative polymerase chain reaction (qPCR) measures the transcriptional expression of various genes by amplifying coding DNA (cDNA) with specific DNA primers.   We determined the baseline transcriptional expression of sstr1, sstr2, sstr3, sstr4 and sstr5 in ZR-75-1 cells relative to reference gene hypoxanthine phosphoribosyltransferase 1 (HPRT1) using qPCR. Total RNA from ZR-75-1 cells was purified using the GenElute^{TM} Mammalian total RNA miniprep kit (Sigma), treated with amplification grade DNase I (Sigma), and measured using a NanoDrop^{TM} spectrophotometer. 2.0 μg of total ZR-75-1 RNA was reverse transcribed in a 20 μL reaction using SuperScript$^®$ VILO^{TM} cDNA synthesis kit (Invitrogen). qPCR was set up in 384-well plates, in a total volume of 10 μL; each reaction containing 1 μL template cDNA, 500 μM forward and reverse primers, 250 μM probe, and 1X SsoAdvanced^{TM} universal probes supermix (BioRad). Each reaction was performed in triplicates and repeated 3 times. Predefined primers (forward and reverse) and probes for all six genes were purchased from IDT. The Quantstudio^{TM} 6K Flex Real-Time PCR system (Thermo Fisher Scientific) was used for amplification and detection. The concentration of each target was determined by interpolating

the C_t value (cycle at which fluorescence reached a certain threshold) from respective standard curves of known concentrations. To construct the standard curves, RNA from cell lines with known expression of sstr subtypes was purified and reverse-transcribed as described above. Target sstr genes were PCR amplified using Q5® high-fidelity DNA polymerase (New England BioLabs) as per the manufacturer's instructions, using the same primers as the qPCR reactions (without the fluorogenic probe). PCR products were separated on a 2% agarose gel, and target bands were extracted and purified using the Monarch® DNA gel extraction kit (New England BioLabs). The amount of DNA was quantified using Qubit® dsDNA HS assay kit (Thermo Fisher) and the number of copies/µL was calculated using the following formula:

$$copies/\mu L = \frac{DNA \ Concentration \ (g/\mu L)}{amplicon \ length \ (bp) \times 650 \ g/mol} \times 6.022 \cdot 10^{23} \ copies/mol$$

Standard curves were constructed from 10-fold serial dilutions (10^5 copies/µL to 1 copy/µL) and assayed by qPCR in triplicates. All standard curves were repeated 2 times (3 times for HPRT1). Sstr1 transcripts were amplified from HeLa cells, sstr2 from ZR-75-1 cells, sstr3 from Jurkat cells, sstr4 from the Chantest™ human sstr4 receptor cell line (irradiated cells, Charles river), and sstr5 and HPRT1 from HEK-sstr5 cells. Standard curves, primer and probe information, and cycling conditions for both PCR and qPCR can be found in Appendix A.

2.7   Cell Culture

All imaging and biodistribution studies were performed using the human breast carcinoma, ER-positive cell model ZR-75-1[140] (ATCC). In addition, HeLa cells (gifted from Dr. Sam Aparicio), Jurkat cells (ATCC) and sstr5-transfected HEK-293 cells (HEK-sstr5, gifted from Dr. Stefan Schultz) were used for qPCR standard curve construction. ZR-75-1 cells were cultured in RPMI 1640 media + GlutaMAX™ (Life Technologies) and supplemented with 10%

fetal bovine serum (FBS) (Seradigm). Jurkat cells were grown in the same base media, and contained 10% heat-inactivated FBS and 1 mM sodium pyruvate. HeLa cells were grown in DMEM + GlutaMAX^{TM} (Life Technologies) with 10% FBS. HEK-sstr5 cells were grown in DMEM + GlutaMAX^{TM} with 10% FBS, and contained 0.5 mg/mL G418 to maintain sstr5 expression. All cell cultures were exposed to 100 I.U./mL penicillin/streptomycin (Life Technologies) and grown in a humidified atmosphere at 37°C.

2.8 Animal Studies

All animal studies were done in compliance with the Canadian Council on Animal Care guidelines and were approved by the Animal Care Committee of University of British Columbia.

2.8.1 17β-Estradiol Pellet Implant and Tumour Inoculation

Immunodeficient female NOD *scid* gamma mice (NOD.Cg-*Prkdc*^{sci}*Il2rg*^{tm1Wjl}/SzJ or NSG) were obtained from an in-house breeding colony at BC Cancer Research Centre and Jackson Laboratory. To sustain the growth of the ER-positive ZR-75-1 cell model, animals were administered a slow-release 17β-estradiol pellet (E2) (Innovative Research of America) subcutaneously in the dorsal space of the neck. An initial pellet dose of 1.7 mg/60 days was used, however, this dose was reduced to 0.72 mg/60 days to minimize E2-related urinary retention and bladder stone formation[150,151]. Animals evaluated with compounds ^{68}Ga-DOTATATE, ^{68}Ga-DOTATOC and ^{68}Ga-NODAGA-JR11 (Chapter 3) received the higher pellet dose of 1.7 mg/60-day. However, studies done with compounds ^{18}F-AmBF$_3$-TOC, ^{18}F-AmBF$_3$-TATE and ^{18}F-AmBF$_3$-JR11 (Chapter 4) received an equal mixture of 0.72 and 1.7 mg/60-day release pellets. Among these groups, animals evaluated at 1 h p.i. with the three different ^{18}F tracers received a similar combination of 0.72 and 1.7 mg/60-day release pellets. However, animals evaluated at 2 h p.i. and 1 h p.i. with blocking received the lower 0.72 mg/60-day dose. 3-5 days post pellet-

43

implant, 1×10^7 ZR-75-1 cells were re-suspended in a mixture of PBS and Matrigel (Corning) and inoculated subcutaneously on the right shoulder. Tumours were grown for 5 - 6 weeks, until they reached a size of 7 - 11 mm in diameter.

2.8.2 *In Vivo* Plasma Stability

In vivo plasma stability studies were done for ^{18}F-fluorinated tracers, ^{18}F-AmBF$_3$-TOC, ^{18}F-AmBF$_3$-TATE and ^{18}F-AmBF$_3$-JR11, to determine metabolic stability at 5 min or 15 min p.i. Naïve mice were injected intravenously with either 10 MBq (for 5 min time point) or 20 MBq (for 15 min time point) tracer and allowed to roam freely in their cage. Following euthanization, blood was collected by cardiac puncture, mixed with an equal volume of MeCN to precipitate proteins, and centrifuged for 15 min. The supernatant was collected and quantified on HPLC using an analytical column with 2 mL/min flow rate, and the following isocratic conditions in H$_2$O (0.1% TFA): 27% MeCN (0.1% TFA) for ^{18}F-AmBF$_3$-TOC and ^{18}F-AmBF$_3$-TATE, and 26% MeCN (0.1% TFA) for ^{18}F-AmBF$_3$-JR11.

2.8.3 Biodistribution Studies

Mice were sedated with 2% isoflurane in oxygen, at a flow-rate of 2 L/min, and administered a radiotracer dose of 1 - 3 MBq intravenously. Biodistribution studies were either done at 1 h p.i. or 2 h p.i. For evaluation of ^{18}F radiotracers (Chapter 4), we also performed blocking studies to determine radioligand specificity for the tumour. For these studies, 50 μg (AmBF$_3$-TOC) or 100 μg (AmBF$_3$-TATE or AmBF$_3$-JR11) of the non-radioactive standards were co-injected with the respective radiotracer. After 1 or 2 h uptake time, animals were sedated with 5% isoflurane (2 L/min) and euthanized by CO$_2$ asphyxiation. Blood was promptly collected by cardiac puncture and weighed. All internal organs were harvested, rinsed in PBS, blotted dry and weighed. Organs were measured in a Wallac WIZARD2 gamma counter (Perkin

Elmer). Measured activity was normalized to the injected dose and the respective weight of the organ and expressed as percent injected dose per gram of tissue (%ID/g).

2.8.4　PET/CT Imaging

Tumour-bearing mice were injected intravenously with 8 - 9 MBq of radio-peptide. Static PET images were acquired 55 min post-injection for 10 min using an Inveon microPET/CT scanner (Siemens) as described previously[144]. A baseline CT scan was used for localization and attenuation correction. Mice were promptly euthanized after imaging, and biodistribution studies were undertaken as described above.

2.9　Statistics

Statistical analyses were performed using GraphPad Prism v6.07 software. Ordinary 1-way analysis of variance (ANOVA) was used in all statistical comparisons. P values ≥ 0.05, < 0.05, < 0.01 and < 0.001 were denoted as ns (non-significant), *, ** and *** respectively.

Chapter 3: Comparison of [68]Ga Agonists and Antagonist Somatostatin Radiotracers for Breast Cancer Imaging

3.1   Introduction

Several studies have reported on the superiority of somatostatin antagonist radiotracers for imaging of sstr2-positive tumours[49,105,106,108-110]. Antagonists are hypothesized to effectively bind to both active and inactive configurations of their target receptors, while agonists bind only when the receptor is in an active state[52]. Thus antagonist probes label more sites on the cell surface, resulting in overall higher uptake despite no internalization ability[52]. When imaging tumours with low or heterogeneous sstr density, such as breast cancers, antagonists may be the preferred choice as to maximize the number of binding sites labeled. Using *in vitro* autoradiography, Cescato *et al.* observed that binding of the antagonist ^{177}Lu-DOTA-BASS to human breast cancer sections was 11-fold higher than the agonist ^{177}Lu-DOTA-TATE[105].

The antagonist PET/CT radiotracer ^{68}Ga-NODAGA-JR11 (or ^{68}Ga-OPS202) showed excellent tumour uptake and biodistribution in both preclinical[108] and pilot clinical[110] studies. The aim of this chapter, in accordance with Aim 1, is to compare the potent antagonist, ^{68}Ga-NODAGA-JR11, with two commonly used agonists, ^{68}Ga-DOTATATE and ^{68}Ga-DOTATOC, for *in vivo* breast cancer imaging using an sstr2-postive breast cancer xenograft model (ZR-75-1). Herein we synthesized and evaluated the binding affinity of non-radioactive standards [nat]Ga-DOTATATE, [nat]Ga-DOTATOC and [nat]Ga-NODAGA-JR11 to sstr2. We radiolabeled the above compounds with ^{68}Ga, and compared their *in vivo* tumour uptake and biodistribution in ZR-75-1

tumour-bearing mice. Additionally, we determined the baseline transcriptional profile of sstr1-5 subtypes in ZR-75-1 cells.

⁶⁸Ga-DOTATOC

⁶⁸Ga-DOTATATE
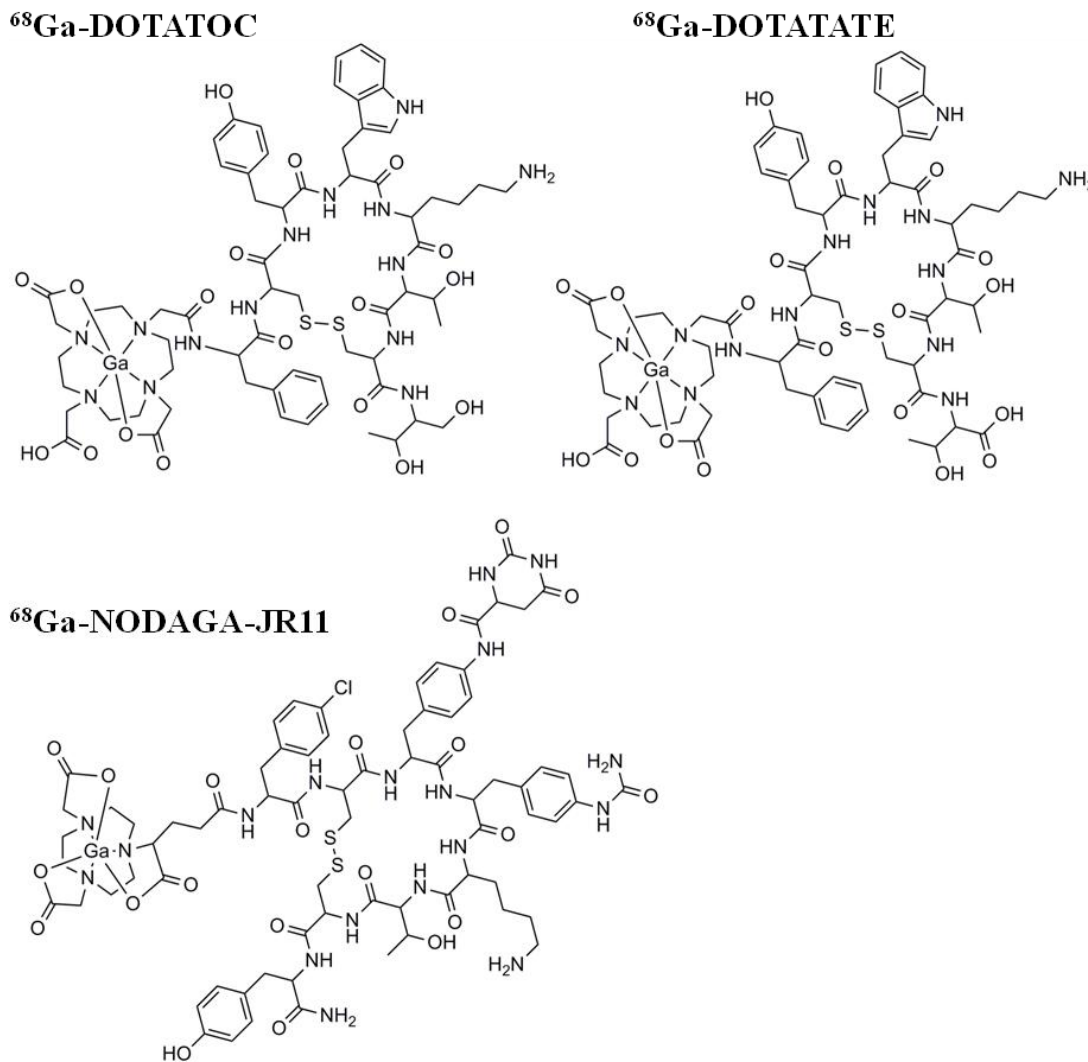
⁶⁸Ga-NODAGA-JR11

Figure 3.1 Chemical structures of ⁶⁸Ga-DOTATOC, ⁶⁸Ga-DOTATATE and ⁶⁸Ga-NODAGA-JR11.

3.2   Materials and Methods

The materials and methods used in this chapter are listed in Chapter 2. Relevant sections are those describing peptide synthesis (Section 2.2), binding affinity (Section 2.3), radiolabeling (Section 2.4.1), q-PCR (Section 2.6), cell culture (Section 2.7), 17β-estradiol pellet implant and tumour inoculation (Section 2.8.1), biodistribution (Section 2.8.3), PET/CT imaging (Section 2.8.4) and statistics (Section 2.9).

3.3   Results

3.3.1   Transcriptional Sstr Expression

We calculated the target gene/HPRT1 copy number ratio for all five somatostatin subtypes and found predominant expression of sstr2. The normalized expression of sstr2 to HPRT1 was 0.055 ± 0.0083 (n = 3), and < 0.00005 for all other subtypes (n = 3 each, $p < 0.001$) (Figure 3.2). For all subtypes except sstr2, we calculated < 10 copies/μL of target transcript in our cDNA preparation. In comparison, we identified $12{,}915.5 \pm 2{,}218.2$ copies/μL (n = 4) HPRT1 transcripts, and 680.8 ± 148.0 (n = 3) copies/μL sstr2 transcripts.
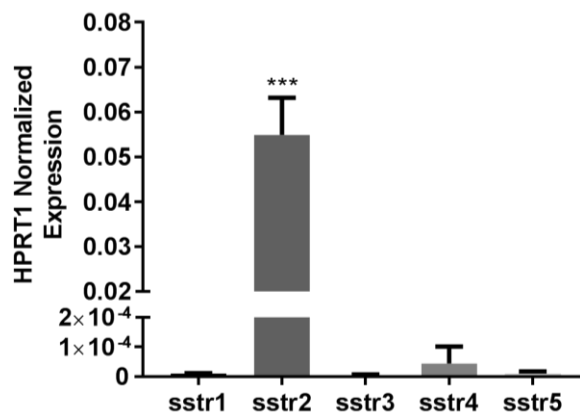
Figure 3.2 Relative transcriptional expression of sstr subtypes normalized to housekeeping gene HPRT1.

3.3.2 Binding Affinity and Radiolabeling

^{nat}Ga-DOTATOC and ^{nat}Ga-DOTATATE had inhibition constants (K_i) in the low nanomolar range (0.9 ± 0.1 nM, n = 4, and 1.4 ± 0.3 nM, n = 3 respectively), while the K_i of ^{nat}Ga-NODAGA-JR11 was much higher (25.9 ± 0.2 nM, n = 3, p < 0.001). The SRIF-28 control had a K_i of 3.7 ± 1.7 nM (n = 5) in our assays. Representative inhibition curves are shown in Figure 3.3. Multiple batches of ^{68}Ga-DOTATOC, ^{68}Ga-DOTATATE and ^{68}Ga-NODAGA-JR11 were prepared in good radiochemical yield (61 ± 5%, 62 ± 8% and 68 ± 13% respectively, n = 3), purity (> 98%) and high specific activity (251.6 ± 33.9, 197.3 ± 85.2 and 138.8 ± 2.6 MBq/nmol respectively, n = 3). The particular tracer preparations used for animals studies corresponded to radiochemical yields of 62%, 66% and 58% respectively, and specific activities of 281.2, 218.3 and 136.9 MBq/nmol for ^{68}Ga-DOTATOC, ^{68}Ga-DOTATATE and ^{68}Ga-NODAGA-JR11 respectively.
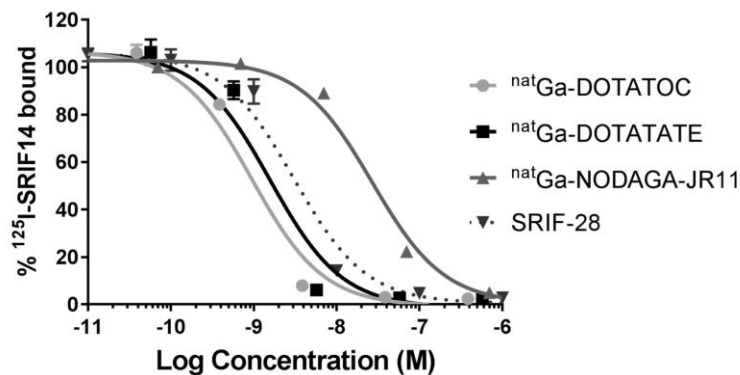
Figure 3.3 Representative competition binding assays of ^{nat}Ga peptides. Peptides ^{nat}Ga-DOTATOC, ^{nat}Ga-DOTATATE, ^{nat}Ga-NODAGA-JR11 and SRIF-28 control were run with purified sstr2-overexpressing membranes and competing radioactive ligand ^{125}I-SRIF14.

3.3.3 Tumour and Organ Uptake

A full overview of tracer biodistribution is presented in Table 3.1. Among the three tested tracers, we found that the antagonist ^{68}Ga-NODAGA-JR11 has the lowest tumour uptake (12.2 $\pm$ 0.78 %ID/g) compared to agonists ^{68}Ga-DOTATOC (18.4 $\pm$ 2.87 %ID/g, $p < 0.001$) and ^{68}Ga-DOTATATE (15.2 $\pm$ 2.20 %ID/g, ns) (see Figures 3.4 and 3.5). The antagonist ^{68}Ga-NODAGA-JR11 also had the lowest tumour-to-blood (15.6 $\pm$ 2.20) and tumour-to-muscle (45.2 $\pm$ 11.6) ratios compared to ^{68}Ga-DOTATOC (41.1 $\pm$ 5.68, $p < 0.001$ and 172 $\pm$ 55.3, $p < 0.01$, respectively) and ^{68}Ga-DOTATATE (44.6 $\pm$ 11.7, $p < 0.001$ and 152.0 $\pm$ 60.8, $p < 0.01$, respectively) (see Figure 3.6). The excretion profile of all three tracers was predominantly renal, with high uptake in the kidneys and bladder. The agonist ^{68}Ga-DOTATATE had the lowest kidney uptake (8.44 $\pm$ 1.73 %ID/g), followed by ^{68}Ga-DOTATOC (9.27 $\pm$ 1.73 %ID/g) and lastly by ^{68}Ga-NODAGA-JR11 (14.1 $\pm$ 1.65 %ID/g, $p < 0.001$).
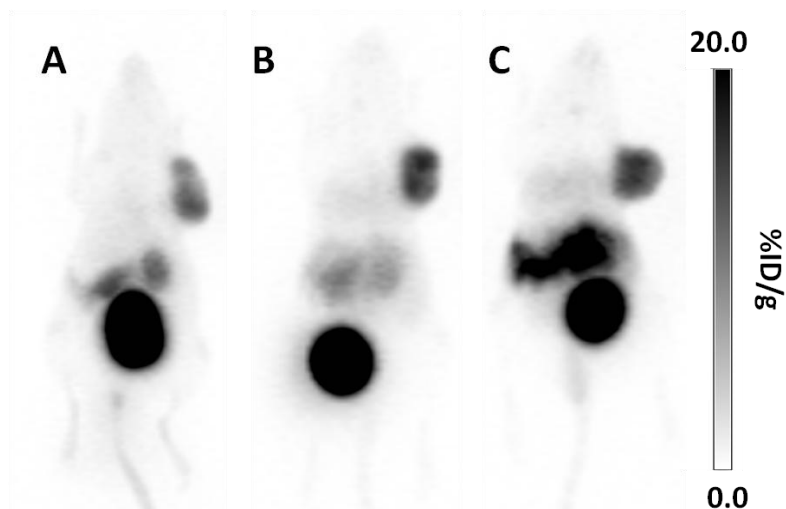
Figure 3.4 Representative PET maximum intensity projection images of ^{68}Ga compounds in a ZR-75-1 tumour model. A. ^{68}Ga-NODAGA-JR11, **B.** ^{68}Ga-DOTATOC and **C.** ^{68}Ga-DOTA-TATE. Note that image **C** is of a mouse treated with ^{68}Ga-DOTATATE, but not included in the biodistribution analysis as it received a lower pellet dose of 0.72 mg/60 d compared to the others.
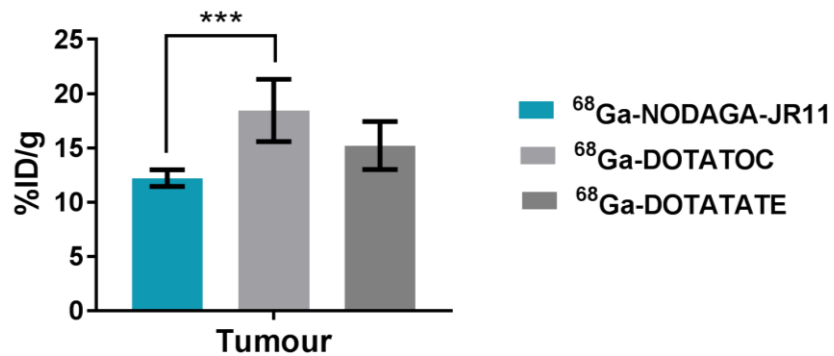
Figure 3.5 ZR-75-1 tumour uptake at 1 h p.i. with ^{68}Ga radiotracers. *** $p < 0.001$.
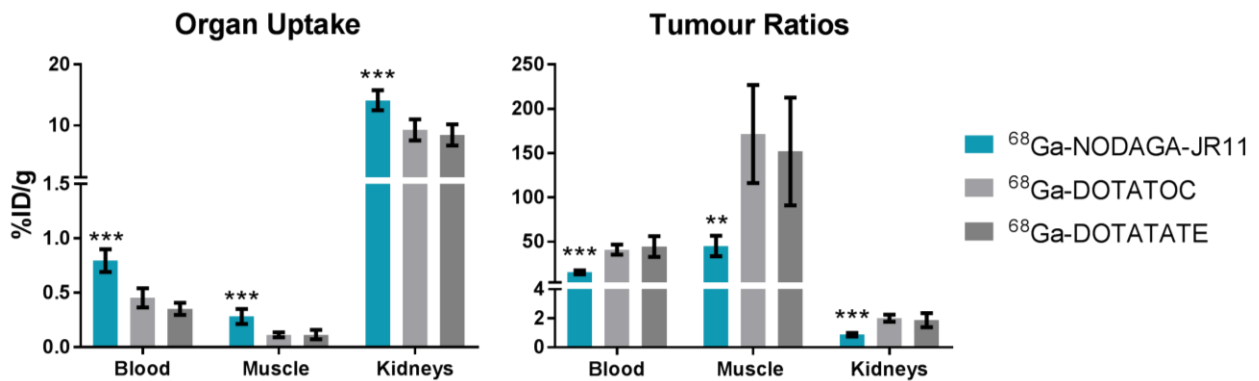
Figure 3.6 Organ uptake and tumour-to-background ratios with ^{68}Ga-radiotracers at 1 h p.i. ^{68}Ga-NODAGA-JR11 had statistically higher uptake in the blood, muscle and kidneys compared to the other two radiotracers, resulting in lower tumour-to-blood, tumour-to-muscle and tumour-to-kidney ratios. ** $p < 0.01$, *** $p < 0.001$.

Table 3.1 Biodistribution of ^{68}Ga-NODAGA-JR11, ^{68}Ga-DOTATOC, and ^{68}Ga-DOTATATE in NOD *scid* gamma tumour-bearing mice.

Organ Uptake (%ID/g)

	^{68}Ga-NODAGA-JR11 (n= 5)		^{68}Ga-DOTATOC (n= 6)		^{68}Ga-DOTATATE (n = 6)	
	Mean	**SD**	**Mean**	**SD**	**Mean**	**SD**
Blood	0.80	0.10	0.45	0.09 ***	0.35	0.06 ***
Fat	0.23	0.11	0.18	0.09	0.28	0.14
Ovaries	0.68	0.22	0.51	0.07	0.89	0.35
Uterus	0.86	0.22	0.54	0.11	0.84	0.10
Intestine	0.90	0.20	2.39	0.30	7.35	0.44
Stomach	1.37	0.78	2.75	1.25	8.29	3.06
Pancreas	9.29	2.03	11.01	1.32	51.56	5.47
Spleen	0.39	0.05	0.46	0.11	0.84	0.38
Kidneys	14.12	1.65	9.27	1.73 ***	8.44	1.73 ***
Adrenals	2.00	0.65	9.52	3.77	15.20	7.26
Liver	0.99	0.12	0.71	0.17	1.95	0.52
Lungs	4.72	0.71	22.93	6.12	28.66	2.94
Heart	0.46	0.06	0.30	0.04	0.67	0.13
Tumour	**12.21**	**0.78**	**18.44**	**2.87 *****	**15.22**	**2.20**
Muscle	0.28	0.07	0.11	0.02 ***	0.11	0.04 ***
Bone	0.26	0.04	0.20	0.03	0.25	0.02
Brain	0.05	0.02	0.03	0.01	0.03	0.01

Tumour to Normal Tissue Ratios

	^{68}Ga-NODAGA-JR11		^{68}Ga-DOTATOC		^{68}Ga-DOTATATE	
	Mean	**SD**	**Mean**	**SD**	**Mean**	**SD**
Blood	15.6	2.20	41.1	5.68 ***	44.6	11.7 ***
Muscle	45.2	11.6	172	55.3 **	152	60.8 **
Kidney	0.88	0.12	2.01	0.24 ***	1.88	0.49 ***

Organ uptake is expressed as mean ± standard deviation in units of percent injected dose per gram of tissue (%ID/g). Statistical comparisons were performed between mean organ uptake of ^{68}Ga-NODAGA-JR11 and ^{68}Ga-DOTATOC and between mean organ uptake of ^{68}Ga-NODAGA-JR11 and ^{68}Ga-DOTATATE. P values < 0.05, < 0.01 and < 0.001 were expressed as *, **, and *** respectively.

3.4 Discussion

In this study, we used a human breast cancer cell model with endogenous sstr2 expression to compare tumour uptake of the antagonist ^{68}Ga-NODAGA-JR11 with two routinely used agonists ^{68}Ga-DOTATOC and ^{68}Ga-DOTATATE. Most studies evaluating sstr tracers *in vivo* typically used a rat pancreatic cell model, i.e. AR42J[152], or HEK cells transfected with somatostatin receptors[49,108,109], which may not adequately represent a breast cancer phenotype.

We looked at the transcriptional expression of all five sstr subtypes in ZR-75-1 cells and found predominant expression of sstr2, with negligible expression of the other four subtypes (Figure 3.2). Previous studies have reported a strong correlation between sstr mRNA and protein expression, suggesting that transcriptional studies are sufficient for profiling this receptor family[89,91,153]. Breast carcinoma samples typically overexpress sstr2[89,91,153], however, co-expression of multiple subtypes is common[72,74].

We evaluated the binding affinity of [nat]Ga-DOTATOC, [nat]Ga-DOTATATE and [nat]Ga-NODAGA-JR11 to human sstr2 in a well-established, filtration-based, competition binding assay. For the agonists [nat]Ga-DOTATOC, [nat]Ga-DOTATATE and SRIF-28 control, our inhibition constants (K_i) were 0.9 ± 0.1 nM, 1.4 ± 0.3 nM and 3.7 ± 1.7 nM respectively. Our K_i values were comparable to the IC_{50} values obtained by Reubi *et al.* (K_i values were not reported), which were 2.5 ± 0.50 nM, 0.20 ± 0.04 nM and 2.7 ± 0.30 nM, respectively[154]. As IC_{50} values are dependent on the concentration of substrates used in a specific assay, they are not reproducible between laboratories, and it is recommended that K_i values are calculated. Although [nat]Ga-DOTATATE was reported to have very high affinity to sstr2 (12 fold higher than [nat]Ga-DOTATOC)[154], we did not observe this in

53

our experiments. This may explain, in part, why the diagnostic performance of both peptides is similar in clinical studies, with perhaps a slight advantage for ^{68}Ga-DOTATOC[103]. The binding affinity of the antagonist ^{nat}Ga-NODAGA-JR11 was significantly lower in our studies (K_i = 25.9 ± 0.2 nM) compared to the IC_{50} reported by Fani *et al.* (IC_{50} = 1.2 ± 0.2 nM)[108]. Differences between our studies and literature reports could be partially attributed to different methodology and assay conditions. We used a filtration-based binding assay, whereas others used an autoradiography approach[108,154]. We attempted to minimize the impact of assay conditions by calculating the K_i instead of IC_{50}, and ensured accurate concentration of our tested peptides by performing amino acid analysis. A direct comparison between classical protein binding assays and autoradiography methods would be valuable to improve our understanding of the structure-activity relationship of these ligands.

When evaluated *in vivo*, all compounds targeted the tumour and sstr-positive organs to varying degrees. Tumour uptake was highest for ^{68}Ga-DOTATOC (18.4 ± 2.9 %ID/g), followed by ^{68}Ga-DOTATATE (15.2 ± 2.2 %ID/g, ns) and finally ^{68}Ga-NODAGA-JR11 (12.2 ± 0.8 %ID/g, p < 0.001). In contrast, sstr2 positive organs such as pancreas, adrenals, intestines and stomach showed the highest uptake with ^{68}Ga-DOTATATE.

We wanted to determine if specific activity played a confounding role in our analysis. Unlike enzymes or protein transporters, peptide receptors saturate at lower amounts, which can have an impact on uptake in tumour or receptor-positive organs[155-157]. To reach the minimum activity requirements for PET/CT image acquisition (typically 5 − 10 MBq per mouse) with low specific activity peptides, a higher amount of non-

radioactive compound will also be co-injected. The co-injected unlabeled or cold-standard peptides may compete for binding sites, saturating receptors and effectively decreasing organ uptake[155-157]. De Jong *et al*. demonstrated that ^{111}In-DOTATOC uptake in the tumour and sstr2-positive organs was a function of the total injected peptide amount, and not specific activity directly[157].

A negative correlation between peptide mass and uptake has, in fact, been observed in several studies, with the maximum tumour uptake reached between 10 - 100 pmol/mouse[156,157]. In other sstr2-positive organs, maximum uptake is reached at even lower peptide amounts, presumably due to lower absolute receptor quantities (lower density or more regionally concentrated) in these organs[156,157]. Studies with ^{111}In-DOTATOC in CA20948-bearing rats (sstr-positive rat pancreatic tumour model) evaluated the relationship between tumour uptake and injected peptide mass and found that a dose of 0.5 µg (equivalent to ~30 pmol/mouse) resulted in optimal tumour uptake at 24 h p.i.[157].

In our data set, we found that ^{68}Ga-DOTATOC (highest tumour uptake) and ^{68}Ga-NODAGA-JR11 (lowest tumour uptake) were injected with comparable peptide amounts (33.0 ± 33.5 pmol/mouse and 40.3 ± 21.5 pmol/mouse respectively) allowing for a fair comparison between the two. Interestingly we saw a slight (but statistically significant) negative correlation between uptake and peptide mass in sstr-positive tissues imaged with ^{68}Ga-NODAGA-JR11 (tumour, pancreas, adrenals, intestine) but not those imaged with ^{68}Ga-DOTATOC (Appendix B Figure B.1) indicating that at lower doses, the antagonist might outperform the agonist.

For ^{68}Ga-DOTATATE, the range of injected peptide in this group was very narrow and much lower than the other two tracers (15.6 ± 4.4 pmol/mouse) (Appendix B Figure B.1). We observed that low capacity organs such as pancreas, adrenals, intestine and stomach, but not high capacity sites like the tumour, showed elevated uptake with ^{68}Ga-DOTATATE compared to both ^{68}Ga-DOTATOC and ^{68}Ga-NODAGA-JR11, indicating this might be a peptide-mass effect.

In our studies, tumour-to-blood and tumour-to-muscle ratios were lowest for ^{68}Ga-NODAGA-JR11 (15.6 ± 2.20 and 45.2 ± 11.6 respectively) compared to ^{68}Ga-DOTATOC (41.1 ± 5.68, $p < 0.001$ and 172 ± 55.3, $p < 0.001$ respectively) and ^{68}Ga-DOTA-TATE (44.6 ± 11.7, $p < 0.001$ and 152 ± 60.8, $p < 0.01$ respectively). ^{68}Ga-NODAGA-JR11 had a ~2 fold higher uptake in the blood and muscle compared to the other two agonists, accounting for the lower tumour contrast.

All three tested peptides had predominant renal clearance. Exogenous E2 pellets are known to cause hydronephrosis and urine retention[150,151], thus we expected higher than normal kidney uptake due to the indirect effects of E2.

3.5 Conclusion

To evaluate the feasibility of using antagonist radiotracers for breast cancer diagnosis, we compared the tumour uptake and biodistribution of two well-known agonists, ^{68}Ga-DOTATOC and ^{68}Ga-DOTATATE, and one potent antagonist, ^{68}Ga-NODAGA-JR11, *in vivo* using a human breast cancer xenograft model with endogenous sstr2 expression. We found that ^{68}Ga-DOTATOC had the highest tumour uptake (18.4 ± 2.9 %ID/g), followed by ^{68}Ga-DOTATATE (15.2 ± 2.2 %ID/g) and ^{68}Ga-NODAGA-JR11 (12.21 ± 0.78 %ID/g). The high uptake of ^{68}Ga-NODAGA-JR11 is still surprising,

considering its significantly poorer binding affinity (25.9 ± 0.2 nM compared to 0.9 ± 0.1 for ^{68}Ga-DOTATOC and 1.4 ± 0.3 nM for ^{68}Ga-DOTATATE).

Peptide mass effects may have played a role in this study. Although we injected comparable amounts of ^{68}Ga-DOTATOC and ^{68}Ga-NODAGA-JR11, we noticed a slight (but statistically significant) negative correlation between uptake and injected peptide mass in sstr2-positive tissues (tumour, pancreas, intestine, stomach) for ^{68}Ga-NODAGA-JR11 but not for ^{68}Ga-DOTATOC. Indeed, tracer uptake is a complex function of several concurrent factors including binding affinity, internalization capacity, peptide mass, and receptor density. Although these studies selected ^{68}Ga-DOTATOC as the best tracer, this may not be the case when injecting even smaller peptide doses.

Chapter 4: Synthesis and Preclinical Evaluation of ^{18}F-labeled Ammoniomethyl Trifluoroborate Somatostatin Analogues for Breast Cancer Imaging

4.1 Introduction

[68]Ga is traditionally the isotope of choice for radiolabeling somatostatin analogues due to its convenient generator production (although limited in quantity) and reliable chelator radiochemistry[55]. However, ^{18}F also offers several advantages and in some cases might be preferred to [68]Ga. [18]F is routinely produced in multi Curie amounts in medical cyclotrons, has excellent imaging properties such as high positron emission (97%), low positron energy (0.64 MeV), and an ideal half-life of 110 minutes[62,63]. Compared to [68]Ga ($t_{1/2}$ = 68 min), ^{18}F affords more time for radiolabeling, quality control and distribution of radiopharmaceuticals to other imaging centers[62,63]. However, ^{18}F-fluoride's poor aqueous reactivity has previously limited its use for peptide tracers, as traditional radiolabeling methods required harsh reaction conditions and lengthy multi-step approaches[62-64].

Perrin and colleagues report a simple labeling approach that uses aqueous ^{18}F in an isotope exchange reaction (IEX) to radiolabel an organotrifluoroborate moiety conjugated to the *N*-terminus of the peptide[69,70,146]. In accordance with Aim 2, we used this method to synthesize the non-radioactive standards AmBF$_3$-TOC, AmBF$_3$-TATE and AmBF$_3$-JR11 and evaluated their binding affinity to sstr2. We radiolabeled these constructs with [18]F (Figure 4.1) and performed imaging and biodistribution at both 1 h post-injection (p.i.) and 2 h p.i., along with accompanying *in vitro* internalization assays and *in vivo* plasma stability. Based on recent reports

describing the superiority of antagonists[49,106,108], we hypothesized that ^{18}F-AmBF$_3$-JR11 will be the best tracer for tumour visualization. Furthermore, we believe these studies will highlight the potential of AmBF$_3$-peptides for breast cancer visualization and demonstrate their utility for centres that lack a ^{68}Ga/[68]Ge generator, are close enough to a cyclotron to receive daily ^{18}F shipments, or prefer to work with ^{18}F due to ^{18}F-FDG familiarity.
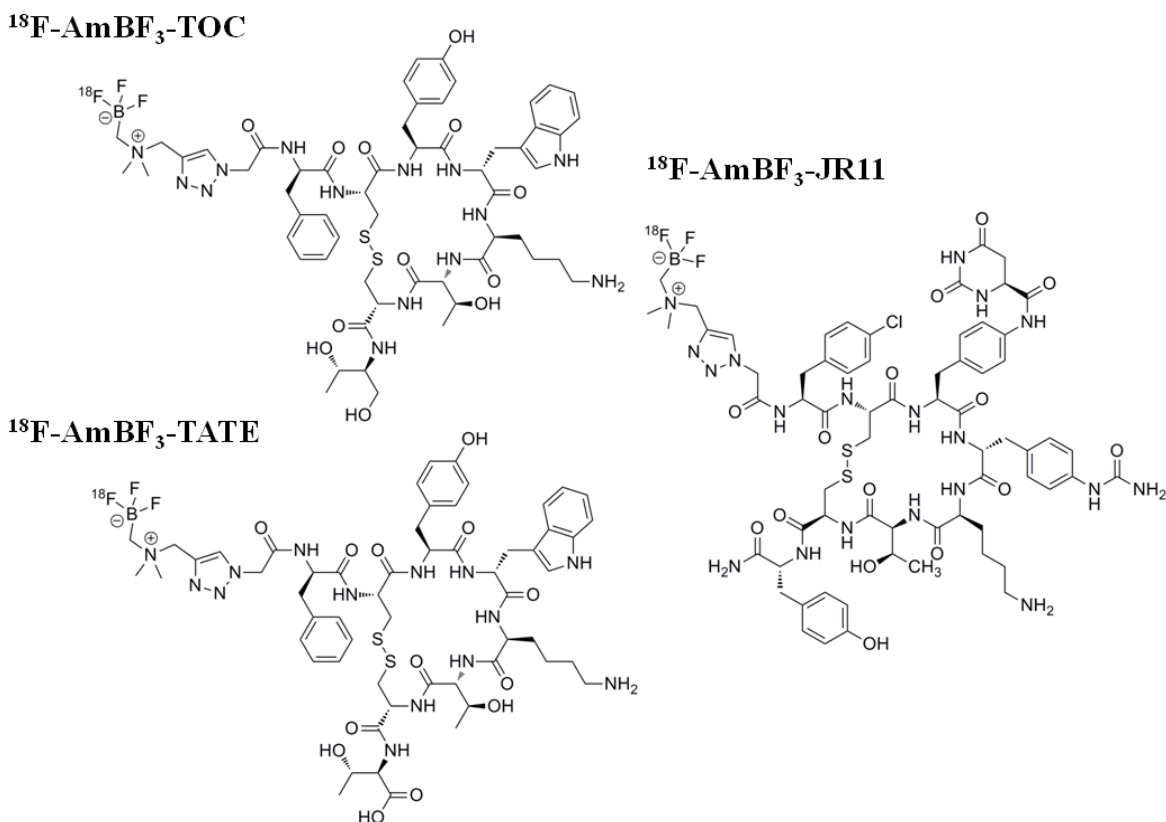
Figure 4.1 Chemical structures of ^{18}F-AmBF$_3$-TOC, ^{18}F-AmBF$_3$-TATE and ^{18}F-AmBF$_3$-JR11

4.2 Materials and Methods

The materials and methods used in this chapter are listed in Chapter 2. Relevant sections are those describing peptide synthesis (Section 2.2), binding affinity (Section 2.3), ^{18}F radiolabeling (Section 2.4.2), internalization assay (Section 2.5), cell culture (Section 2.7), 17β-

59

estradiol pellet implant and tumour inoculation (Section 2.8.1), *in vivo* plasma stability (Section 2.8.2), biodistribution (Section 2.8.3), PET/CT imaging (Section 2.8.4) and statistics (Section 2.9).

4.3 Results

4.3.1 Chemistry and Radiochemistry

Peptides were successfully synthesized on solid support and modified with an azide at the *N*-terminus. Radiolabeling of ^{18}F-AmBF$_3$-JR11, ^{18}F-AmBF$_3$-TOC and ^{18}F-AmBF$_3$-TATE was achieved in > 97% radiochemical purity, 55.5 ± 18.5 to 122.1 ± 62.9 MBq/nmol specific activity and 13 ± 5 to 28 ± 9% decay-corrected radiochemical yield (RCY). The chemical structures of the three radiotracers are shown in Figure 4.1, and individual radiochemical data is summarized in Table 4.1.

Table 4.1 Radiochemistry and *in vivo* plasma stability results for compounds ^{18}F-AmBF$_3$-JR11, ^{18}F-AmBF$_3$-TOC and ^{18}F-AmBF$_3$-TATE.

Tracer	RCY (%) (n = 4)	Radiochemical Purity (%) (n = 4)	Specific Activity (MBq/nmol) (n = 4)	Plasma Stability (% Intact) 5 min (n = 2)	15 min (n = 2)
^{18}F-AmBF$_3$-JR11	18 ± 7	99 ± 1	55.5 ± 18.5	> 95	> 95
^{18}F-AmBF$_3$-TOC	13 ± 5	97 ± 1	55.5 ± 3.7	> 95	> 95
^{18}F-AmBF$_3$-TATE	28 ± 9	97 ± 2	122.1 ± 62.9	> 95	> 95

4.3.2 *In Vitro* Binding Affinity and Internalization Studies

All trifluoroborate-modified peptides retained their *in vitro* binding affinity to sstr2. Representative inhibition curves are illustrated in Figure 4.2. SRIF-28 was run as a control under the same assay conditions and had an inhibition constant (K_i) of 3.7 ± 1.7 nM (n = 5). AmBF$_3$-

TATE had the highest binding affinity, with a K_i of 0.6 ± 0.3 nM, followed by AmBF$_3$-TOC (1.3 $\pm$ 0.2 nM, ns) and lastly AmBF$_3$-JR11 (18.8 $\pm$ 1.0 nM, p < 0.001).
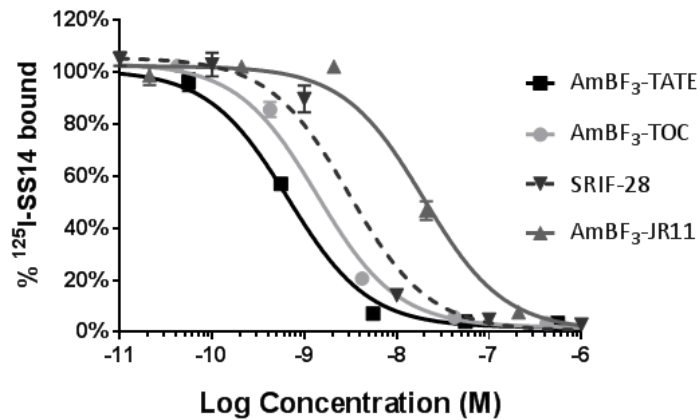
Figure 4.2 Representative competition binding assays of ^{18}F radiotracers. AmBF$_3$-TATE, AmBF$_3$-TOC, AmBF$_3$-JR11 and SRIF-28 control were run with competing radioactive ligand ^{125}I-SRIF14 and human-sstr2 purified membranes.

In vitro internalization assays confirmed that radiotracers ^{18}F-AmBF$_3$-TOC and ^{18}F-AmBF$_3$-TATE maintained agonist activity, and localized to both surface and internalized cell fractions. ^{18}F-AmBF$_3$-JR11 was predominantly found on the cell surface, indicating antagonist activity (see Figure 4.3).
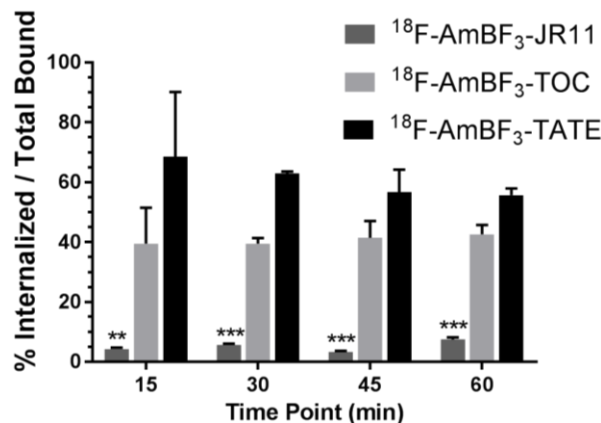
Figure 4.3 Internalized fractions of ^{18}F-AmBF$_3$-JR11, ^{18}F-AmBF$_3$-TOC and ^{18}F-AmBF$_3$-TATE on ZR-75-1 cells. ** p < 0.01, *** < p < 0.001

61

4.3.3 *In Vivo* Plasma Stability

All three radiotracers demonstrated excellent *in vivo* plasma stability, with > 95% of the compound stable at 15 min p.i. (see Table 4.1 for results, and Figure 4.4 for representative radio-HPLC chromatograms of mouse plasma). This analysis could not be performed at later time points, as peptide radiotracers clear rapidly from circulation and thus would not be detected at longer time points.
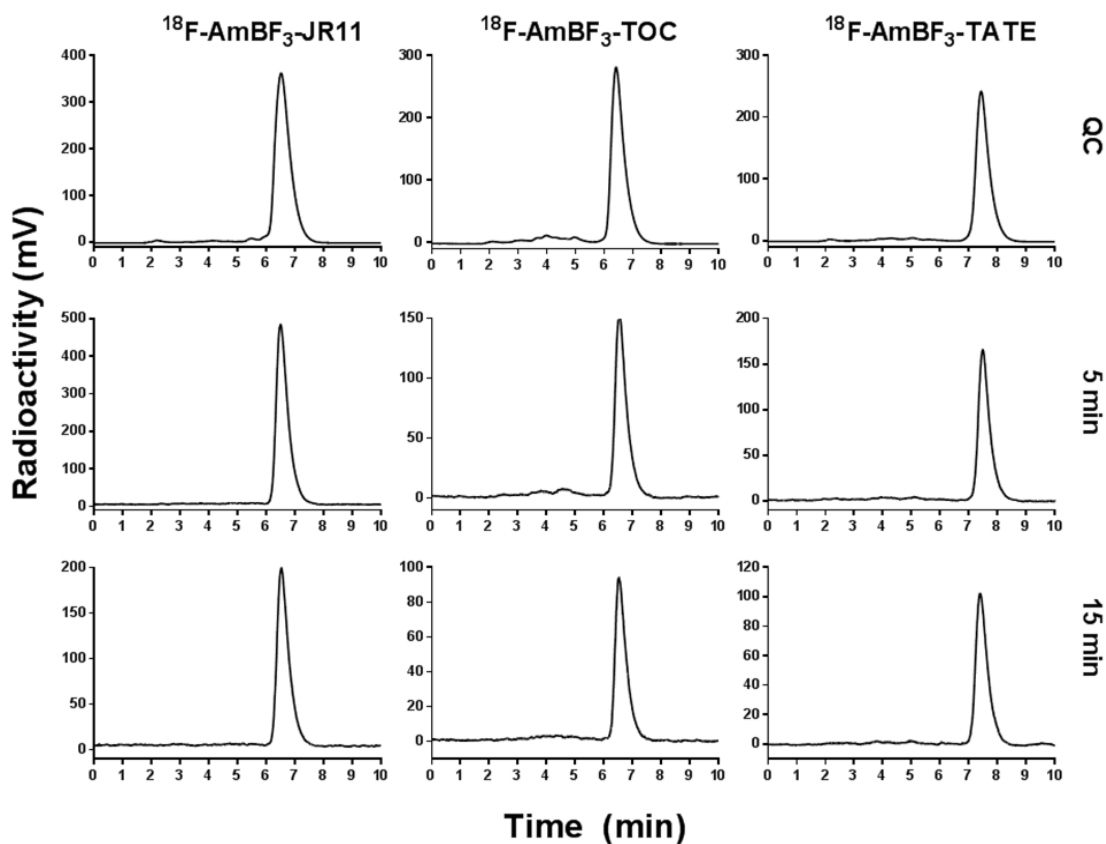
Figure 4.4 Representative radio-HPLC chromatographs of plasma samples collected from mice treated with ^{18}F tracers at 5 min and 15 min p.i. Columns (from left to right) represent tracers ^{18}F-AmBF$_3$-JR11, ^{18}F-AmBF$_3$-TOC and ^{18}F-AmBF$_3$-TATE. Rows (from top to bottom) represent tracer quality control (QC), 5 min time point and 15 min time point.

4.3.4   Tumour and Organ Uptake

All three tracers successfully targeted sstr-positive organs such as tumour, pancreas, stomach, intestine, adrenal glands and lung[158-160]; see Figure 4.5, Figure 4.6 and Table 4.2 for biodistribution results. At 1 h p.i., tumour uptake was highest for ^{18}F-AmBF$_3$-JR11 (13.4 ± 2.15 %ID/g) compared to ^{18}F-AmBF$_3$-TOC (9.96 ± 3.69 %ID/g, ns) and ^{18}F-AmBF$_3$-TATE (10.2 ± 3.26 %ID/g, ns) (Figure 4.6). At 2 h p.i, tumour uptake was highest for ^{18}F-AmBF$_3$-TATE (15.3 ± 3.24 %ID/g), followed by ^{18}F-AmBF$_3$-JR11 (13.1 ± 3.47 %ID/g, ns) and ^{18}F-AmBF$_3$-TOC (11.9 ± 2.63 %ID/g, ns) (Figure 4.6). As expected, all three radiotracers progressively cleared from background organs, resulting in improved tumour contrast at 2 h p.i. compared to 1 h p.i. (Figure 4.7). At the later time point, both agonists ^{18}F-AmBF$_3$-TOC and ^{18}F-AmBF$_3$-TATE showed significantly better contrast compared to the antagonist ^{18}F-AmBF$_3$-JR11 (Figure 4.7 and Table 4.2). At 2 h p.i. tumour-to-blood and tumour-to-muscle ratios were 36.9 ± 4.5 and 100 ± 9.5 respectively for ^{18}F-AmBF$_3$-JR11, compared to 63.5 ± 11.3 ($p < 0.05$) and 230 ± 46.2 ($p < 0.01$) for ^{18}F-AmBF$_3$-TOC and 76.4 ± 20.5 ($p < 0.001$) and 187 ± 85.7 ($p < 0.05$) for ^{18}F-AmBF$_3$-TATE.

A co-injection of excess non-radioactive standard resulted in a tumour blocking efficiency of 86 − 96% for all three radiotracers, indicating tracer specificity. *In vivo* de-fluorination was minimal, indicated by the low bone uptake (< 0.31 %ID/g). See Figure 4.5 for PET/CT images of mice injected with the three tested compounds.
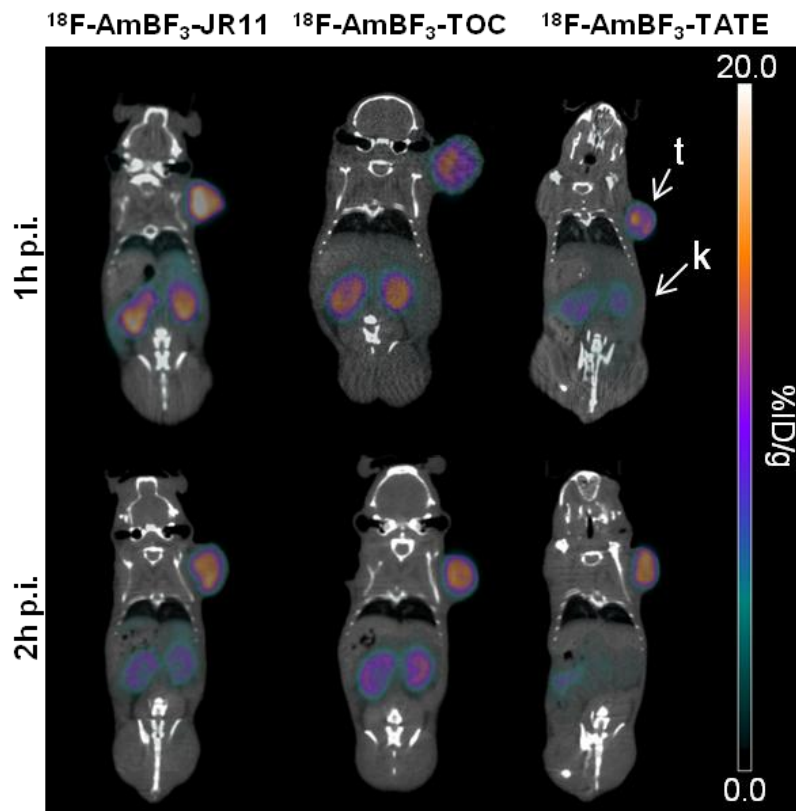
Figure 4.5 Coronal PET/CT images of 6 different ZR-75-1 tumour bearing mice injected with ^{18}F-AmBF$_3$-JR11, ^{18}F-AmBF$_3$-TOC and ^{18}F-AmBF$_3$-TATE and imaged 1 and 2 h p.i. t = tumour, k = kidneys.
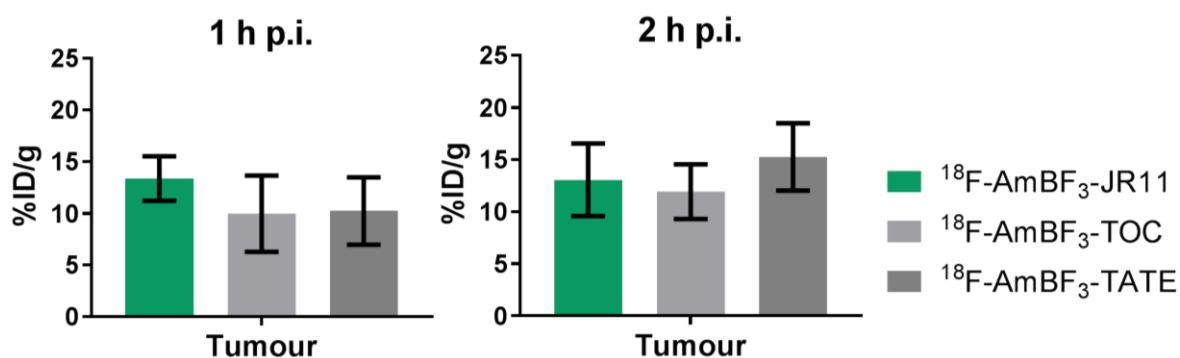
Figure 4.6 ZR-75-1 tumour uptake with ^{18}F radiotracers at 1 h and 2 h p.i. No statistical differences found between any groups.

Figure 4.7 Background uptake and tumour ratios with ^{18}F-radiotracers at 1 h p.i. and 2 h p.i. Kidney uptake at both 1 h and 2 h p.i. is significantly lower for ^{18}F-AmBF$_3$-TATE compared to both other radiotracers. Uptake with ^{18}F-AmBF$_3$-JR11 at 2 h p.i. is slightly higher in blood and muscle compared to the other two tracers. * $p < 0.05$, *** $p < 0.001$.

Table 4.2 Biodistribution of ^{18}F-AmBF$_3$-JR11, ^{18}F-AmBF$_3$-TOC and ^{18}F-AmBF$_3$-TATE at 1 and 2 h p.i. in ZR-75-1 tumour bearing mice. Uptake is expressed as mean ± SD in units of %ID/g.

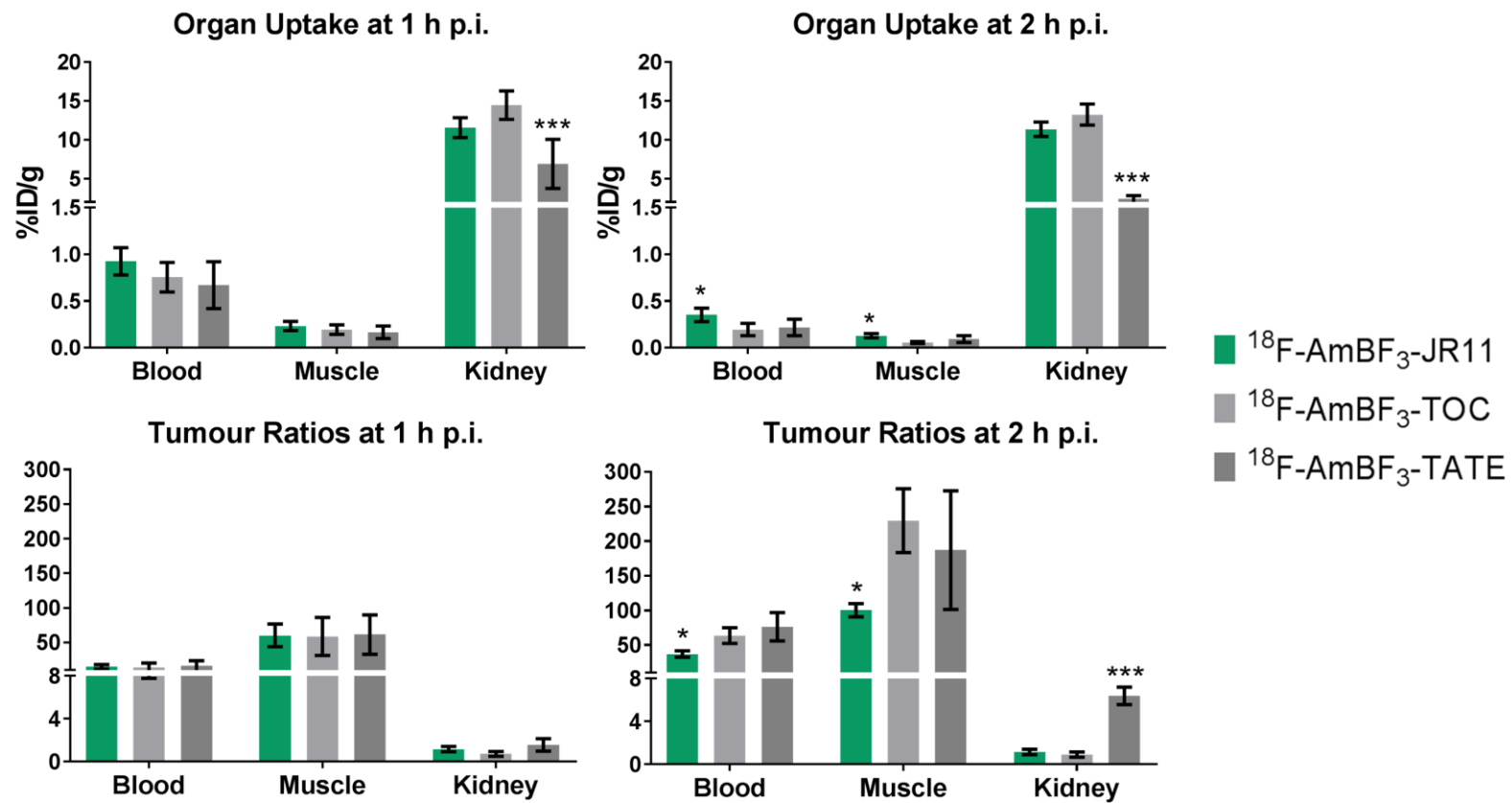|	^{18}F-AmBF$_3$-JR11			^{18}F-AmBF$_3$-TOC			^{18}F-AmBF$_3$-TATE		
	1h p.i (n=9)	2h p.i. (n=6)	1h p.i. Blocked (n=4)	1h p.i. (n=12)	2h p.i. (n=6)	1h p.i. Blocked (n=3)	1h p.i. (n=11)	2h p.i. (n=6)	1h p.i. Blocked (n=3)
Blood	0.93 ± 0.15	0.35 ± 0.07	0.84 ± 0.25	0.76 ± 0.16	0.20 ± 0.06	2.90 ± 1.78	0.67 ± 0.25	0.22 ± 0.09	0.54 ± 0.10
Fat	0.21 ± 0.04	0.11 ± 0.02	0.30 ± 0.12	0.21 ± 0.09	0.06 ± 0.02	0.39 ± 0.04	0.20 ± 0.09	0.13 ± 0.13	0.09 ± 0.01
Uterus	1.12 ± 0.13	0.53 ± 0.08	1.12 ± 0.14	0.77 ± 0.21	0.21 ± 0.05	1.66 ± 0.37	0.64 ± 0.19	0.28 ± 0.07	0.51 ± 0.07
Intestine	3.94 ± 0.37	4.77 ± 0.80	2.50 ± 1.21	3.25 ± 0.47	4.43 ± 0.76	3.51 ± 0.08	3.19 ± 0.80	6.00 ± 1.28	1.85 ± 0.21
Stomach	2.03 ± 0.97	1.86 ± 1.04	0.21 ± 0.07	1.08 ± 0.42	1.23 ± 0.28	0.39 ± 0.07	1.85 ± 1.25	3.63 ± 1.55	0.31 ± 0.32
Pancreas	14.2 ± 4.64	8.75 ± 1.78	0.34 ± 0.08	4.41 ± 1.65	3.31 ± 0.87	0.58 ± 0.02	10.8 ± 7.48	12.4 ± 2.72	0.16 ± 0.06
Spleen	0.59 ± 0.09	0.50 ± 0.13	0.47 ± 0.15	0.45 ± 0.10	0.22 ± 0.08	0.70 ± 0.10	0.30 ± 0.09	0.18 ± 0.02	0.14 ± 0.03
Kidneys	11.6 ± 1.28	11.3 ± 0.93	12.5 ± 3.37	14.4 ± 1.82	13.2 ± 1.36	33.8 ± 10.5	6.89 ± 3.16	2.40 ± 0.43	5.09 ± 0.91
Adrenals	2.62 ± 0.81	1.65 ± 0.86	0.57 ± 0.24	2.24 ± 0.97	2.05 ± 0.65	0.98 ± 0.09	2.47 ± 1.49	3.47 ± 1.16	0.25 ± 0.03
Liver	3.83 ± 0.50	3.40 ± 0.12	2.86 ± 1.15	0.87 ± 0.08	0.46 ± 0.09	1.59 ± 0.07	0.59 ± 0.17	0.32 ± 0.07	0.36 ± 0.01
Lungs	7.23 ± 2.04	3.75 ± 0.48	1.35 ± 1.17	4.44 ± 2.50	5.47 ± 1.53	2.98 ± 0.36	6.17 ± 4.76	6.31 ± 2.78	0.60 ± 0.12
Heart	0.43 ± 0.16	0.26 ± 0.06	0.38 ± 0.12	0.39 ± 0.10	0.13 ± 0.04	0.67 ± 0.13	0.30 ± 0.09	0.17 ± 0.04	0.19 ± 0.04
Tumour	**13.4 ± 2.15**	**13.1 ± 3.47**	**1.52 ± 1.17**	**9.96 ± 3.69**	**11.9 ± 2.63**	**1.40 ± 0.08**	**10.2 ± 3.26**	**15.3 ± 3.24**	**0.36 ± 0.15**
Muscle	0.23 ± 0.05	0.13 ± 0.02	0.18 ± 0.07	0.19 ± 0.05	0.05 ± 0.01	0.55 ± 0.14	0.17 ± 0.07	0.09 ± 0.04	0.11 ± 0.01
Bone	0.31 ± 0.10	0.26 ± 0.05	0.19 ± 0.17	0.31 ± 0.08	0.14 ± 0.01	0.56 ± 0.00	0.22 ± 0.13	0.15 ± 0.03	0.18 ± 0.02
Brain	0.03 ± 0.01	0.02 ± 0.00	0.26 ± 0.29	0.03 ± 0.01	0.02 ± 0.00	0.05 ± 0.01	0.04 ± 0.02	0.03 ± 0.00	0.02 ± 0.00
Tumour to Background Ratios									
Blood	14.8 ± 3.15	36.9 ± 4.54	1.89 ± 1.24	14.0 ± 6.22	63.5 ± 11.3	0.61 ± 0.31	16.1 ± 7.45	76.4 ± 20.5	0.65 ± 0.17
Muscle	60.2 ± 16.4	100 ± 9.53	10.9 ± 9.47	58.7 ± 27.6	230 ± 46.2	2.71 ± 0.85	61.6 ± 28.5	187 ± 85.7	3.31 ± 1.36
Kidney	1.17 ± 0.24	1.14 ± 0.25	0.13 ± 0.09	0.73 ± 0.23	0.91 ± 0.25	0.05 ± 0.02	1.57 ± 0.58	6.38 ± 0.82	0.07 ± 0.02

4.4   Discussion

The AmBF$_3$ method was previously used to synthesize several tracers, including ^{18}F-AmBF$_3$-TATE, which showed high tumour uptake at 1 h p.i. ($10.11 \pm 1.67\%$ID/g) in the AR42J rat pancreatic tumour model[146]. Herein, we report two additional sstr2-targeting radiotracers, ^{18}F-AmBF$_3$-TOC and ^{18}F-AmBF$_3$-JR11 and compared them to ^{18}F-AmBF$_3$-TATE in the human breast cancer xenograft, ZR-75-1. We hypothesized that the antagonist ^{18}F-AmBF$_3$-JR11 would show the highest tumour uptake and contrast among the three peptides.

We assessed the *in vitro* binding affinity of the three non-radioactive standards to sstr2 and found that AmBF$_3$-TATE and AmBF$_3$-TOC maintained high binding affinity, with a K_i of 0.6 ± 0.3 nM and 1.3 ± 0.2 nM respectively; both having better affinities then the endogenous ligand SRIF-28 ($K_i = 3.7 \pm 1.7$ nM). AmBF$_3$-JR11 had a much lower binding affinity ($K_i = 18.8 \pm 1.0$ nM, $p < 0.001$) than both AmBF$_3$-TOC and AmBF$_3$-TATE. This affinity is also lower than that reported by Fani *et al.* for DOTA-JR11 ($IC_{50} = 0.72 \pm 0.12$ nM) but comparable to ^{nat}Ga-DOTA-JR11 ($IC_{50} = 29 \pm 2.7$ nM)[108]. Despite poor binding affinity, Fani *et al.* showed that tumour uptake with ^{68}Ga-DOTA-JR11 was still promising, and in fact, higher than with high-affinity agonist ^{68}Ga-DOTATATE[108]. As hypothesized by others, it is possible that the number of receptor sites available for antagonist binding can compensate for lower binding affinity, resulting in high tumour uptake[49,50,52,105].

We used a cell-based internalization assay to validate the agonist/antagonist identity of our AmBF$_3$-modified peptides. ^{18}F-AmBF$_3$-TOC and ^{18}F-AmBF$_3$-TATE maintained their agonist capacity, and internalized into the ZR-75-1 cells as early as 15 min post-treatment. Similarly, ^{18}F-AmBF$_3$-JR11 remained an antagonist, and was not able to internalize into the cytoplasm (Figure 4.3).

We evaluated our ^{18}F-labed radiotracers *in vivo* at both 1 h and 2 h p.i. in ZR-75-1 tumour bearing mice. All three compounds targeted sstr-positive tissues such as tumour, pancreas, and adrenal glands with high and specific uptake. At 1 h p.i., tumour uptake was highest for ^{18}F-AmBF$_3$-JR11 (13.4 ± 2.15 %ID/g) compared to ^{18}F-AmBF$_3$-TATE (10.3 ± 3.26 %ID/g) and ^{18}F-AmBF$_3$-TOC (9.96 ± 3.69%ID/g), although differences were not statistically significant (see Figure 4.6). Despite low binding affinity, ^{18}F-AmBF$_3$-JR11 uptake was comparable to ^{18}F-AmBF$_3$-TOC and ^{18}F-AmBF$_3$-TATE, in line with the current model of antagonist binding. Tumour-to-normal-tissue ratios were comparable among all three tracers at 1 h p.i. (Figure 4.7).

We evaluated the metabolic stability of all three radiotracers, and found that all had excellent *in vivo* plasma stability (> 95% intact after 15 min p.i.) suggesting that imaging at a longer time point is feasible and could result in better tumour contrast. At 2 h p.i., tumour uptake was 15.3 ± 3.24 %ID/g for ^{18}F-AmBF$_3$-TATE, followed by 13.1 ± 3.47 %ID/g for ^{18}F-AmBF$_3$-JR11 and 11.9 ± 2.63 %ID/g for ^{18}F-AmBF$_3$-TOC (not statistically significant). All tracers showed significantly higher tumour-to-background radios from 1 h to 2 h p.i. due to wash-out from non-specific binding sites (Figure 4.7).

Similar to the ^{68}Ga-derivatives discussed in Chapter 3, we were interested in analysing the effects of injected mass on the biodistribution of ^{18}F-labelled tracers. For 1 h p.i. studies, ^{18}F-AmBF$_3$-TOC, ^{18}F-AmBF$_3$-TATE and ^{18}F-AmBF$_3$-JR11 were injected in comparable amounts (152.5 ± 116.6, 95.9 ± 77.5 and 111.5 ± 76.1 pmol/mouse respectively), enabling an accurate comparison between radiotracers. Similar to ^{68}Ga-DOTATOC, we found that ^{18}F-AmBF$_3$-TOC tumour uptake was the most tolerant to peptide mass differences, while ^{18}F-AmBF$_3$-JR11 and

^{18}F-AmBF$_3$-TATE showed a saturation effect in tumour and other sstr-positive organs (Appendix B, Figure B.2).

At 2 h p.i., ^{18}F-AmBF$_3$-JR11 no longer had the highest tumour uptake (although differences were not statistically significant). In line with this observation, the injected peptide content of ^{18}F-AmBF$_3$-JR11 was higher (94.3 ± 33.85 pmol/mouse) than that of ^{18}F-AmBF$_3$-TOC (53.6 ± 25.3 pmol/mouse, p < 0.05) and ^{18}F-AmBF$_3$-TATE (23.5 ± 10.3 pmol/mouse, p < 0.001), possibly accounting for the lower tumour uptake. Although all radiotracers were HPLC-purified to achieve the highest possible specific activity, variability in radiolabeling reactions resulted in differences in specific activities for 2 h p.i. experiments, and therefore differences in amounts of co-injected cold peptide. Therefore, a direct comparison of tumour uptake at this later time point is not possible. These studies still provide valuable information on the uptake in background organs, which did not appear to be mass dependant in our studies (data not shown) or other reports[157,161].

Overall, we found that background uptake at 2 h p.i. was generally higher with ^{18}F-AmBF$_3$-JR11 compared to the other two tracers (Figure 4.7). Blood uptake was 0.35 ± 0.15 %ID/g with ^{18}F-AmBF$_3$-JR11 compared to 0.20 ± 0.06 %ID/g for ^{18}F-AmBF$_3$-TOC (p < 0.01) and 0.22 ± 0.09 %ID/g for ^{18}F-AmBF$_3$-TATE (p < 0.05). Muscle uptake was lowest for ^{18}F-AmBF$_3$-TOC (0.05 ± 0.01 %ID/g, p < 0.05), and kidney uptake was lowest for ^{18}F-AmBF$_3$-TATE (2.40 ± 0.043 %ID/g, p < 0.001). Liver uptake was significantly higher with ^{18}F-AmBF$_3$-JR11 at both 1 h and 2 h p.i. (3.83 ± 0.50 %ID/g, p < 0.001 and 3.40 ± 0.12 %ID/g, p < 0.001 respectively), which, in a clinical setting, could compromise the visibility of sstr-positive metastases in the liver (common for both NETs[79] and breast cancers[162]).

The excretion profile of all three tracers is predominantly renal, resulting in high kidney uptake (7-14 %ID/g at 1 h p.i.). Our animals were treated with exogenous E2 pellets to support the growth of the ER-positive tumour, which are known to cause hydronephrosis and urine retention[150,151]. Thus, we expect kidney and bladder uptake to be unusually high. ^{18}F-AmBF$_3$-TATE had the lowest kidney uptake at both 1 h p.i. (6.89 ± 3.16 %ID/g, $p < 0.001$), and 2 h p.i. (2.40 ± 0.43 %ID/g, $p < 0.001$). A fast wash-out from excretory organs, as seen with ^{18}F-AmBF$_3$-TATE is favorable, especially for patients with renal sensitivities.

4.5   Conclusion

We evaluated three ^{18}F-radiolabeled somatostatin analgoues for breast cancer visualization and found that the two agonists ^{18}F-AmBF$_3$-TOC and ^{18}F-AmBF$_3$-TATE and one antagonist ^{18}F-AmBF$_3$-JR11 were very comparable in terms of tumour uptake and contrast. At 1 h p.i. ^{18}F-AmBF$_3$-JR11 had the highest tumour uptake (13.4 ± 2.15 %ID/g), followed by ^{18}F-AmBF$_3$-TATE (10.3 ± 3.26 %ID/g) and ^{18}F-AmBF$_3$-TOC (9.96 ± 3.69 %ID/g). All tracers were stable *in vivo* and tumour uptake was sustained at 2 h p.i. ^{18}F-AmBF$_3$-JR11 (similar to ^{68}Ga-NODAGA-JR11) suffers from increased non-specific uptake in background organs, compromising tumour contrast. Overall, we did not find imaging with the antagonist ^{18}F-AmBF$_3$-JR11 to be superior then with the other two agonists. However, we did find that ^{18}F-AmBF$_3$-TATE had lower kidney uptake, and could provide an advantage to patients with renal sensitivities or those intolerant to amino acid treatment.

Chapter 5: Conclusion and Future Direction

5.1 Significance and Summary of Results

Our studies were motivated by the long-standing knowledge that breast cancers overexpress sstr2, and could hence be imaged using somatostatin analogs[87-93]. Breast cancers with high sstr expression have a Luminal A molecular profile and are ER/PR-positive[163,164]. Imaging with sstr analogues can provide surrogate information on the cancer phenotype, monitor response to anti-hormone therapies, and determine the extent of metastatic disease to sentinel and auxiliary lymph nodes. We believe that somatostatin analogues radiolabeled with PET isotopes would be promising imaging agents for breast cancer visualization.

Most somatostatin analogues are labeled with the radio-metal ^{68}Ga, although ^{18}F has many desirable properties, and in some cases might be preferred. While both ^{68}Ga and ^{18}F have short half-lives well-matched with peptide pharmacokinetics, ^{18}F has a lower positron range enabling better image resolution[62]. Additionally, ^{18}F is readily produced in all nuclear medicine facilities equipped for ^{18}F-FDG production, and by virtue of its slightly longer half-life, can also be distributed from a centralized radio-pharmacy to other imaging centres nearby[62].

The main objectives of this thesis were to compare agonists and antagonist radiotracers labeled with ^{68}Ga and ^{18}F for breast cancer imaging. We hypothesized that agonists TOC and TATE and antagonist JR11 can be radiolabeled with ^{68}Ga and ^{18}F, and that antagonist radiotracers will have a higher tumour uptake in breast cancer xenografts (ZR-75-1 cell line) compared to agonists.

Our first aim was to synthesize compounds ^{68}Ga-DOTATOC, ^{68}Ga-DOTATATE and ^{68}Ga-NODAGA-JR11, and compare their tumour uptake and biodistribution in ZR-75-1 tumour

71

bearing mice. As described in Chapter 3, the three compounds were achieved in high radiochemical yield, purity and specific activity. When evaluated *in vivo*, ^{68}Ga-DOTATOC had the highest tumour uptake, followed by ^{68}Ga-DOTATATE and finally by ^{68}Ga-NODAGA-JR11. Tumour-to-background-tissue ratios were significantly higher with agonist compared to the antagonist.

Our second aim was to use the AmBF$_3$ method described by Perrin and colleagues[69] to synthesize and radiolabel compounds ^{18}F-AmBF$_3$-TOC, ^{18}F-AmBF$_3$-TATE and ^{18}F-AmBF$_3$-JR11 (Chapter 4). All three compounds showed excellent metabolic stability, with > 95% of the radiolabeled compounds intact after 15 min in mouse circulation. This enabled sustained tumour uptake at 2 h p.i. The antagonist ^{18}F-AmBF$_3$-JR11 had similar tumour uptake, and tumour-to-background ratios compared to agonists ^{18}F-AmBF$_3$-TOC and ^{18}F-AmBF$_3$-TATE at 1 h p.i. Due to differences in injected mass, we could not properly compare tumour uptake at 2 h p.i., however we did notice that uptake in background organs was higher with ^{18}F-AmBF$_3$-JR11 compare to the other two, potentially compromising tumour contrast.

We accept our first hypothesis, namely that somatostatin analogs TOC, TATE and JR11 can be radiolabeled with ^{68}Ga and ^{18}F in sufficiently high yield, purity and specific activity to enable imaging. We could not accept our second hypothesis, stating that ZR-75-1 tumour uptake is higher in mice imaged with antagonist analogues compared to agonists. In Chapter 3 we observed that ^{68}Ga-NODAGA-JR11 had the lowest tumour uptake and contrast compared to the other two agonists; in Chapter 4 we found all three ^{18}F-peptides to be comparable. We do not deny that antagonists are superior to agonists for tumour imaging, but perhaps the difference is not as striking in this tumour model. The high tumour uptake of antagonists ^{68}Ga-NODAGA-JR11 and ^{18}F-AmBF$_3$-JR11 is still surprising, considering their low binding affinity. Further

evaluation of binding affinity, normalization of injected peptide mass and validation of *in vivo* sstr2 expression levels will be important, as addressed in the limitations section below.

5.2 Thesis Limitations

Based on previous literature reports, we did not expect to find such low sstr2 binding affinity for our JR11-based peptides. The K_i of ^{nat}Ga-NODAGA-JR11 and AmBF$_3$-JR11 in our studies was 25.8 ± 0.2 nM and 18.8 ± 1.0 nM respectively, which is 7.0-fold and 5.1-fold higher than the K_i for SRIF-28 (3.7 ± 1.7 nM). In contrast, previous studies using an autoradiography approach reported an IC$_{50}$ of 0.7 ± 0.1 nM for DOTA-JR11[107] and 1.2 ± 0.2 nM for ^{nat}Ga-NODAGA-JR11[108], which is 3.9-fold and 2.3-fold lower than the IC$_{50}$ observed for SRIF-28 (2.7 ± 0.3 nM)[154] using the same method. Although unlikely, it could be hypothesized that our JR11 based probes were structurally different than those reported in literature, leading to the lower binding affinity and tumour uptake. The JR11 peptide and ^{68}Ga-NODAGA-JR11 radiotracer were prepared according to literature procedures, molecular weights were validated by mass spectroscopy, and the stereochemistry of in-house modified amino acids (Aph(Hor) and D-Aph(Cbm)) was confirmed using an optical rotation test. It is more likely that differences in binding affinity are due to the different assay methods. We used a membrane filtration assay (explained in Section 2.3), however previous studies use an autoradiography approach. A direct comparison between these two methods will be valuable in elucidating the inconsistencies observed in binding affinity (Figure 5.1). We have worked towards this goal in our lab, however, we experienced low and unspecific binding of our referenced radioactive ligand ^{125}I-Tyr^{11}-SRIF14 to sstr2-positive tumour sections. More work is needed towards optimizing assay conditions, potentially using the radioactive ligand ^{125}I-[Leu^8, D-Trp^{22}, Tyr^{25}]-somatostatin-28, employed in most autoradiography applications reported in literature[107,108,154].

Membrane Filtration

Add to each well:

- 0.05 nM ^{125}I-SRIF14
- 25 µg membranes (overexpressing sstr2)
- 0.001 – 100 nM ligand

Incubate at 27 °C, 1 h

filter-bottom plate

Attach plate to vacuum manifold and wash each well with excess buffer to remove unbound ligand

Remove each filter and count individually in gamma counter

Autoradiography

20 µm-thick cryostat sections of cell membrane pellets on glass slides (prepared from sstr overexpressing cell line)

Add to each section:

- 15,000 cpm/100µL ^{125}I-[Leu^8, D-Trp^{22}, Tyr^{25}]-SRIF28
- 0.1 – 1000 nM ligand

Incubate at room temperature, 2 h

Wash with buffer and expose to X-ray film (7 d) in light tight cassette

Quantify intensity using computer-assisted image processing system

Figure 5.1 Methodological differences between competition binding assays done using filtration versus autoradiography methods. Autoradiography information (right panel) was based on methods described by Fani *et al.*[108].

When evaluating tumour and organ uptake of peptide radiopharmaceuticals, it is important to also consider the total mass of injected peptide[155,156]. When imaging relatively low-density target systems, such as peptide receptors, the degree of receptor-occupancy will influence tumour uptake, especially when receptors approach saturation[155,156]. As a general rule, tumour uptake will increase with decreasing peptide mass, up to a limit of 10-100 pmol per mouse[156]. We observed saturation effects with ^{68}Ga-NODAGA-JR11, ^{18}F-AmBF$_3$-TOC, ^{18}F-AmBF$_3$-JR11

and ^{18}F-AmBF$_3$-TATE in tumour and sstr2-positive organs such as pancreas, adrenals, intestine and stomach (Appendix B, Figures B.1, B.2 and B.3). In future studies, normalizing the injected peptide content between animals will enable direct comparisons between tracers with comparable receptor-occupancy levels.

Finally, we did not fully consider the functional relationship between 17β-estradiol (E2) and sstr2 expression. The ZR-75-1 breast cancer model used in our studies is ER-positive and requires exogenous E2 administration to grow *in vivo*. We used subcutaneously implanted slow-release E2 pellets to sustain tumour growth *in vivo*. Although pellets are intended to deliver a steady amount of E2, Ingburg *et al.* observed that mice treated with high-dose pellets, such as the ones used in our studies, showed very high variability in E2 plasma levels week-to-week[151]. This variability may have affected the sstr2 expression levels on ZR-75-1 cells *in vivo*. Previous studies have reported on the upregulation of sstr2 mRNA in response to E2 in ZR-75-1 cells[96,97,165], however, no upregulation was seen at the protein level[96,165]. In future studies it is recommended to validate the sstr2 protein levels of ZR-75-1 xenografts by flow cytometry or western blotting at the time of imaging to ensure consisted sstr2 expression between different radiotracer groups.

5.3 Future Direction

5.3.1 Peptide Receptor Radionuclide Therapy in Breast Cancer

Therapy with ^{177}Lu-DOTATATE and ^{177}Lu-DOTA-JR11 has been compared in both animal models[115], and pilot clinical studies[106]. Both studies demonstrated that the antagonist ^{177}Lu-DOTA-JR11 delivered a higher radiation dose to the tumour compared to the agonist ^{177}Lu-DOTATATE. We have shown that ZR-75-1 tumour xenografts can be successfully targeted with diagnostic somatostatin radiotracers, however, we have yet to evaluate the

therapeutic potential of ^{177}Lu-labeled somatostatin compounds in the same model. As ^{68}Ga-DOTATOC showed the highest tumour uptake in our ZR-75-1 studies at 1 h p.i., a comparison between ^{177}Lu-DOTATOC and ^{177}Lu-DOTA-JR11 would be worthwhile. ZR-75-1 tumour xenografts can be grown as reported herein, although care must be taken to ensure consistent pellet doses and validation of sstr2 protein expression. Biodistribution studies can be performed with ^{177}Lu-DOTATOC and ^{177}Lu-DOTA-JR11 at different time points. As ^{177}Lu has a long half-life ($t_{1/2}$ = 6.7 d), SPECT imaging and biodistribution can be done as early as 4 h p.i. and up to 7 d p.i. Dalm and colleagues demonstrated that a peptide dose of 0.5µg/30MBq resulted in the highest absorbed tumour dose[115]. For treatment studies, mice can be administered a single dose of 0.5 µg ^{177}Lu-radiotracer once tumours reach ~500 mm^3 in volume. Monitoring of tumour size, mouse weight and general health status can be done daily until a humane end-point is reached.

5.3.2 Clinical Translation of ^{18}F-AmBF$_3$-TATE

All three ^{18}F-radiolabeled tracers described in Chapter 4 would be excellent candidates for clinical translation, as all had comparable tumour uptake, low background and excellent *in vivo* tracer stability. Because ^{18}F-AmBF$_3$-TATE showed the fastest kidney wash-out, and significantly lower liver uptake than ^{18}F-AmBF$_3$-JR11, ^{18}F-AmBF$_3$-TATE should be the first of such tracers to be pursued for clinical translation, as imaging would result in a lower dose-burden for patients.

To obtain approval for a clinical trial application, the radiotracer and non-radioactive standard must be prepared under good laboratory practice (GLP) conditions and evaluated for acute toxicity and dosimetry in rodents[166]. Toxicological studies are performed by administrating a single dose of the non-radioactive equivalent (AmBF$_3$-TATE) at 100 times the expected peptide mass required for imaging. Animals will be inspected for changes in body weight, blood

chemistry, urine, and histology of key organs (kidneys, liver, pancreas, bone marrow, intestine, adrenal glands, stomach)[167]. Single-dose studies are sufficient, as patients will be administered the radiotracer only at the time of imaging, potentially weeks or months apart[166]. Dosimetry data will be acquired by performing biodistribution studies with ^{18}F-AmBF$_3$-TATE in healthy rodents over multiple time points. The uptake in organs will be used to calculate the predicted human effective radiation doses (mSv) using the OLINDA/EXM software[168]. The Investigation Drug Program at our facility, the BC Cancer Agency, is well equipped for performing toxicity and biodistribution studies under GLP conditions.

5.4   Concluding Remarks

In this thesis we evaluated ^{68}Ga- and ^{18}F- radiolabeled somatostatin analogues *in vivo*, using a breast cancer xenograft model with endogenous sstr2 expression. We hypothesized that antagonist peptides are better visualization agents compared to agonists, having both higher tumour uptake and contrast. Based on the results reported herein, we could not accept this hypothesis. However, all six tested compounds were able to clearly visualize the tumour indicating the potential of sstr imaging in breast cancers. Along with its high tumour uptake, ^{18}F-AmBF$_3$-TATE showed particularly fast background clearance, and could be a valuable imaging agent in facilities that prefer to use ^{18}F over traditional ^{68}Ga approaches.

Bibliography

1. Celler A. Nuclear medicine: SPECT and PET imaging principles. *Medical Imaging: Principles, Detectors, and Electronics.* 2009:101-126.

2. Gambhir SS. Molecular imaging of cancer with positron emission tomography. *Nature Reviews Cancer.* 2002;2:683-693.

3. Townsend DW. Combined positron emission tomography–computed tomography: the historical perspective. Paper presented at: Seminars in Ultrasound, CT and MRI, 2008.

4. Rosenkrantz AB, Friedman K, Chandarana H, et al. Current Status of Hybrid PET/MRI in Oncologic Imaging. *American Journal of Roentgenology.* 2016;206:162-172.

5. Fani M, Maecke HR. Radiopharmaceutical development of radiolabelled peptides. *European journal of nuclear medicine and molecular imaging.* 2012;39:11-30.

6. Vaidyanathan G, Zalutsky MR. Targeted therapy using alpha emitters. *Physics in Medicine and Biology.* 1996;41:1915.

7. Jadvar H, Parker JA. *Clinical PET and PET/CT*: Springer-Verlag London; 2006.

8. Cyclotron Produced Radionuclides: Physical Characteristics and Production Methods. *International Atomic Energy Agency.* 2009.

9. RA Pillai M, Dash A, F Knapp F. Rhenium-188: availability from the 188W/188Re generator and status of current applications. *Current Radiopharmaceuticals.* 2012;5:228-243.

10. Dash A, Pillai MRA, Knapp Jr FF. Production of 177Lu for targeted radionuclide therapy: available options. *Nuclear Medicine and Molecular Imaging.* 2015;49:85-107.

11. Saha GB. Diagnostic uses of radiopharmaceuticals in nuclear medicine. *Fundamentals of Nuclear Pharmacy*: Springer; 2010:257-339.

12. Lopci E, Nanni C, Castellucci P, et al. Imaging with non-FDG PET tracers: outlook for current clinical applications. *Insights into Imaging.* 2010;1:373-385.

13. Pauwels E, Sturm E, Bombardieri E, Cleton F, Stokkel M. Positron-emission tomography with [18F] fluorodeoxyglucose. *Journal of Cancer Research and Clinical Oncology.* 2000;126:549-559.

14. Nabi HA, Zubeldia JM. Clinical applications of 18F-FDG in oncology. *Journal of Nuclear Medicine Technology.* 2002;30:3-9.

15. Hoh CK. Clinical use of FDG PET. *Nuclear Medicine and Biology.* 2007;34:737-742.

16. Vander Heiden MG, Cantley LC, Thompson CB. Understanding the Warburg effect: the metabolic requirements of cell proliferation. *Science.* 2009;324:1029-1033.

17. Almuhaideb A, Papathanasiou N, Bomanji J. 18 F-FDG PET/CT imaging in oncology. *Annals of Saudi medicine.* 2011;31:3.

18. Hillner BE, Siegel BA, Liu D, et al. Impact of positron emission tomography/computed tomography and positron emission tomography (PET) alone on expected management of patients with cancer: initial results from the National Oncologic PET Registry. *Journal of Clinical Oncology.* 2008;26:2155-2161.

19. Garland S, Morrison A. Publicly Funded Uses of PET Scans in Canada. *Canadian Agency for Drugs and Technologies in Health (CADTH).* 2015:1-11.

20. Buck AK, Herrmann K, Stargardt T, Dechow T, Krause BJ, Schreyogg J. Economic evaluation of PET and PET/CT in oncology: evidence and methodologic approaches. *J Nucl Med Technol.* 2010;38:6-17.

21. Healthcare resource statistics - technical resources and medical technology. *Eurostate Statistics Explained* [January 16, 2017; http://ec.europa.eu/eurostat/statistics-explained/index.php/Healthcare_resource_statistics_-_technical_resources_and_medical_technology#Further_Eurostat_information. Accessed January 18, 2017.

22. Eckelman WC, Reba RC, Kelloff GJ. Targeted imaging: an important biomarker for understanding disease progression in the era of personalized medicine. *Drug Discovery Today.* 2008;13:748-759.

23. Wang L, Tang K, Zhang Q, et al. Somatostatin receptor-based molecular imaging and therapy for neuroendocrine tumors. *BioMed Research International.* 2013;2013.

24. Okarvi SM, Maecke HR. Chapter Eight-Radiometallo-Labeled Peptides in Tumor Diagnosis and Targeted Radionuclide Therapy. *Advances in Inorganic Chemistry.* 2016;68:341-396.

25. Reubi JC. Peptide receptors as molecular targets for cancer diagnosis and therapy. *Endocrine Reviews.* 2003;24:389-427.

26. Fani M, Maecke H, Okarvi S. Radiolabeled peptides: valuable tools for the detection and treatment of cancer. *Theranostics.* 2012;2:481-501.

27. Graham MM, Menda Y. Radiopeptide imaging and therapy in the United States. *Journal of Nuclear Medicine.* 2011;52:56S-63S.

28. U.S. Food and Drug Administration, Center for Drug Evaluation and Research. NETSPOT NED 208547 approval letter, June, 1 2016. http://www.accessdata.fda.gov/drugsatfda_docs/nda/2016/208547Orig1s000Approv.pdf. Accessed November 11, 2016.

29. Kähkönen E, Jambor I, Kemppainen J, et al. In vivo imaging of prostate cancer using [68Ga]-labeled bombesin analog BAY86-7548. *Clinical Cancer Research.* 2013;19:5434-5443.

30. Maina T, Bergsma H, Kulkarni HR, et al. Preclinical and first clinical experience with the gastrin-releasing peptide receptor-antagonist [68Ga] SB3 and PET/CT. *European Journal of Nuclear Medicine and Molecular Imaging.* 2016;43:964-973.

31. Sah B-R, Burger IA, Schibli R, et al. Dosimetry and first clinical evaluation of the new 18F-radiolabeled bombesin analogue BAY 864367 in patients with prostate cancer. *Journal of Nuclear Medicine.* 2015;56:372-378.

32. Wieser G, Mansi R, Grosu AL, et al. Positron emission tomography (PET) imaging of prostate cancer with a gastrin releasing peptide receptor antagonist–from mice to men. *Theranostics.* 2014;4:412-419.

33. Mansi R, Minamimoto R, Mäcke H, Iagaru AH. Bombesin-Targeted PET of Prostate Cancer. *Journal of Nuclear Medicine.* 2016;57:67S-72S.

34. Hanahan D, Weinberg RA. Hallmarks of cancer: the next generation. *Cell.* 2011;144:646-674.

35. Chen H, Niu G, Wu H, Chen X. Clinical application of radiolabeled RGD peptides for PET imaging of integrin αvβ3. *Theranostics.* 2016;6:78.

36. Fischer G, Schirrmacher R, Wängler B, Wängler C. Radiolabeled heterobivalent peptidic ligands: an approach with high future potential for in vivo imaging and therapy of malignant diseases. *ChemMedChem.* 2013;8:883-890.

37. Fröberg AC, de Jong M, Nock BA, et al. Comparison of three radiolabelled peptide analogues for CCK-2 receptor scintigraphy in medullary thyroid carcinoma. *European Journal of Nuclear Medicine and Molecular Imaging.* 2009;36:1265-1272.

38. Reubi JC, Waser B. Unexpected high incidence of cholecystokinin-B/gastrin receptors in human medullary thyroid carcinomas. *International Journal of Cancer.* 1996;67:644-647.

39. Christ E, Wild D, Ederer S, et al. Glucagon-like peptide-1 receptor imaging for the localisation of insulinomas: a prospective multicentre imaging study. *The Lancet Diabetes & Endocrinology.* 2013;1:115-122.

80

40. Körner M, Christ E, Wild D, Reubi JC. Glucagon-like peptide-1 receptor overexpression in cancer and its impact on clinical applications. *Frontiers in Endocrinology.* 2012;3:158.

41. Luo Y, Pan Q, Yao S, et al. Glucagon-Like Peptide-1 Receptor PET/CT with 68Ga-NOTA-Exendin-4 for Detecting Localized Insulinoma: A Prospective Cohort Study. *Journal of Nuclear Medicine.* 2016;57:715-720.

42. Tang B, Yong X, Xie R, Li Q-W, Yang S-M. Vasoactive intestinal peptide receptor-based imaging and treatment of tumors (Review). *International journal of oncology.* 2014;44:1023-1031.

43. Buchegger F, Bonvin F, Kosinski M, et al. Radiolabeled neurotensin analog, 99mTc-NT-XI, evaluated in ductal pancreatic adenocarcinoma patients. *Journal of Nuclear Medicine.* 2003;44:1649-1654.

44. George GP, Pisaneschi F, Nguyen QD, Aboagye EO. Positron emission tomographic imaging of CXCR4 in cancer: challenges and promises. *Molecular imaging.* 2014;13.

45. Philipp-Abbrederis K, Herrmann K, Knop S, et al. In vivo molecular imaging of chemokine receptor CXCR4 expression in patients with advanced multiple myeloma. *EMBO Molecular Medicine.* 2015;7:477-487.

46. Wang Z, Zhang M, Wang L, et al. Prospective Study of (68)Ga-NOTA-NFB: Radiation Dosimetry in Healthy Volunteers and First Application in Glioma Patients. *Theranostics.* 2015;5:882-889.

47. Jamous M, Haberkorn U, Mier W. Synthesis of peptide radiopharmaceuticals for the therapy and diagnosis of tumor diseases. *Molecules.* 2013;18:3379-3409.

48. Sun X, Li Y, Liu T, Li Z, Zhang X, Chen X. Peptide-based imaging agents for cancer detection. *Advanced Drug Delivery Reviews.* 2016.

49. Ginj M, Zhang H, Waser B, et al. Radiolabeled somatostatin receptor antagonists are preferable to agonists for in vivo peptide receptor targeting of tumors. *Proceedings of the National Academy of Sciences.* 2006;103:16436-16441.

50. Cescato R, Maina T, Nock B, et al. Bombesin receptor antagonists may be preferable to agonists for tumor targeting. *Journal of Nuclear Medicine.* 2008;49:318-326.

51. Sleight AJ, Stam NJ, Mutel V, Vanderheyden PM. Radiolabelling of the human 5-HT 2A receptor with an agonist, a partial agonist and an antagonist: effects on apparent agonist affinities. *Biochemical Pharmacology.* 1996;51:71-76.

52. Perrin MH, Sutton SW, Cervini LA, Rivier JE, Vale WW. Comparison of an agonist, urocortin, and an antagonist, astressin, as radioligands for characterization of corticotropin-releasing factor receptors. *Journal of Pharmacology and Experimental Therapeutics.* 1999;288:729-734.

53. Saha GB. Internal Radiation Dosimetry. *Fundamentals of Nuclear Pharmacy*: Springer; 2010:193-206.

54. Forrer F, Valkema R, Kwekkeboom DJ, de Jong M, Krenning EP. Peptide receptor radionuclide therapy. *Best Practice & Research Clinical Endocrinology & Metabolism.* 2007;21:111-129.

55. Price EW, Orvig C. The Chemistry of Inorganic Nuclides (86Y, 68Ga, 64Cu, 89Zr, 124I). *The Chemistry of Molecular Imaging.* 2014:105-135.

56. Cal-González J, Herraiz J, España S, Desco M, Vaquero JJ, Udías JM. Positron range effects in high resolution 3D PET imaging. Paper presented at: 2009 IEEE Nuclear Science Symposium Conference Record (NSS/MIC), 2009.

57. Šimeček J, Hermann P, Wester HJ, Notni J. How is 68Ga labeling of macrocyclic chelators influenced by metal ion contaminants in 68Ge/68Ga generator eluates? *ChemMedChem.* 2013;8:95-103.

58. Spang P, Herrmann C, Roesch F. Bifunctional Gallium-68 Chelators: Past, Present, and Future. *Seminars in nuclear medicine.* 2016;46:373-394.

59. Price EW, Orvig C. Matching chelators to radiometals for radiopharmaceuticals. *Chemical Society reviews.* 2014;43:260-290.

60. Notni J, Simecek J, Hermann P, Wester HJ. TRAP, a powerful and versatile framework for gallium-68 radiopharmaceuticals. *Chemistry (Weinheim an der Bergstrasse, Germany).* 2011;17:14718-14722.

61. Simecek J, Zemek O, Hermann P, Wester HJ, Notni J. A monoreactive bifunctional triazacyclononane phosphinate chelator with high selectivity for gallium-68. *ChemMedChem.* 2012;7:1375-1378.

62. Roeda D, Dollé F. Recent Developments in the Chemistry of [18F] Fluoride for PET. *The Chemistry of Molecular Imaging.* 2014:55-77.

63. Richter S, Wuest F. 18F-Labeled peptides: the future is bright. *Molecules.* 2014;19:20536-20556.

64. Smith GE, Sladen HL, Biagini SC, Blower PJ. Inorganic approaches for radiolabelling biomolecules with fluorine-18 for imaging with positron emission tomography. *Dalton Transactions.* 2011;40:6196-6205.

65. Zeng J-L, Wang J, Ma J-A. New strategies for rapid 18F-radiolabeling of biomolecules for radionuclide-based in vivo imaging. *Bioconjugate chemistry.* 2015;26:1000-1003.

66. McBride WJ, Sharkey RM, Karacay H, et al. A novel method of 18F radiolabeling for PET. *Journal of Nuclear Medicine.* 2009;50:991-998.

67. Bernard-Gauthier V, Wängler C, Schirrmacher E, et al. 18 F-Labeled Silicon-Based Fluoride Acceptors: Potential Opportunities for Novel Positron Emitting Radiopharmaceuticals. *BioMed Research International.* 2014;2014.

68. Bernard-Gauthier V, Bailey JJ, Liu Z, et al. From Unorthodox to Established: The Current Status of 18F-Trifluoroborate-and 18F-SiFA-Based Radiopharmaceuticals in PET Nuclear Imaging. *Bioconjugate Chemistry.* 2015;27:267-279.

69. Liu Z, Lin K-S, Bénard F, et al. One-step 18F labeling of biomolecules using organotrifluoroborates. *Nature Protocols.* 2015;10:1423-1432.

70. Liu Z, Pourghiasian M, Radtke MA, et al. An Organotrifluoroborate for Broadly Applicable One-Step 18F-Labeling. *Angewandte Chemie International Edition.* 2014;53:11876-11880.

71. McBride WJ, D'Souza CA, Karacay H, Sharkey RM, Goldenberg DM. New lyophilized kit for rapid radiofluorination of peptides. *Bioconjugate Chemistry.* 2012;23:538-547.

72. Mariniello B. Somatostatin Receptor. *Encyclopedia of Signaling Molecules.* 2012:1759-1765.

73. Weckbecker G, Lewis I, Albert R, Schmid HA, Hoyer D, Bruns C. Opportunities in somatostatin research: biological, chemical and therapeutic aspects. *Nature Reviews Drug Discovery.* 2003;2:999-1017.

74. Ritter SL, Hall RA. Fine-tuning of GPCR activity by receptor-interacting proteins. *Nature Reviews Molecular Cell Biology.* 2009;10:819-830.

75. Barbieri F, Bajetto A, Pattarozzi A, et al. Peptide receptor targeting in cancer: the somatostatin paradigm. *International Journal of Peptides.* 2013;2013.

76. Krenning E, Kwekkeboom DJ, Bakker Wea, et al. Somatostatin receptor scintigraphy with [111In-DTPA-D-Phe1]-and [123I-Tyr3]-octreotide: the Rotterdam experience with more than 1000 patients. *European Journal of Nuclear Medicine and Molecular imaging.* 1993;20:716-731.

77. Reubi J, Waser B, Schaer J-C, Laissue JA. Somatostatin receptor sst1–sst5 expression in normal and neoplastic human tissues using receptor autoradiography with subtype-selective ligands. *European Journal of Nuclear Medicine and Molecular Imaging.* 2001;28:836-846.

78. Sollini M, Erba PA, Fraternali A, et al. PET and PET/CT with 68gallium-labeled somatostatin analogues in Non GEP-NETs Tumors. *The Scientific World Journal.* 2014;2014.

79. Klöppel G. Tumour biology and histopathology of neuroendocrine tumours. *Best Practice & Research Clinical Endocrinology & Metabolism.* 2007;21:15-31.

80. Modlin IM, Moss SF, Oberg K, et al. Gastrointestinal neuroendocrine (carcinoid) tumours: current diagnosis and management. *Medical Journal of Australia.* 2010;193:46-52.

81. Hallet J, Law CHL, Cukier M, Saskin R, Liu N, Singh S. Exploring the rising incidence of neuroendocrine tumors: A population-based analysis of epidemiology, metastatic presentation, and outcomes. *Cancer.* 2015;121:589-597.

82. Yao JC, Hassan M, Phan A, et al. One hundred years after "carcinoid": epidemiology of and prognostic factors for neuroendocrine tumors in 35,825 cases in the United States. *Journal of Clinical Oncology.* 2008;26:3063-3072.

83. Pape U-F, Berndt U, Müller-Nordhorn J, et al. Prognostic factors of long-term outcome in gastroenteropancreatic neuroendocrine tumours. *Endocrine-Related Cancer.* 2008;15:1083-1097.

84. Reubi J, Laissue J, Krenning E, Lamberts S. Somatostatin receptors in human cancer: incidence, characteristics, functional correlates and clinical implications. *The Journal of Steroid Biochemistry and Molecular Biology.* 1992;43:27-35.

85. Reubi J-C, Krenning E, Lamberts S, Kvols L. Somatostatin receptors in malignant tissues. *The Journal of Steroid Biochemistry and Molecular Biology.* 1990;37:1073-1077.

86. Volante M, Rosas R, Allia E, et al. Somatostatin, cortistatin and their receptors in tumours. *Molecular and Cellular Endocrinology.* 2008;286:219-229.

87. Prevost G, Hosford D, Thomas F. Receptors for Somatostatin and Somatostatin Analogues in Human Breast Tumors. *Annals of the New York Academy of Sciences.* 1994;733:147-154.

88. Reubi J, Waser B, Foekens J, Klijn J, Lamberts S, Laissue J. Somatostatin receptor incidence and distribution in breast cancer using receptor autoradiography: relationship to EGF receptors. *International Journal of Cancer.* 1990;46:416-420.

89. Schaer JC, Waser B, Mengod G, Reubi JC. Somatostatin receptor subtypes sst1, sst2, sst3 and sst5 expression in human pituitary, gastroentero-pancreatic and mammary tumors: comparison of mRNA analysis with receptor autoradiography. *International Journal of Cancer.* 1997;70:530-537.

90. Evans AA, Crook T, Laws SA, Gough AC, Royle GT, Primrose JN. Analysis of somatostatin receptor subtype mRNA expression in human breast cancer. *British journal of cancer.* 1997;75:798-803.

91. Kumar U, Grigorakis SI, Watt HL, et al. Somatostatin receptors in primary human breast cancer: quantitative analysis of mRNA for subtypes 1--5 and correlation with receptor protein expression and tumor pathology. *Breast cancer research and treatment.* 2005;92:175-186.

92. Vikic-Topic S, Raisch KP, Kvols LK, Vuk-Pavlovic S. Expression of somatostatin receptor subtypes in breast carcinoma, carcinoid tumor, and renal cell carcinoma. *Journal of Clinical Endocrinology Metabolism.* 1995;80:2974-2979.

93. Schulz S, Schmitt J, Wiborny D, et al. Immunocytochemical detection of somatostatin receptors sst1, sst2A, sst2B, and sst3 in paraffin-embedded breast cancer tissue using subtype-specific antibodies. *Clinical Cancer Research.* 1998;4:2047-2052.

94. Orlando C, Raggi CC, Bianchi S, et al. Measurement of somatostatin receptor subtype 2 mRNA in breast cancer and corresponding normal tissue. *Endocrine-Related Cancer.* 2004;11:323-332.

95. Reubi JC, Torhorst J. The relationship between somatostatin, epidermal growth factor, and steroid hormone receptors in breast cancer. *Cancer.* 1989;64:1254-1260.

96. Van Den Bossche B, D'haeninck E, De Vos F, et al. Oestrogen-mediated regulation of somatostatin receptor expression in human breast cancer cell lines assessed with 99mTc-depreotide. *European Journal of Nuclear Medicine and Molecular Imaging.* 2004;31:1022-1030.

97. Xu Y, Song J, Berelowitz M, Bruno JF. Estrogen regulates somatostatin receptor subtype 2 messenger ribonucleic acid expression in human breast cancer cells. *Endocrinology.* 1996;137:5634-5640.

98. Xu Y, Berelowitz M, Bruno JF. Characterization of the promoter region of the human somatostatin receptor subtype 2 gene and localization of sequences required for estrogen-responsiveness. *Molecular and Cellular Endocrinology.* 1998;139:71-77.

99. Bajetta E, Procopio G, Ferrari L, et al. A randomized, multicenter prospective trial assessing long-acting release octreotide pamoate plus tamoxifen as a first line therapy for advanced breast carcinoma. *Cancer.* 2002;94:299-304.

100. Mikołajczak R, Maecke HR. Radiopharmaceuticals for somatostatin receptor imaging. *Nuclear Medicine Review.* 2016;19:126-132.

101. Lamberts S, Barker W, Reubi J-C, Krenning E. Somatostatin-receptor imaging in the localization of endocrine tumors. *New England Journal of Medicine.* 1990;323:1246-1249.

102. Kabasakal L, Demirci E, Ocak M, et al. Comparison of 68Ga-DOTATATE and 68Ga-DOTANOC PET/CT imaging in the same patient group with neuroendocrine tumours. *European Journal of Nuclear Medicine and Molecular imaging.* 2012;39:1271-1277.

103. Poeppel TD, Binse I, Petersenn S, et al. 68Ga-DOTATOC versus 68Ga-DOTATATE PET/CT in functional imaging of neuroendocrine tumors. *Journal of Nuclear Medicine.* 2011;52:1864-1870.

104. Bass RT, Buckwalter BL, Patel BP, et al. Identification and characterization of novel somatostatin antagonists. *Molecular pharmacology.* 1996;50:709-715.

105. Cescato R, Waser B, Fani M, Reubi JC. Evaluation of 177Lu-DOTA-sst2 antagonist versus 177Lu-DOTA-sst2 agonist binding in human cancers in vitro. *Journal of Nuclear Medicine.* 2011;52:1886-1890.

106. Wild D, Fani M, Behe M, et al. First clinical evidence that imaging with somatostatin receptor antagonists is feasible. *Journal of Nuclear Medicine.* 2011;52:1412-1417.

107. Cescato R, Erchegyi J, Waser B, et al. Design and in vitro characterization of highly sst2-selective somatostatin antagonists suitable for radiotargeting. *Journal of Medicinal Chemistry.* 2008;51:4030-4037.

108. Fani M, Braun F, Waser B, et al. Unexpected sensitivity of sst2 antagonists to N-terminal radiometal modifications. *Journal of Nuclear Medicine.* 2012;53:1481-1489.

109. Fani M, Del Pozzo L, Abiraj K, et al. PET of somatostatin receptor-positive tumors using 64Cu- and 68Ga-somatostatin antagonists: the chelate makes the difference. *Journal of Nuclear Medicine.* 2011;52:1110-1118.

110. Nicolas G, Kaul F, Mena R, Bouterfa H, Fani M, Wild D. First clinical data on 68Ga-labeled somatostatin receptor antagonists: a phase I/II study comparing 68Ga-OPS202 with 68Ga-DOTATOC PET/CT. *Journal of Nuclear Medicine.* 2015;56:266-266.

111.   Fani M, Maecke HR. Radiolabeled Somatostatin Receptor Antagonists. *Somatostatin Analogues: From Research to Clinical Practice.* 2015:306-321.

112.   Kaltsas G, Papadogias D, Makras P, Grossman A. Treatment of advanced neuroendocrine tumours with radiolabelled somatostatin analogues. *Endocrine-Related Cancer.* 2005;12:683-699.

113.   Kwekkeboom DJ, Mueller-Brand J, Paganelli G, et al. Overview of results of peptide receptor radionuclide therapy with 3 radiolabeled somatostatin analogs. *Journal of Nuclear Medicine.* 2005;46:62S-66S.

114.   Strosberg J, Wolin E, Chasen B, et al. NETTER-1 Phase III in Patients with Midgut Neuroendocrine Tumors Treated with 177Lu-Dotatate: Efficacy and Safety Results. *Journal of Nuclear Medicine.* 2016;57:629-629.

115.   Dalm SU, Nonnekens J, Doeswijk GN, et al. Comparison of the Therapeutic Response to Treatment with a 177Lu-Labeled Somatostatin Receptor Agonist and Antagonist in Preclinical Models. *Journal of Nuclear Medicine.* 2016;57:260-265.

116.   Wild D, Fani M, Fischer R, et al. Comparison of somatostatin receptor agonist and antagonist for peptide receptor radionuclide therapy: a pilot study. *Journal of Nuclear Medicine.* 2014;55:1248-1252.

117.   Canadian Cancer Society's Advisory Committee on Cancer Statistics. *Canadian Cancer Statistics 2016.*Toronto, ON: Canadian Cancer Society; 2016.

118.   Stewart B, Wild CP. World cancer report 2014. *World.* 2016.

119.   Allred DC. Ductal carcinoma in situ: terminology, classification, and natural history. *Journal of the National Cancer Institute Monographs.* 2009;2010:134-138.

120.   PDQ® Adult Treatment Editorial Board. PDQ Breast Cancer Treatment. Bethesda, MD: National Cancer Institute. Updated 10/12/2016. Available at: http://www.cancer.gov/types/breast/patient/breast-treatment-pdq. Accessed 11/08/2016. [PMID: 26389406].

121.   Prat A, Pineda E, Adamo B, et al. Clinical implications of the intrinsic molecular subtypes of breast cancer. *The Breast.* 2015;24:S26-S35.

122.   Yersal O, Barutca S. Biological subtypes of breast cancer: Prognostic and therapeutic implications. *World Journal of Clinical Oncology.* 2014;5:412-424.

123.   Dawood S, Hu R, Homes MD, et al. Defining breast cancer prognosis based on molecular phenotypes: results from a large cohort study. *Breast cancer research and treatment.* 2011;126:185-192.

124. Howlader N, Altekruse SF, Li CI, et al. US incidence of breast cancer subtypes defined by joint hormone receptor and HER2 status. *Journal of the National Cancer Institute.* 2014;106.

125. Voduc KD, Cheang MC, Tyldesley S, Gelmon K, Nielsen TO, Kennecke H. Breast cancer subtypes and the risk of local and regional relapse. *Journal of Clinical Pncology : Official Journal of the American Society of Clinical Oncology.* 2010;28:1684-1691.

126. Alcantara D, Leal MP, García-Bocanegra I, García-Martín ML. Molecular imaging of breast cancer: present and future directions. *Frontiers in Chemistry.* 2014;2.

127. Prasad S, Houserkovaa D. The role of various modalities in breast imaging. *Biomed Pap Med Fac Univ Palacky Olomouc Czech Repub.* 2007;151:209-218.

128. Sree SV, Ng EY-K, Acharya RU, Faust O. Breast imaging: A survey. *World Journal of Clinical Oncology.* 2011;2:171-178.

129. Care CTFoPH. Recommendations on screening for breast cancer in average-risk women aged 40–74 years. *Canadian Medical Association Journal.* 2011;183:1991-2001.

130. Wilson CM. Screening Mammography Program of BC. http://www.bccancer.bc.ca/family-oncology-network-site/Documents/SMPPresentationIncludingDigital_V06_FINAL.pdf. Accessed Nov 11, 2016.

131. Garcia EM, Storm ES, Atkinson L, Kenny E, Mitchell LS. Current breast imaging modalities, advances, and impact on breast care. *Obstetrics and Gynecology Clinics of North America.* 2013;40:429-457.

132. Munnink TO, Nagengast W, Brouwers A, et al. Molecular imaging of breast cancer. *The Breast.* 2009;18:S66-S73.

133. Bénard F, Turcotte É. Imaging in breast cancer: Single-photon computed tomography and positron-emission tomography. *Breast Cancer Research.* 2005;7:153-162.

134. Fletcher JW, Djulbegovic B, Soares HP, et al. Recommendations on the use of 18F-FDG PET in oncology. *Journal of Nuclear Medicine.* 2008;49:480-508.

135. Kenny L, Coombes RC, Vigushin DM, Al-Nahhas A, Shousha S, Aboagye EO. Imaging early changes in proliferation at 1 week post chemotherapy: a pilot study in breast cancer patients with 3′-deoxy-3′-[18F] fluorothymidine positron emission tomography. *European Journal of Nuclear Medicine and Molecular imaging.* 2007;34:1339-1347.

136. MacDonald L, Edwards J, Lewellen T, Haseley D, Rogers J, Kinahan P. Clinical imaging characteristics of the positron emission mammography camera: PEM Flex Solo II. *Journal of Nuclear Medicine.* 2009;50:1666-1675.

137. Kalinyak JE, Berg WA, Schilling K, Madsen KS, Narayanan D, Tartar M. Breast cancer detection using high-resolution breast PET compared to whole-body PET or PET/CT. *European Journal of Nuclear Medicine and Molecular imaging.* 2014;41:260-275.

138. Dalm SU, Melis M, Emmering J, Kwekkeboom DJ, de Jong M. Breast cancer imaging using radiolabelled somatostatin analogues. *Nuclear Medicine and Biology.* 2016;43:559-565.

139. Droog M, Beelen K, Linn S, Zwart W. Tamoxifen resistance: from bench to bedside. *European Journal of Pharmacology.* 2013;717:47-57.

140. Engel LW, Young NA. Human breast carcinoma cells in continuous culture: a review. *Cancer Research.* 1978;38:4327-4339.

141. Subik K, Lee J-F, Baxter L, et al. The expression patterns of ER, PR, HER2, CK5/6, EGFR, Ki-67 and AR by immunohistochemical analysis in breast cancer cell lines. *Breast Cancer: Casic and Clinical Research.* 2010;4:35.

142. Prat A, Karginova O, Parker JS, et al. Characterization of cell lines derived from breast cancers and normal mammary tissues for the study of the intrinsic molecular subtypes. *Breast cancer research and treatment.* 2013;142:237-255.

143. Pourghiasian M. *Novel radiolabeled peptides to improve breast and prostate cancer diagnosis by PET*, University of British Columbia; 2015.

144. Lin K-S, Pan J, Amouroux G, et al. In vivo radioimaging of bradykinin receptor B1, a widely overexpressed molecule in human cancer. *Cancer Research.* 2015;75:387-393.

145. Heppeler A, Froidevaux S, Mäcke HR, et al. Radiometal-Labelled Macrocyclic Chelator-Derivatised Somatostatin Analogue with Superb Tumour-Targeting Properties and Potential for Receptor-Mediated Internal Radiotherapy. *Chemistry - A European Journal.* 1999;5:1974-1981.

146. Liu Z, Pourghiasian M, Bénard F, Pan J, Lin K-S, Perrin DM. Preclinical evaluation of a high-affinity 18F-trifluoroborate octreotate derivative for somatostatin receptor imaging. *Journal of Nuclear Medicine.* 2014;55:1499-1505.

147. Jiang G, Stalewski J, Galyean R, et al. GnRH antagonists: a new generation of long acting analogues incorporating p-ureido-phenylalanines at positions 5 and 6. *Journal of Medicinal Chemistry.* 2001;44:453-467.

148. Bylund DB, Deupree JD, Toews ML. Radioligand-binding methods for membrane preparations and intact cells. *Receptor Signal Transduction Protocols.* 2004:1-28.

149. Yung-Chi C, Prusoff WH. Relationship between the inhibition constant (K i) and the concentration of inhibitor which causes 50 per cent inhibition (I 50) of an enzymatic reaction. *Biochemical Pharmacology.* 1973;22:3099-3108.

150. Gakhar G, Wight-Carter M, Andrews G, Olson S, Nguyen TA. Hydronephrosis and urine retention in estrogen-implanted athymic nude mice. *Veterinary pathology.* 2009;46:505-508.

151. Ingberg E, Theodorsson A, Theodorsson E, Strom JO. Methods for long-term 17beta-estradiol administration to mice. *General and comparative endocrinology.* 2012;175:188-193.

152. Froidevaux S, Eberle AN, Christe M, et al. Neuroendocrine tumor targeting: study of novel gallium-labeled somatostatin radiopeptides in a rat pancreatic tumor model. *International Journal of Cancer.* 2002;98:930-937.

153. Wang F, Wang Z, Wu J, et al. The role of technetium-99m-labeled octreotide acetate scintigraphy in suspected breast cancer and correlates with expression of SSTR. *Nuclear Medicine and Biology.* 2008;35:665-671.

154. Reubi JC, Schär J-C, Waser B, et al. Affinity profiles for human somatostatin receptor subtypes SST1–SST5 of somatostatin radiotracers selected for scintigraphic and radiotherapeutic use. *European Journal of Nuclear Medicine.* 2000;27:273-282.

155. Jagoda E, Vaquero JJ, Seidel J, Green MV, Eckelman WC. Experiment assessment of mass effects in the rat: implications for small animal PET imaging. *Nuclear Medicine and Biology.* 2004;31:771-779.

156. Notni J, Steiger K, Hoffmann F, et al. Variation of Specific Activities of ^{68}Ga-Aquibeprin and ^{68}Ga-Avebetrin Enables Selective PET Imaging of Different Expression Levels of Integrins α5β1 and αvβ3. *Journal of Nuclear Medicine.* 2016;57:1618-1624.

157. de Jong M, Breeman WA, Bernard BF, et al. Tumour uptake of the radiolabelled somatostatin analogue [DOTA0, TYR3]octreotide is dependent on the peptide amount. *European Journal of Nuclear Medicine.* 1999;26:693-698.

158. Allen JP, Canty AJ, Schulz S, Humphrey P, Emson PC, Young HM. Identification of cells expressing somatostatin receptor 2 in the gastrointestinal tract of Sstr2 knockout/lacZ knockin mice. *Journal of Comparative Neurology.* 2002;454:329-340.

159. Froidevaux S, Heppeler A, Eberle AN, et al. Preclinical Comparison in AR4–2J Tumor-Bearing Mice of Four Radiolabeled 1, 4, 7, 10-Tetraazacyclododecane-1, 4, 7, 10-

Tetraacetic Acid-Somatostatin Analogs for Tumor Diagnosis and Internal Radiotherapy 1. *Endocrinology.* 2000;141:3304-3312.

160. Schloos J, Raulf F, Hoyer D, Bruns C. Identification and pharmacological characterization of somatostatin receptors in rat lung. *British journal of pharmacology.* 1997;121:963-971.

161. Breeman WA, Kwekkeboom DJ, Kooij PP, et al. Effect of dose and specific activity on tissue distribution of indium-111-pentetreotide in rats. *Journal of Nuclear Medicine.* 1995;36:623-627.

162. Kennecke H, Yerushalmi R, Woods R, et al. Metastatic behavior of breast cancer subtypes. *Journal of clinical oncology : official journal of the American Society of Clinical Oncology.* 2010;28:3271-3277.

163. Dalm SU, Sieuwerts AM, Look MP, et al. Clinical Relevance of Targeting the Gastrin-Releasing Peptide Receptor, Somatostatin Receptor 2, or Chemokine C-X-C Motif Receptor 4 in Breast Cancer for Imaging and Therapy. *Journal of Nuclear Medicine.* 2015;56:1487-1493.

164. Frati A, Rouzier R, Lesieur B, et al. Expression of somatostatin type-2 and -4 receptor and correlation with histological type in breast cancer. *Anticancer research.* 2014;34:3997-4003.

165. Rivera JA, Alturaihi H, Kumar U. Differential regulation of somatostatin receptors 1 and 2 mRNA and protein expression by tamoxifen and estradiol in breast cancer cells. *Journal of carcinogenesis.* 2005;4:10.

166. Sharma R, Aboagye E. Development of radiotracers for oncology--the interface with pharmacology. *British journal of pharmacology.* 2011;163:1565-1585.

167. Maina T, Konijnenberg MW, KolencPeitl P, et al. Preclinical pharmacokinetics, biodistribution, radiation dosimetry and toxicity studies required for regulatory approval of a phase I clinical trial with (111)In-CP04 in medullary thyroid carcinoma patients. *European Journal of Pharmaceutical Sciences.* 2016;91:236-242.

168. Stabin MG, Sparks RB, Crowe E. OLINDA/EXM: the second-generation personal computer software for internal dose assessment in nuclear medicine. *Journal of Nuclear Medicine.* 2005;46:1023-1027.

Appendices

Appendix A qPCR Parameters

IDT PrimeTime[®] qPCR Assays:

sstr1: Hs.PT.58.3617180.g; sstr2: Hs.PT.58.4519773; sstr3: Hs.PT.58.2857882;

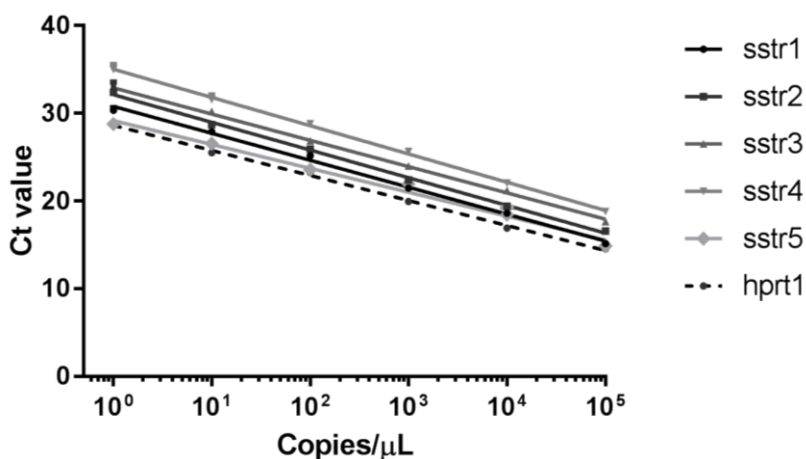Sstr4: Hs.PT.58.25532554.g; Sstr5: Hs.PT.58.25896367.g; HPRT1: Hs.PT.58v.45621572

Figure A.1 Representative standard curves for absolute quantification qPCR experiments.

Table A.1 Standard curve parameters

Target	Efficiency (%) (n=2)	Curve Fit (R^2) (n=2)
Sstr1	101.6	0.9969
Sstr2	107.5	0.9941
Sstr3	112.5	0.9937
Sstr4	104.7	0.9970
Sstr5	113.0	0.9910
HPRT1 (n=3)	125.09	0.9575

Table A.2 PCR cycling conditions

Denaturation	98 °C	30 sec
40 Cycles:		
Denaturation	98 °C	10 sec
Annealing	sstr1: 60 °C sstr2: 57 °C sstr3: 58 °C sstr4: 57 °C sstr5: 60 °C HPRT1: 57 °C	10 sec
Extension	72 °C	20 sec
Final Extension	72 °C	2 min
Hold	4 °C	

Table A.3 qPCR cycling conditions

Hot Start	95 °C	15 sec
40 cycles		
Denaturation	95 °C	10 sec
Annealing /Extension	sstr1: 60 °C sstr2: 57 °C sstr3: 58 °C sstr4: 58 °C sstr5: 60 °C HPRT1: 58 °C	60 sec

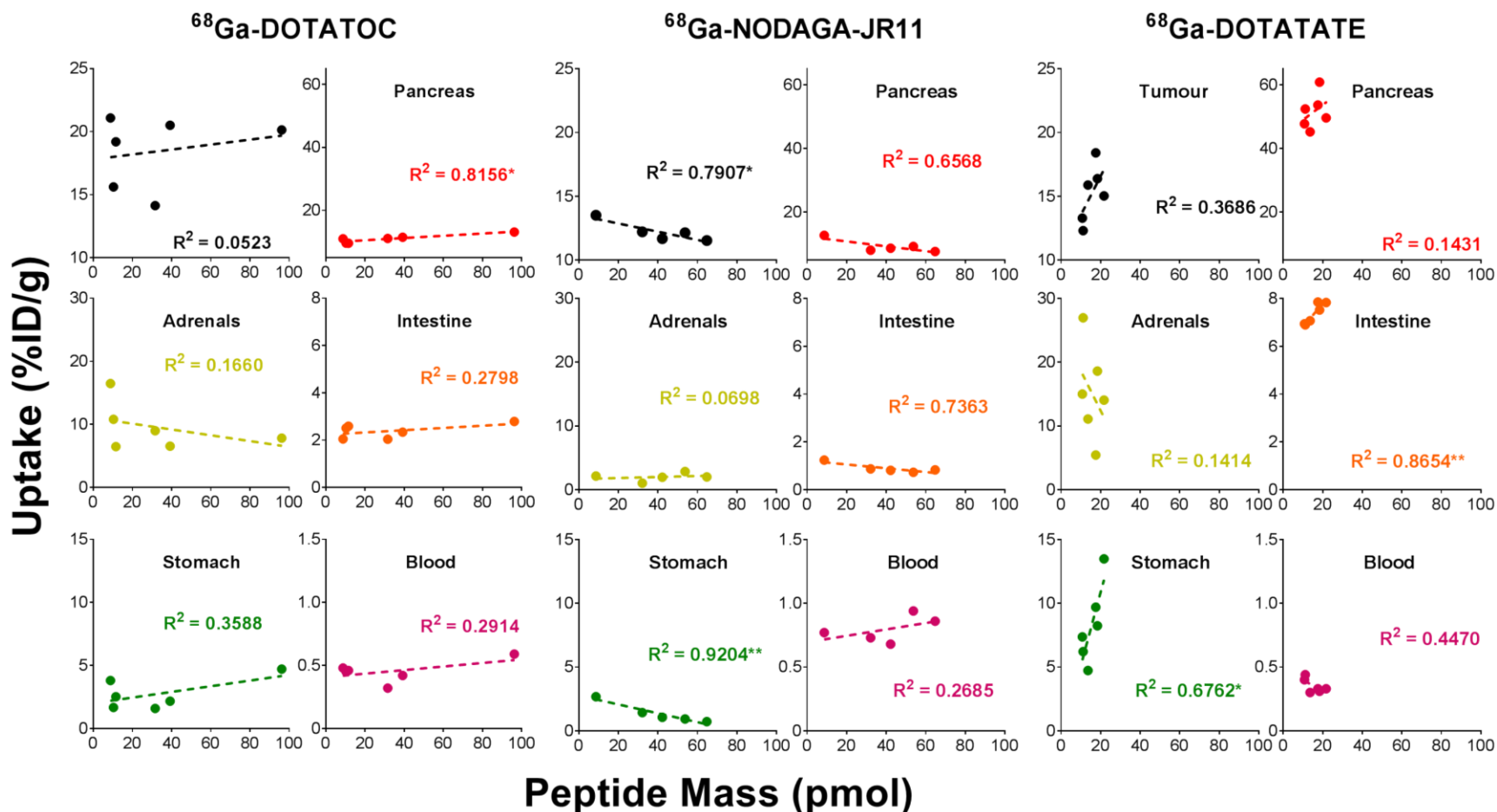## Appendix B Relationship between Peptide Mass and Organ Uptake

Figure B.1 Correlation between injected peptide mass and uptake in sstr-positive organs and blood with ^{68}Ga-NODAGA-JR11, ^{68}Ga-DOTATOC and ^{68}Ga-DOTATATE. * $p < 0.05$, **$p < 0.01$.
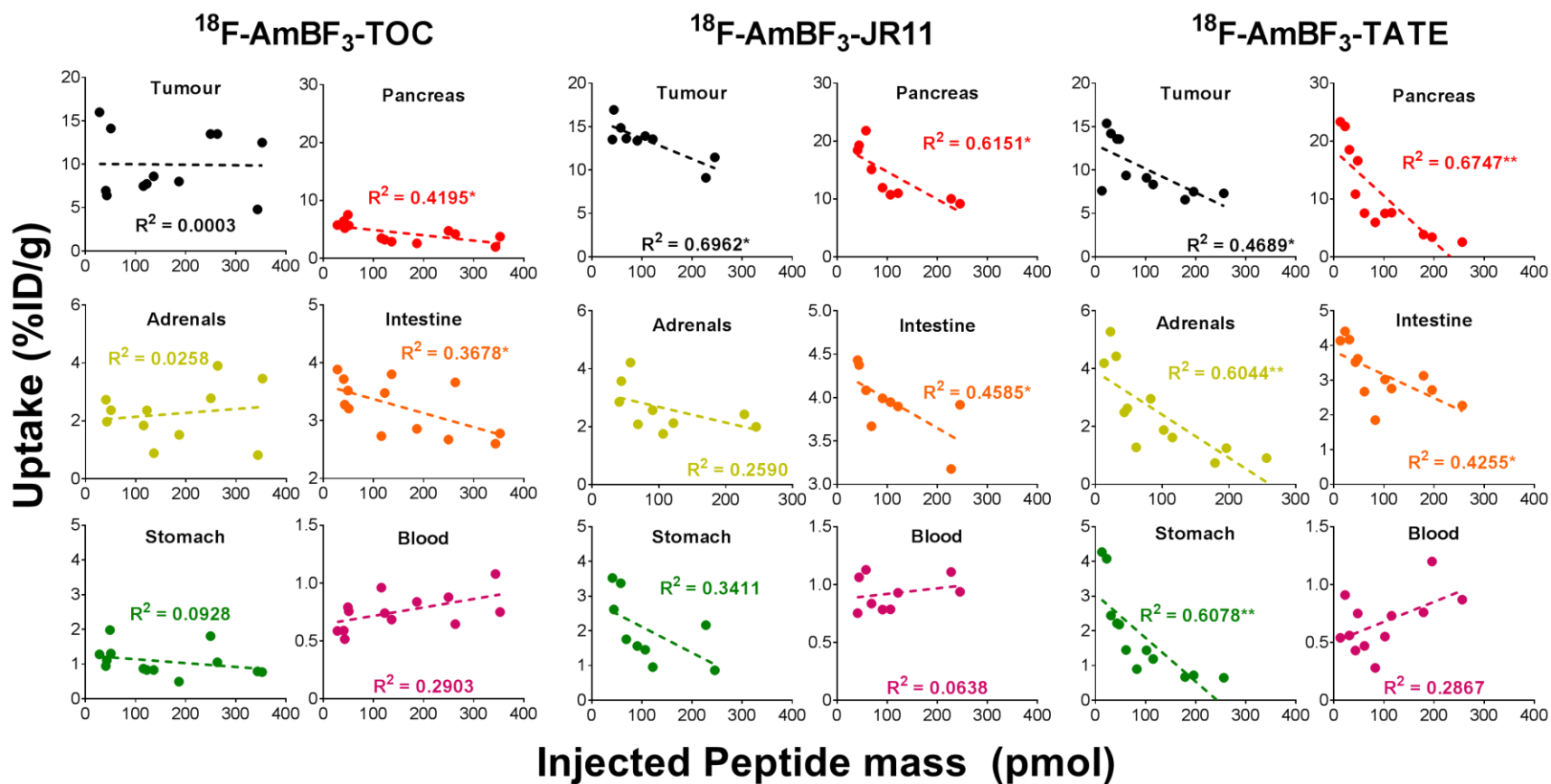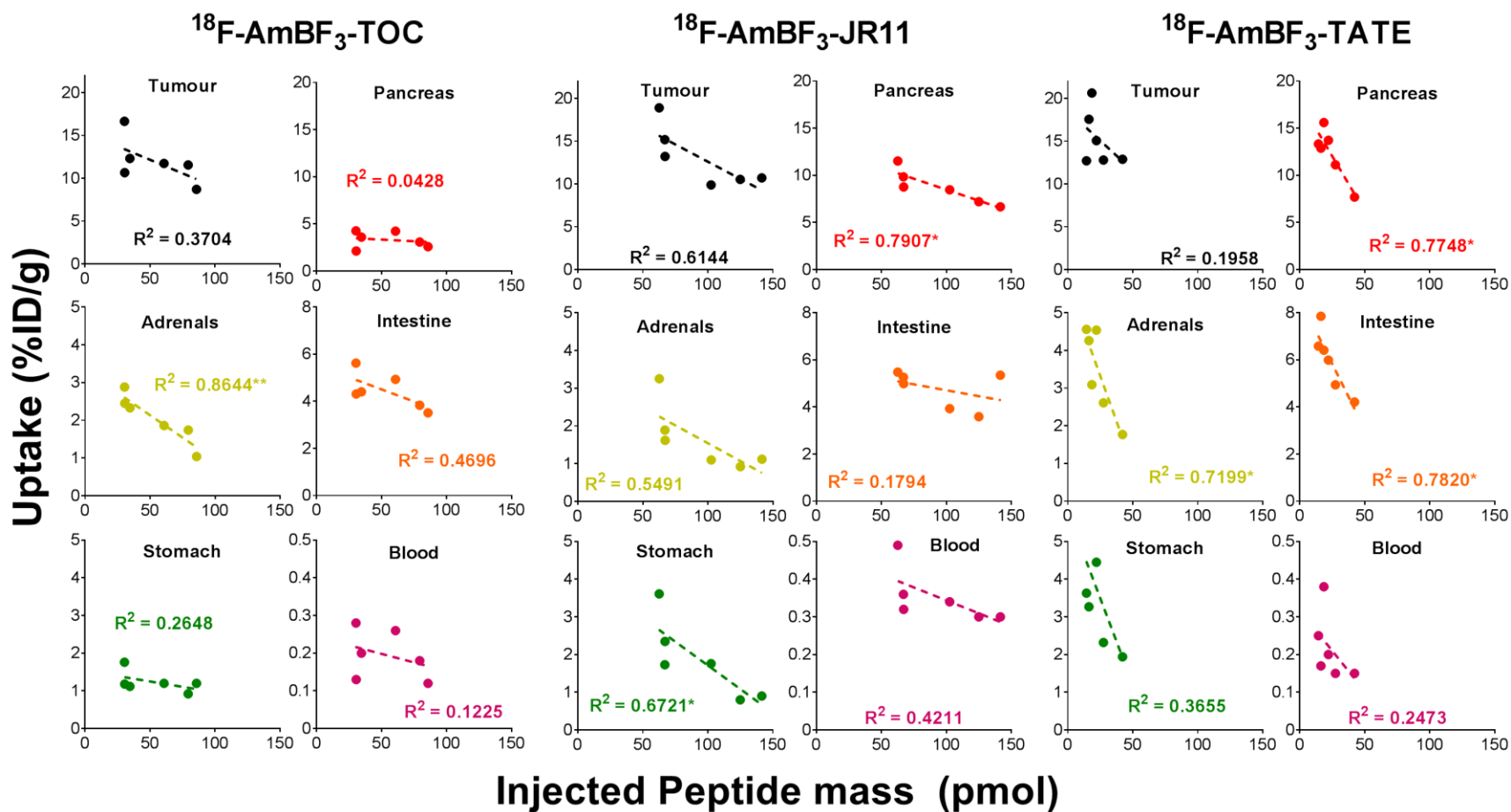
Figure B.2 Correlation between injected peptide mass and uptake in sstr-positive organs and blood with ^{18}F-AmBF$_3$-TOC, ^{18}F-AmBF$_3$-JR11, and ^{18}F-AmBF$_3$-TATE at 1h p.i. $* p < 0.05$, $**p < 0.01$.

Figure B.3 Correlation between injected peptide mass and uptake in sstr-positive organs and blood with ^{18}F-AmBF$_3$-TOC, ^{18}F-AmBF$_3$-JR11, and ^{18}F-AmBF$_3$-TATE at 2 h p.i. * $p < 0.05$, **$p < 0.01$.